VNIVERSITAT E VALÈNCIA

Instituto Interuniversitario de Reconocimiento Molecular y Desarrollo Tecnológico.

Doctorado en Química

Design, Synthesis and Evaluation of chemosensors for NOx detection

PhD Thesis

Submitted by:
Luis Alberto Juárez Díaz

PhD supervisors:
Prof. Ana María Costero Nieto
Prof. Margarita Parra Álvarez

València, Mayo 2016.

Ana Maria Costero Nieto, PhD in Chemistry and Professor at the Universitat de València, and Margarita Parra Álvarez, PhD in Chemistry and Professor at the Universitat de València.

CERTIFY:

That the work *"Design, Synthesis and Evaluation of chemosensors for NOx detection"* has been developed by **Luis Alberto Juárez Díaz** under their supervision in the Instituto Interuniversitario de Reconocimiento Molecular y Desarrollo Tecnólogico (IDM) of the Universitat de València, as a thesis Project in order to obtain the degree of PhD in Chemistry at the Universitat de València.

València, May 2016.

Prof. Ana María Costero Nieto   Prof. Margarita Parra Álvarez

a mi Madre

Abstract

The present PhD thesis entitled "Design, Synthesis and Evaluation of chemosensors for NOx detection" is focused on the development of new chromo-fluorogenic sensors following principle of molecular recognition.

The first part of this thesis is focused on the design, synthesis characterization and evaluation of organic compounds suitable to act as sensors for nitrogen dioxide. The synthetized receptors employ either functionalized biphenylsor BODIPY-dyes as signalling subunit. The strategy is based on the generation of aromatic aldehydes from trimethylsilyl benzyl ethers and oximes in the presence of NO_2. The formed aldehyde would change the electronic properties of the ligand with the result of a change in the chromo-fluorogenic properties. The prepared sensors have remarkable low limits of detection and highly selectivity. The sensing abilities are retained in solid support, allowing practical applications of the systems in real-time monitoring as simple colorimetric tests.

The remaining part of this first section is centre in the development of new mesoporous materials functionalized with molecular gates and their applications in sensing. The design, synthesis and evaluation of suitable modified MCM-41 materials with the liberation of the cargo controlled by the target molecule were described.

The second part is centered in the design, synthesis, characterization and evaluation of a copper(II) BODIPY-complex for nitric oxide detection. The displacement assay approach has been used in this case to develop a selective and highly sensitive sensor for NO (g). The demetalation of the BODIPY-complex, induced by the cation reduction, causes an enhancement of the emission. The limit of detection was in the ppb range. The probe was successfully used to detect NO release in cells.

Resumen

La presente tesis doctoral titulada "Design, Syntehsis and Evaluation of chemosensors for NOx detection (Diseño, síntesis y evaluación de sensores químicos para la detección de NOx)" está centrada en el desarrollo de nuevos sensores cromo-fluorogénicos basados en los principios del reconocimientos molecular.

La primera parte de esta tesis doctoral se centra en el diseño, síntesis, caracterización y evaluación de compuestos orgánicos adecuados para actuar como sensores de dióxido de nitrógeno. Los receptores sintetizados emplean bifenilos adecuadamente funcionalizados o BODIPY como subunidades señalizadoras. La estrategia se basa en la capacidad regeneración de los grupos aldehídos aromáticos a partir de trimetilsilil benzil éteres u oximas en presencia de NO_2. El aldehído obtenido cambia las propiedades electrónicas de sistema con el consecuente cambio en las propiedades cromo-fluorogénicas. Los límites de detección alcanzados son muy interesantes. La capacidad de detección se mantiene cuando el sensor se deposita en un soporte sólido, lo que permite la aplicación práctica para medidas en tiempo real mediante ensayos colorimétricos sencillos.

La parte restante de esta primera sección se centra en el desarrollo de nuevos materiales mesoporosos funcionalizados con puertas moleculares para su empleo como sensores químicos. Se ha llevado a cabo el diseño, síntesis y evaluación de MCMC-41 materiales convenientemente modificados y el estudio de la liberación de la carga frente a las moléculas objetivo.

La segunda parte del trabajo se centra en el diseño, síntesis, caracterización y evaluación de un complejo con Cu(II) de un derivado de BODIPY para la detección de óxido nítrico. En este caso, se ha usado la aproximación de ensayo de desplazamiento y se ha desarrollo un sensor selectivo y altamente sensible para NO (g). La desmetalización del complejo de Bodipy causada por la reducción del Cu(II) a Cu(I) origina un aumento considerable de la emisión. Los límites de detección se encuentran en el rango de los ppb. El sensor preparado se ha mostrado útil para detectar la liberación de NO en células.

Abbreviations and acronyms.

BODIPY	4,4-difluoro-4-bora-3a,4a-diaza-s-indacene
^{13}C-NMR	Carbon Nuclear Magnetic Resonance
^{1}H-NMR	Proton Nuclear Magnetic Resonance
abs	Absorbance
Ar	Argon
$BF_3 \cdot Et_2O$	Boron trifluoride diethyl etherate
CD_3CN	Acetonitrile-d3
$CDCl_3$	Chloroform-d
CH_2Cl_2	Dichloromethane
CH_3Cl	Chloromethane
CH_3CN	Acetonitrile
Cl	Chloride
CT	Charge transfer
d	Doublet
δ	Chemical Shift
D_2O	Deuterium Oxide
dd	Doublet of doublets
DDQ	2,3-Dichloro-5,6-dicyano-1,4-benzoquinone
DMF	Dimethylformamide
DMSO	Dimethylsulfoxide
dt	Doublet of triplets
em	Emission
Et_3N	Triethylamine
EtOH	Ethanol
FRET	Fluorescence Resonance Energy Transfer
GC/MS Gas	Gas Chromatography–Mass Spectrometry
GC-FID Gas	Gas Chromatography – Flame Ionization Detector
h	Hours
H_2	Hydrogen
H_2SO_4	Sulfuric Acid
HCl	Hydrochloric acid
He	Helium
Hex	Hexane
HOMO	Highest Ocupied Molecular Orbital
HRMS	High Resolution Mass Spectrometry
Hz	Hertz
ICT	Internal Change Transfer
J	J-coupling
K_2CO_3	Potassium Carbonate

KOH	Potassium Hydroxide
$LiAlH_4$	Lithium aluminium hydride
LOD	Limit of detection
LUMO	Lowerst Unnocupied Molecular Orbital
m	Multiplet
MeOH	Methanol
$MgSO_4$	Magnesium Sulfate
min	Minutes
mL	Mililitres
Na	Sodium
$NaHCO_3$	Sodium bicarbonate
NaOH	Sodium hydroxide
n-BuLi	n-Buthyllithium
NH_4OAc	Ammonium acetate
NO	Nitric oxide
NO_2	Nitrogen dioxide
OH	Hydroxil
φ	Quantum yield
Pd	Palladium
Pd/C	Palladium on Carbon
PET	Photoinduced Electron Transfer
ppb	Parts per billion
ppm	Parts per million
PTC	Photoinduced Charge Transfer
q	Quartet
S	Single excited state
s	Singulet
SE	Electrophilic substitution
SEAr	Electrophilic aromatic substitution
SNAr	Nucleophilic aromatic substitution
t	Triplet
T	Triple excited state
TBAOH	Tetrabutylammonium hydroxide solution
TEA	Triethylamine
TFA	Trifluoroacetic acid
THF	Tetrahydrofuran
TLC	Thin Layer Chromathography
UV	Ultraviolet
λ	Wavelength
ε	Molar absorption coefficient

Table of contents

Chapter 1:
General Introduction

1. The reactive species of nitrogen: NOx

In recent years, environmental awareness has significantly grown. This fact can be attributed to social dissatisfaction with the state of the environment. As a result, more rigours environmental laws have been introduced.

Air pollution constitutes one of the major problems in urban areas where many sources of air pollutants are concentrated. The notion "air pollutant" covers all substances which may harm humans, animals, vegetation and material. The main sources of air pollution are the combustion processes of fossil fuels used in power plants, vehicles and other incineration processes. Key combustion-generated air contaminants are sulphur oxides, particulate matter, carbon monoxide, unburned hydrocarbons and nitrogen oxides (NOx).[1]

NOx are considered the primary pollutants of the atmosphere, since they are responsible for environmental problems such as photochemical smog, acid raid, tropospheric ozone, ozone layer depletion, … Further to the above, they cause many health problems in humans when they are exposed to high concentration of these gases.
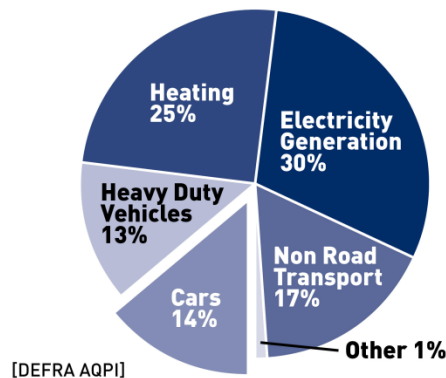

Fig. 1. Contribution of different sources to NOx emission (Europe, 2014)

---

[1] US Environmental Protection Agency Publications, http://www.epa. Gov/airquality/nitrogenoxides/index.html. (February 2016)
K. Skalska, J. S. Miller, S. Ledakowicz, *Sci. Total Environ*. **2010**, 408, 3976

Thus NOx concentration in urban areas is directly related with respiratory problems.[2] An exposition, for longer periods than 15 min, at concentrations higher than 5 ppm is known to produce intolerable irritations or irreversible modifications on pulmonary tissues. Even lower concentrations also can be irritant[3].

NOx is the generic term for the nitrogen oxides: nitric oxide (NO) and nitrogen dioxide (NO_2). NOx are produced from the reaction among nitrogen, oxygen and hydrocarbons during combustion at high temperatures (mainly in internal combustion engine and in power generation stations) (Fig. 1). NOx are usually describing for the total concentration of NO and NO_2, these concentrations are in equilibrium, the ratio NO/NO_2 is determinate by light and ozone (Scheme 1)

$$O_3 + h\nu \rightarrow O_2 + O$$
$$NO + O \rightarrow NO_2$$
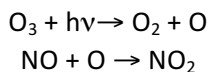
**Scheme 1:** NO_2 formation from ozone and light

Regardless of being the major component of NOx, nitric oxide is much less toxic than nitric dioxide

1.1 Environmental impact

Deforestation in the northern hemisphere by contamination is considered one of the most important ecological problems. Although responsibility might be directed toward a variety of factors, acid rain remains a major contributor among them. Rain is generally a slightly acid with pH value around 5-6, but acid rain pH has lower values, between 4 and 4.5. Acid rain is due to SO_2 and NO_2 present in the atmosphere.

[2] M. A. Gomez-Garcia, V. Pitchon, A. Kiennemann, *Environ. Int*. **2005**, 31, 445.
[3] S. C. Barman, N. Kumar, R. Singh, G. C. Kisku, A. H. Khan, M. M. Kidwai, R. C. Murthy M. P. S. Negi, P. Pandey, A. K. Verma, G. Jain, S. K.Bhargava, *J. Environ. Biol*., **2010**, 31, 913.
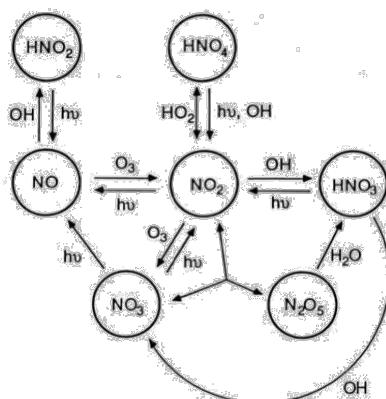
Scheme 2. Principal tropospheric reactions of the nitrogen oxides

Nitrogen oxides play an influential role in the photochemistry of both troposphere and stratosphere[4]. Nitrogen oxides are rapidly oxidised by ozone while radicals such as HO• and HOO•transformNO_2 into HNO_2 the principal component of the acid rain (Scheme 2). Acid rain is usually formed high up in the clouds, a place where nitrogen oxides react with water, oxygen and other oxidants. These compounds are transformed into HNO_3 that then acidifies rain, snow or fog because of its solubility in water. These acid precipitations greatly perturb the aquatic ecosystems and can cause the biological death of lakes and rivers.

1.2 Emission regulations

Starting in the early 1970s, the policy has gradually evolved in various countries, notably Japan, the United States and Germany, to establish a program of reducing emission levels of pollutants in flue gases from stationary sources. [5]

The Gothenburg Protocol (1999) was unique in the sense that it established reductions of four pollutants to abate three effects (acidification, eutrophication and the effects of tropospheric ozone on human health and vegetation). The protocol was signed by 29 European

---

[4] J.N. Armor, *Catal Today*, **1996**, 31, 191; R.C. Cohen, J.G. Murphy, *Chem. Rev*., **2003**, 103, 4985.
[5] J. W. Erisman, P. Grennflet, M. Sutton, *Environ Int*., **2003**, 19, 311.

countries together with Canada and U.S.A. Apart from the protocols, the member states have to fulfil several directives[6].
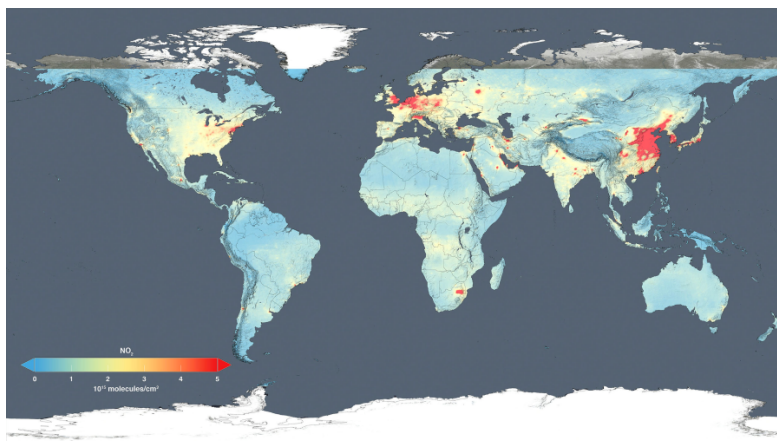

Fig. 2. Global air quality levels in 2014

Annual emission (Figure 2) reported by parties to the CLRTRAP (Convention of long-large transboundary air pollution) are summarised by EMEP (a co-operative program for the monitoring and evaluation of the long-range transmission of air pollutants in Europe). Updated information related to pollutant emissions can be obtained at the European Environment Agency (EEA), which interprets emission data, co-ordinates the development of the spatial distribution of emissions, and provides information on policies and scenarios[7].

1.3 Nitric oxide relevant properties in biology.

Nitic oxide (NO) is a small uncharged gaseous free radical containing one unpaired electron. NO exists in the space as an interstellar molecule and it has been also detected in the atmosphere of Venus and Mars. On the earth, NO has been recognized as an atmospheric pollutant and potential health hazard[8].

[6] a) A. Anon, *Air Pollut consult*, **1995**, 13. b) S. Devahasdin, Ch. Fan, K. Li, DH. Chen, *J. Photochem. Photobiol. A,* **2003**, 156, 161.

[7] V. Vestreng, E. Storen, Analysis of the UNECE/EMEP Emission Data. MSC-W Status Report 2000. Norwegian Meteorogical Intitute: Blindern, Oslo, 2000.

[8] T. Nagano, *Chem. Rev.*, **2002**, 102, 2135.

However, NO is also an important neurotransmitter. It was reported to be the long-sought endothelium-derived relaxing factor (EDRF) known to regulate blood vessel relaxation in the cardiovascular system. This finding initiated tremendous research efforts to understand how NO functions in the organism. Consequent discoveries of its involvement in a range of processes such as signal transduction in the brain and inmate defence against parasitic infections in the immune system led the magazine Science to designate NO as Molecule of the Year in 1992.

A growing body of evidence demonstrates that the role that NO plays in diverse systems is concentration dependent, and thus it is not surprising that defective NO production has been implicated in a range of disorders. Unquestionably, reliable measurement of both NO production and its levels is important. Detection and quantification of NO in biological systems present significant analytical challenges for several reasons being the low concentration of NO in vivo a major concern. NO is endogenously generated by NO synthases (NOS), of which there are three isoforms (nNOS, eNOS and iNOS). In general, nNOS and eNOS release NO in the nanomolar range, whereas iNOS can release NO in the micromolar range for extended periods.

1.4 NOx actual detection systems.

Due to the ubiquitous presence of NOx and its health effects, the development of selective and sensitive sensing methods for its detection and quantification is a hot area of research. An extensive number of analytical techniques for detection of NO_2, such as those based on laser-photoacoustic spectroscopy[9], surface acoustic waves (SAW)[10], transition metal oxide devices[11], or carbon quantum dot-functionalized aerogels have been developed[12]. However, these methods still show certain limitations such as scarce selectivity, operational complexity, non-portability or difficulties in real time monitoring.

---

[9] A. Mukherjee, M. Prasanna, M. Lane, R. Go, I. Dunayevskiy, A. Tsekoun, C. Kumar, N. Patel, *Applied Optics*, **2008**, 47, 4884.

[10] A. Venema, E. Nieuwkoop, M. J. Vellekoop, M. S. Nieuwenhuizen, A. W. Barendsz, *Sensors and actuators*, **1986**, 10, 47.

[11] a) Md. W. K. Nomani, D. Kersey, J. James, D. Diwan, T. Vogt, Rochard A. Webb, G. Koley, *Sensors and actuators B: Chemical*, **2011**, 160, 251. b) Z. Liang, S. Yang, J. Li, H. Zhang, Q. Diao, W. Zhao, G. Lu, *Sensors and Actuators B*, **2011**, 158, 1.

[12] R. Wang, G. Li, Y. Dong, Y. Chi, G. Chen, *Anal. Chem.*, **2013**, 85, 8065.

The importance on a large variety of bioregulatory and immune response roles for NO has been reported in the literature and for this reason insensitive experimental research for its detection are being continuously developed. Some techniques for analysing NO such as those based on chemiluminiescence[13] , colorimetry[14], electron paramagnetic resonance[15] and electrochemistry[16]have been reported[17]. Even through these methods have certain benefits they usually present some limitations such as low sensibility, poor specify, or expensive experimental apparatus which restrict its application in practice[18].

Recently the development of chromo-fluorogenic chemosensor has gained increasing interest[19] as an alternative to these instrumental procedures.

[13] J. F. Brien, B. E. McLaughlin, K. Nakatsu, G. S. Marks, *Methods Enzymol*., **1996**, 268, 83.

[14] F. Brown, N. J. Finnerty, F. B. Bolger, J. Millar, J. P. Lowry, *Anal. Bioanal. Chem*., **1982**, 126, 131.

[15] a) H. Kosaka, M. Watanabe, H. Yoshihara, N. Harada, T. Shiga, *Biochem. Biophys. Res. Commun*., **1992**, 184, 1119. b) Y. Katayama, N. Soh, M. Maeda, *Chem. PhysChem*., **2001**, 2, 655

[16] a) T. Malinski, Z. Taha, *Nature*, **1992**, 358, 676. b) F. Bedioui, N. Villeneuve, *Electroanalysis*, **2003**, 15, 5.

[17] a) M. D. Pluth, M. R. Chan, L. E. McQuade, S. J. Lippard, *Inorg. Chem*., **2011**, 50, 9385. b) S. Ma, D. C.Fang, B. Ning, M. Li, L. He, B. Gong, *Chem. Commun*., **2014**, 50, 6475.

[18] a) S. M. Cristescu, J. Mandon, M. F. J. Harren, P. Meriläinen, M. J. Högman, *Breath Re*., **2013**, 7, 1752. b) L. A. J. Mura, J. Mandonb, S. M. Cristescub, F. J. M. Harrenb, E. Prats, *Plant Science*, **2011**, 181, 509.

[19] S. Ohira , E. Wanigasekara, D.M. Rudkevich, P. K. Dasgupta, *Talanta*, **2001**, 14, 20.

2. Molecular recognition and sensing

At the end of 19th century, H. E. Fisher defined the principle in which molecular recognition is based when he suggested that the enzyme-substrate interactions take the form of "lock and key". J. M. Lehn introduced the term *supramolecule* as an organized complex entity that is created from the association of two or more chemical species held together by intermolecular forces. Whereas the term supramolecular chemistry can be defined as the selective interaction between host molecule (receptor) and a guest molecule (substrate) through non-covalent interactions. To produce this recognition event, specific conditions of spatial and electronic compatibility must be satisfied; in which the guest has a geometric size or shape complementary to the host. This concept laid the basis for molecular recognition (Figure 3) i.e. the discrimination by a host between different guests.
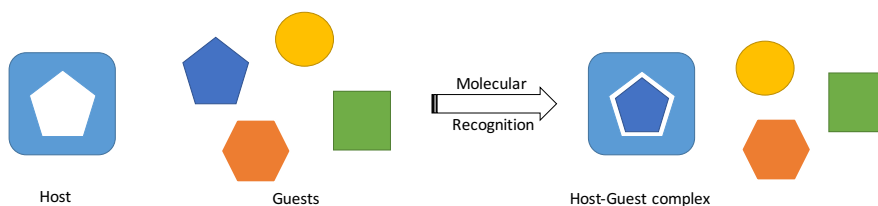

Fig. 3. Molecular recognition event by specific host-guest interactions.

Bearing in mind this concept, in order to design a suitable receptor for a specific guest, some factors of the guest should be considered, as for example, size, charge, geometry, hydrophobicity or lipophilicity or possible formation of hydrogen bonds.

The first receptors, based on this principle, were synthesized by Pedersen.[20] They were crown ether capable of coordinate alkali and alkaline cations. In the last decades, many advances have been achieved in this area and myriad of receptors that mimic the behaviour of biological systems have been described. These synthesized abiotic receptors are able to recognize cations, anions and neutral molecules.[21]

---

[20] C. J. Pedersen, *J. Am. Chem. Soc.*, **1967**, 89, 7017-7036.

[21] a) M. D. Best, S. L. Tobey, E. V. Anslyn, Coord. *Chem. Rev.*, **2003**, 240,3-15, b) K. Severin, *Coord. Chem. Rev.*, **2003**, 245, 3-10, c) J. M. Llinares, D. Powell, K. Bowman-James, *Coord. Chem. Rev.*, **2003**, 240, 57-75. d) K. A. Schung, W. Lindner, *Chem. Rev.*, **2005**, 105, 67-113. e) P. Blondeau, M. Segura, R. Perez-Fernandez, J. De Mendoza, Chem. Soc.

Molecular recognition chemistry is closely related with the concept of chemical sensing. A chemosensor is a molecule or supermolecule that recognizes and interacts with a specific analyte producing a detectable signal which reveals the presence of the guest[22]

2.1 Chemosensors

A molecular sensor or chemosensor is a molecule that specifically interacts with an analyte producing a detectable and easy-to measure signal. In this sensing process, information at the molecular levels, such as the presence or not of a certain guest, is amplified to a macroscopic level; hence, molecular sensing opens the door to the determination (qualitative and/or quantitative) of certain guests[23]. A good chemosensor must fulfil a number of requirements such as selective recognition. On the other hand the interaction should be reversible and not slow to allow real-time readings. The chemosensor is usually composed by two units:
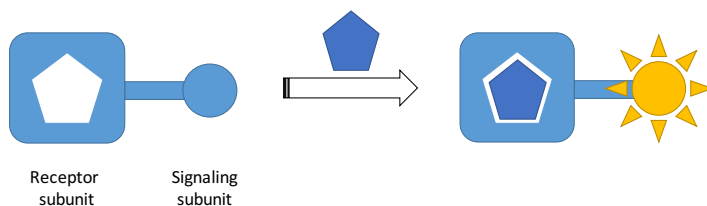

Receptor
subunit

Signaling
subunit

Fig. 4. Schematic representation of a chemosensors.

- Receptor unit. It is responsible of the recognition event and grants the specific interaction with a particular analyte allowing the discrimination.
- Signalling unit. It acts as a signal transducer and informs about the recognition process that occurs at molecular level, through changes in a measurable macroscopic signal. Traditionally changes in the optical properties or electrochemical properties are used.

Rev.,**2007**, 36, 189-197. f) J. W. Steed, *Chem. Soc. Rev*., **2009**,38, 506-519. g) Z. Xu, S. K. Kim, J. Yoon, *Chem. Soc. Rev*., **2010,** 39, 1457-1466. h) T. Pradhan, H. S. Jun, J. H. Jang, T. W. Kim, C. Kang, J. S. Kim, *Chem. Soc. Rev.*, **2014**, 43, 4684-4713.

[22] W. C. Rogers, M.O. Woolf, *Coord. Chem. Rev.*, **2002**, 233, 341.

[23] a) R. Martinez-Mañez, F. Sancenon, *Chem. Rev*., **2003**, 103, 4419. b) M. Moragues, R. Martinez-Mañez, F. Sancenon, *Chem. Soc. Rev*., **2011**, 40, 2593.

Three main approaches can be used for designing optical chemosensors (Fig. 5). The choice of one or another format depends on the selectivity to be achieved and the synthetic effort required to obtain the sensor/chemosensor.

- **Binding site-signalling subunit approach**: Chemosensors based on this approach are formed by two subunits namely "binding site" and "signalling subunit" that are covalently linked. The interaction of guest with the binding site changes the electronic properties of the signalling subunit resulting in a sensing event via colour or emission modulation[24].

- **Displacement approach**: In this approach, the selected receptor (binging site/receptor unit) forms an inclusion complex with a dye. The sensing paradigm relies on a displacement reaction because the coordination of the target molecule with the receptor induces the release of the dye. An optical response is obtained because the signalling subunit colour or emission in the sensing ensemble are different than those present when it is free in solution[25]. Based on this principle, the main requirement is that the stability constant of the "receptor-dye" complex should be lower than the stability constant of the "receptor-target molecule" complex.

- **Chemodosimeter approach**: In this approach, the target molecule induces specific chemical reactions (generally irreversible) and commonly involves the rupture and/or formation of covalent bonds. In general, there is a remarkable chemical modification of the molecular probe after the reaction with the target molecule and therefore this approach is usually associated with remarkable spectroscopic modulations.[26]

---

[24] a) T. S. Snowden, E. V. Anslyn, *Chem. Biology*, **1999**, 3, 740. b) T. Gunnlaugsson, M. Glynn, G. M. Tocci, P. E. Kruger, F. M. Pfeffer, *Coord. Chem. Rev.*, **2006**, 250, 3094.
[25] a) S. L. Wiskur, H. Ait-Haddou, J. J. Lavigne, E. V. Anslyn, *Acc. Chem. Res.*, **2011**, 34, 963. b) B. T. Nguyen, E. V. Anslyn, *Coord. Chem. Rev.*, **2006**, 250, 3118.
[26] M-y. Chae, A. W. Czarnik, *J. Am. Chem. Soc.*, **1992**, 114, 9704. b) S. Sole, F. P. Gabbaï, *Chem. Commun.*, **2004**, 1284.
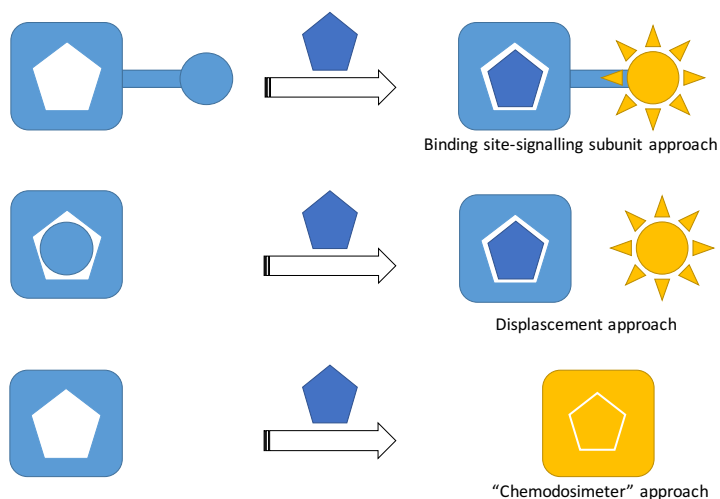
Fig. 5. Schematic representation of the three main paradigms used in the development of chemosensors.

Practically, all reported examples of chromo-fluorogenic chemosensors described in the literature are constructed by the application of one of these approaches. Chromo-fluorogenic sensor offers significant advantages over other analytical detection methods such as: no need of sample pre-treatment, non-destructive detection methods, uses of simple and extended instrumentation, need of small amounts of samples and, in some cases, *in situ* detection and in real-time measurements[27].

Colorimetric sensor induced noticeable colour changes, observable with the naked eye, and they can be used for rapid qualitative determinations. On the other hand, fluorogenic sensors have a high degree of sensibility and specificity due to the possibility of specifying excitation and emission wavelengths, and normally allow achieving lower limits of detection when compared with colorimetric techniques.

2.2 Optical sensors

Optical sensors represent a group of chemical sensors in which electromagnetic radiation is used as signal after analytical recognition. Optical sensor can be based on various optical principles (absorbance,

---

[27] J. Wu, B. Kwon, W. Liu, E. V. Anslyn, P. Wang, J. S. Kim, *Chem. Rev.,* **2015**, 115, 7893

reflectance, luminescence, fluorescence), covering different regions of the spectrum (UV, visible, IR, NIR) allowing measurement not only of the intensity of light but also other related properties as lifetime, refractive index, diffraction, etc.

However, for sensor applications, the most commonly applied methods in optical sensing are those based on light absorption or light emission.

2.2.1 Optical detection principles

Colour is a visual perception generated in the brain to interpret nerve signals perceived by the photoreceptors of the ocular retina, which in turn is able to interpret and disguise the different wavelength of the electromagnetic spectrum (Fig. 6). Every illuminated surface absorbs some of the electromagnetic waves and reflects the others. The reflected waves are captured by the retina and interpreted by the brains as colours. The colour depends on the spectrum of the incident light and the absorption of the object, that determines which waves are reflected.
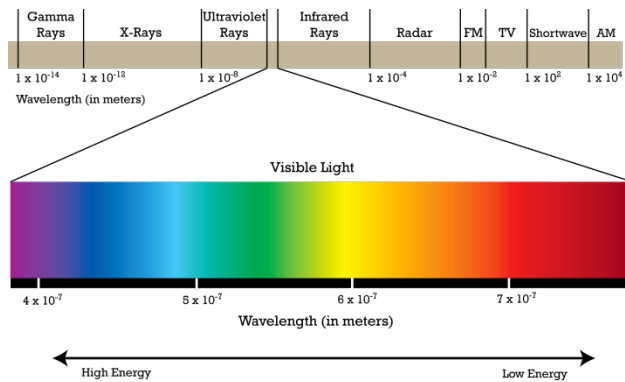

Fig. 6. Electromagnetic spectra.

The observed colours are determined by the spectral distribution of the transmitted radiation[28]. Electromagnetic radiation such as visible light is commonly treated as a wave phenomenon, characterized by a wavelength or frequency. Visible wavelengths cover a range from approximately 400 to 800 nm

---

[28] R. C. Denney, R. Sinclair, *Visible and Ultraviolet Spectroscopy*, John Wiley & Sons. Ed., **1987.**

The absorption of visible or ultraviolet radiation may result in the electron transitions between the ground state and the excited states of the atoms and/or molecules[29].

The electron in molecules can be of one of three types namely:
- σ electrons (single bond) are in the lowest energy level and they are the most stable electrons. These electrons would require a lot of energy to be displaces to higher energy levels.
- π electrons (multiple bond) are placed in much higher energy levels for the ground state. These electrons are therefore relatively unstable.
- n electrons (non-bonding; cause by lone pairs) are in higher energy levels and can be excited by ultraviolet and visible light.

These electrons when interact with energy in the form of light radiation get excited from the highest occupied molecular orbital (HOMO) to the lowest unoccupied molecular orbital (LUMO) and the resulting species is known as the excited state or anti-bonding sate. Most of the absorption in ultraviolet-visible spectroscopy occurs due to π-π^* electron transition or n-π^* electron transitions (Fig. 7).
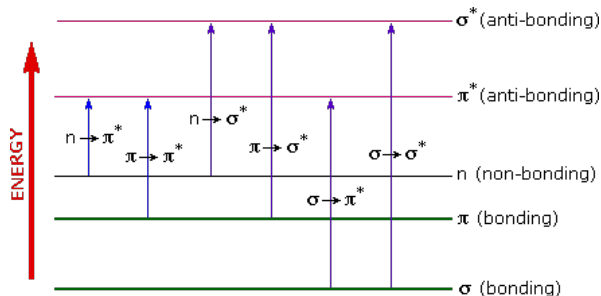

Fig. 7. Electron transitions in ultraviolet/visible spectroscopy

2.2.2   Chromogenic sensors

Colour changes as signalling events have been widely used because it requires the use of inexpensive equipment or no equipment at all as colour changes can be detected by naked eye. Organic compounds become coloured by absorbing electromagnetic radiation in the visible range and investigations related with the correlation between chemical

---

[29] T. Engel, P. Reid, *Physical Chemistry*, Pearson new International edition, **2012**.

structure and colour in organic dyes have been carried out extensively. Many dyes contain systems of conjugated bonds, and the gap between the HOMO and the LUMO is critical in determining the colour of a certain organic dye. It is well-established that the larger the conjugated system is, the shorter the difference between fundamental and excited states, resulting in a more bathochromic shift of the absorption band of lesser energy[30].

Along with incremental conjugation, the absorption wavelength can be modified by anchoring electron donor (NR_2, NHR, NH_2, OH, OMe, etc.) or electron acceptor (NO_2, SO_3H, SO_3^-, COOH, CN, etc.) groups to the conjugated system. When both an electron donor and an electron acceptor group are connected through a conjugated system in a certain molecule, a Charge Transfer (CT) band can be observed (Fig. 8). That is important in relation to the design of chromogenic sensors, the interaction of the analyte with the donor or acceptor groups in those systems affect the position of the charge transfer band resulting in a colour modulation.
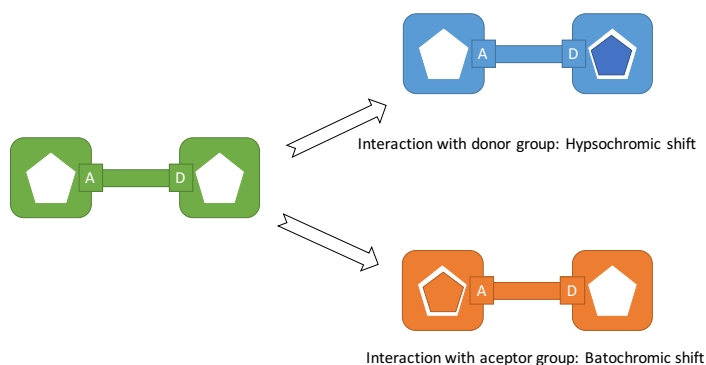

Fig. 8. CT in chromogenic electron donor-acceptor sensors

2.2.3   Fluorescent sensors

Fluorescence imaging and fluorescence indicators are nowadays indispensable tools in various fields in modern science and medicine, including clinical diagnostics, biotechnology, molecular biology and biochemistry, materials science and analytical and environmental

---

[30] H. Zollinguer, *Colour chemistry*, VCH, Weincheim, **1991**.

chemistry. [31] This is due to the fine instrument manipulability, commercial viability, lower detection limits and *in situ* and *in vivo* detection ability[32].

There are different photoluminiscent mechanisms involved in the detection of analytes. The most widely used are:

- Photoinduced Electron Transfer (PET): fluorescence in a molecule is observed when an excited electron, for instance in the LUMO, goes to the HOMO, releasing the excess of energy as light. The PET process appears when there is a lone electron pair located in an orbital of the fluorophore itself or an adjacent molecule and, the energy of this orbital lies between those of the HOMO and LUMO. In this case, an efficient electron transfer of one electron of the pair to the hole created in the HOMO by the light absorption may occur, this process is followed by the transfer of the initially excited electron to the lone pair orbital providing a mechanism for non-radiative deactivation of the excited state. The complete process leads to a "quenching" of the fluorescence[33].

- Photoinduces Charge Transfer (PCT): Electronic excitation involves some degree of charge transfer. In fluorophores containing electron donors and acceptor substituents, this charge transfer may occur over long distances and be associated with major dipole moment changes. This make the process particularly sensitive to the microenvironment of the flurophore[34]

- Excimer formation: An excimer can be defined as a complex formed by interaction of a fluorophore in the excited state with another fluorophore of the same structure in its ground state[35].

[31] a) E. V. Anslym, Curr. Opin. *Chem. Biol*., **1999**, 3, 740. b) M. E. Jun, B. Roy, K. H. Ahn, *Chem. Commun*., **2011**,47, 7583. c) N. Boens, V. Leen, W. Dehaen, *Chem. Soc. Rev.,* **2012,** 41, 1130.
[32] H. Kobayashi, M. Ogawa, R. Alfrod, P. L. Choyke, Y. Urano, *Chem. Rev.* **2010**, 110, 2620.
[33] a) H. F. Ji, G. M. Brown, R. Dabestani, *Chem. Commun*. **1999**, 7, 609. b) J. S. Kim, D. T. Quang, *Chem. Rev.* **2007**, 107, 3780.
[34] a) M. Narita, Y. Higuchi, F. Hamada, H. Kimagai, *Tetrahedron Lett*., **1998**, 39, 8687. b) R. Metivier, I. Leray, B. Valeu, *Chem. Commun*., **2003**, 8, 996.
[35] a) R. Martinez-Mañez, F. Sancencon, *Chem. Rem*. **2003**, 103, 4419. b) A. M. Costero, M. Colera, P. Gaviña, S. Gil, *Chem. Commun*., **2006**, 761.

Compared with the monomer the excimer typically provides redshifted and broad emission bands. In several cases both emission (monomer and excimer) are observed simultaneously[36].

- Fluorescence Resonance Energy Transfer (FRET): Förster Resonance Energy Transfer; is a non-radiative process between a pair of dissimilar fluorophores in which one act as a donor of energy from the excited-state to the acceptor. The donor returns to the electronic ground state, and the observed emission is from the acceptor fluorophore. FRET is influenced by two factors: the distance between the donor emission and the acceptor absorption spectrum, the relative orientation of the donor emission dipole moment and acceptor absorption moment. [37]

Summarizing, an optical sensor consists in a compound incorporating a binding site and a mechanism for communication[38]. In presence of the target molecule, the receptor modifies their electronic properties displaying changes in either colour and/or fluorescence.

In view of the benefits showed by these systems, we decided to design new chromo-fluorogenic chemosensors for the detection of NOx. Among the numerous classes of colorimetric and fluorescent dyes[39], probes based on 4,4-difluoro-4-bora-3a,4a-diaza-sindacene[40] (hereafter known as BODIPY; difluoroboron dipyrromethene) are perhaps the most promising and they have been the base of most of the sensors designed and evaluated in this thesis.

---

[36] M. A. McKewey, E. M. Seward, G. Ferguson, B. Ruhl, S. J. Harrisc, *Chem. Commun.*, **1985**, 388.

[37] a) Z. Zhou, M. Yu, H. Yang, F. Li, T. Yi, C. Huang, *Chem. Commun*,. **2008**, 29, 3387. b) K. Sreenath, J. R. Allen, W. M. Davidson, L. Zhu*, Chem. Commun.*, **2011**, 47, 11730.

[38] A. W. Czarnik, *Acc. Chem. Res.*, **1994**, 27, 302.

[39] R. P. Haugland, The handbook guide to Fluorescent Probes and Labeling Technologies, Molecular Probes, Invitrogen, Carslbad, Ca, 10th ed. **2005**.

[40] A. Loudet, K. Burgess, *Chem. Rev.*, **2007**, 207, 4891.

3. BODIPY dyes

Even though the first BODIPY was reported by Treibs and Kreuzer in 1968[41], it was not until the mid-1990s that the possible uses of BODIPY derivatives for biological labelling, electroluminescent devices, as tuneable laser dyes, potential candidate for solid-state concentrators, fluorescent switches and fluorophores in sensors and labels were fully recognized [42]. Since then, the number of research publications and patents has increased very significantly. This growing success can be explained because of their outstanding photo physical properties such as excitation/emission wavelengths in the visible spectra (about 500 nm), the relatively high molar absorption coefficients and quantum yields, fluorescent lifetimes in the nanosecond range and negligible triplet-sate formation. BODIPYs are relatively insensitive to the pH and they present good solubility, resistance towards self-aggregation in solution and robustness against light and chemicals[43]. Moreover, the spectroscopic and photo physical profiles can be switches by introducing different electron releasing/withdrawing groups at the appropriate positions of the BODIPY-core.

3.1 BODIPY core.

Numbering system for BODIPY dyes is different to that used by IUPAC for dipyrromethenes[44], however, the terms α-, β-positions, and meso- are used in the same way for both systems. The numbering of any substituents follows rules set up for the carbon polycycle *s*-indacenes (Fig. 9). All the positions of the BODIPY core are possible sites for functionalization.
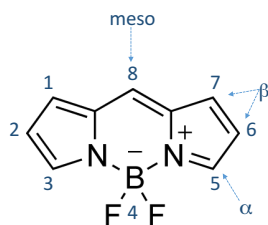

Fig. 9. The BODIPY core numbering

[41] A. Treibs, F. H. Kreuzer, Liebigs. *Ann. Chem*., **1968**, 718, 208.

[42] N. Boens, V. Leen, W. Dehaen, *Chem. Soc. Rev*., **2012**, 41, 1130.

[43] a) R. Ziessel, G. Ulrich, A. Harriman, *New. J. Chem*., **2007**, 31, 496. b) G. Ulrich, R. Ziessel, A. Harriman, *Angew. Chem. Int. Ed*., **2008**, 47, 1184.

[44] H. B. F. Dixon, A. Cornish-Bowden, C. Liebecq, K. L. Loening, G. P. Moss, J. Reedijk, S. F. Velick, P. Venetianer, J. F. G. Vliegenthart, *Pure Appl. Chem*., **1987**, 59, 779.

The BODIPY core is relatively easy to prepare from commercially available pyrrole-based materials, often in high yield and multi-gram quantity. Different approaches have been described for the synthesis of BODIPY dyes:

- Synthesis from pyrroles and aldehydes (Scheme 3): The acid-catalyzed condensation of aldehydes with pyrrole affords dipyrromethanes (III), which are used immediately after preparation (they are sensitive to light, air and acid). Oxidation of dipyrromethane yields a dipyrromethene (or dipyrrin) (IV). This oxidation can be carried out with 2,3-dichloro-5,6-dicyano-*p*-benzoquinone (DDQ) or 2,3,5,6-tetrachloro-*p*-benzoquinone (*p*-chloranil). The boron difluoride bridging unit is introduced by treatment with boron trifluoride diethyl etherate (BF$_3$·Et$_2$O) in the presence of base[45].
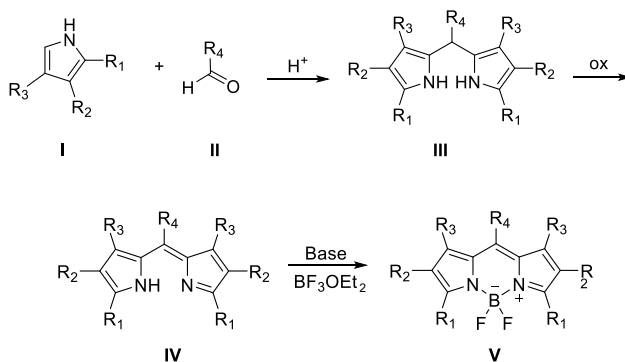
Scheme 3. Outline of a typical synthesis by condensation of a pyrrole with an aldehyde.

- Synthesis from pyrroles and acid chlorides or anhydrides: Other route is condensation of pyrroles with an acylium equivalent. The intermediate acylpyrrole reacts under acidic conditions with an excess of pyrrole to form a dipyrrinium salt. Again, the use of an excess of base and BF$_3$·Et$_2$O yields the BODIPY core[46]. The particular advantage of this approach lies in the possibility of

---

[45] a) R. W. Wagner, J. S. Lindsey, *Pure Appl. Chem*., **1996**, 68, 1373. b) S. Y. Moon, N. R. Cha, Y. H. Kim, S. K. Chang, *J. Org. Chem*., **2004**, 69, 181. c) M. Baruah, W. Qin, N. Basaric, M. De Borggraeve, M. Wim, N. Boens, *J. Org. Chem*., **2005**, 70, 4152.
[46] M. Shah, K. Thangaraj, M. L. Soong, L. T. Wolford, J. H. Boyer, I. R. Politzer, T. G. Pavlopoulos, *Heteroat. Chem*., **1990**, 1, 389.

preparing asymmetric BODIPY dyes, because the isolated acylpyrrole can be combined with a different pyrrole moiety in an acidic condensation.

- Synthesis from an acylated pyrrole: This route is an alternative described by Wu and Burgess[47]. It is the condensation of an acylated pyrrole. A second pyrrole equivalent is no always required, and phosphorus oxychloride is able to promote the selfcondensation of pyrrole-2-carbaldehyde. The phosphorus oxychloride substitutes the aldehyde oxygen, resulting in a chlorinated azafulvene, which is attacked by a second pyrrole aldehyde. The subsequent chloride nucleophilic attack , followed by the decomposition of the unstable intermediate, yields dipyrrinium. The dipyrromethene can undergo complexation with excess of base and $BF_3 \cdot Et_2O$ to yield the symmetric BODIPY. The products, arising from a one-pot procedure and requiring minor purification, are generally obtained in high yields.

3.2 Derivatization of the BODIPY core.

The synthetic adaptability of the BODIPY scaffold is an important advantage in the design of chemosensors. Progresses in BODIPY chemistry make possible to build dyes by post-functionalization of the BODIPY core (Fig. 11) instead of starting from appropriately substituted pyrroles. By connecting suitable electro releasing/withdrawing groups to the BODIPY core, the spectroscopic and photophysical profiles can be tuned.
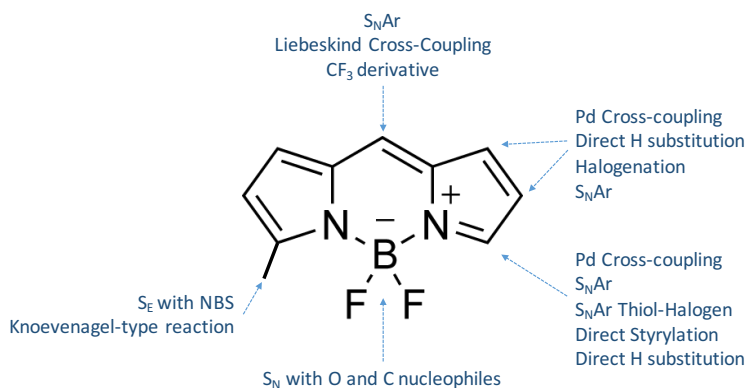

Fig. 10. Derivatization of BODIPY-core

---

[47] L. Wu, K. Burgess, *Chem. Commun.*, **2008**, 4933.

The 3,5-positions can undergo nucleophilic aromatic substitution (S_NAr), direct hydrogen substitutions, direct styrylation, and Pd-catalyzed cross-coupling or electrophilic substitution with NBS and Knovenagel-type reaction on methyl groups[48]. It is possible to carry out electrophilic aromatic substitution (S_EAr), direct hydrogen substitutions and Pd-catalyzed cross-coupling in the 2,6-positions[49]. The 1,7-positions can be halogenated and further substituted by S_NAr or Pd-Catalyzed cross coupling reactions[50]. S_NAr, Liebeskind cross-coupling and installation of a meso-CF_3 group at the 8-position are possible[51]. In addition, nucleophilic substitutions (S_N) of fluorine by oxygen or carbon nucleophiles on the boron centre have been reported[52].

In addition to the numerous synthetic advantages offered by BODIPY dyes, they are tolerant to a wide range of photochemical, thermal, pH, polarity and solubility conditions. Their stability in physiological environments makes them a prime choice for image techniques and protein labelling[53]. On the other hand, the use of the BODIPY core as signalling subunit in chemosensors is widely extended. In the present thesis different derivatization of BODIPY have been used to prepare chemosensors for the studied analytes. The benefits of the BODIPY core is particularly appealing because:

[48] a) B. Verbelen, V. Leen, L. Wang, N. Boens, W. Dehaen, *Chem. Commun.*, **2012**, 48, 9129. b) L. Y. Niu, Y. S. Guan, Y. Z. Chen, L. Z. Wu, C. H. Tung, Q. Z. Yang, *J. Am. Chem. Soc.*, **2012**, 134, 18928. c) G. Ulrich, R. Ziessel, A. Haefele, *J. Org. Chem.*, **2012**, 77, 4298. d) L. Wang, B. Verbelen, C. Tonnele, D. Beljonne, R. Lazzaroni, V. Leen, W. Dehaen, N. Boens, *Photochem. Photobio. Sci.*, **2013**, 12, 835.
[49] a) H. He, D. K. P. Ng, *Org. Biomol. Chem.*, **2011**, 9, 2610. b) W. Wu, H. Guo, W. Wu, S. Ji, J. Zhao, *J. Org. Chem.*, **2011**, 76, 7056. c) W. J. Shi, P. C. Lo, A. Singh, I. Ledow-Rak, D. K. P. Ng, *Tetrahedron*, **2012**, 68. 8712. d) A. Bessette, G. S. Hanan, *Chem. Soc. re.*, **2014**, 43, 3342.
[50] V. Leen, D. Miscoria, S. Yin, A. Filarowski, J. Molisho-Ngongo, M. Van der Auweraer, N. Boens, W. Dehaen, *J. Org. Chem.*, **2011**, 76, 8168.
[51] a) T. V. Goud, A.Tutar, J. F. Biellemann, *Tetrahedron*, **2006**, 62, 5084. b) E. Peña-Cabrera, A. Aguilar-Aguilar, M. Gonzalez-Dominguez, E. Lager, R. Zamudio-Vazquez, J. Godoy-Vargas, F. Villanueva-Garcia, *Org. Lett.*, **2007**, 9, 3985. c) L. N. Sobenina, A. M. Vasiltsov, O. V. Petrova, K. B. Petrushenko, I. A. Ushakov, G. Clavier, R. Meallet-Renault, A. I. Mikhaleva, B. A. Trofimov, *Org. Lett.*, **2011**, 13, 2524.
[52] a) C. Goze, G. Ulrich, L. J. Mallon, B. D. Allen, A. Harriman, R. Ziessel, *J. Am. Chem. Soc.*, **2006**, 128, 10231. b) C. Tahtaoui, C. Thomas, F. Rohmer, P. Klotz, G. Duportail, Y. Mely, D. Bonnet, M. Hibert. *J. Org. Chem.*, **2007**, 72, 269. c) P. Didier, G. Ulrich, Y. Mely, R. Ziessel, *Org. Biomol. Chem.*, **200**9, 7, 3630.

- They require easily, low-cost and widely used instrumentation
- They offer the possibility of detecting the target molecule by the naked eye
- They are non-destructive methods.
- They require small amounts of sample
- They perform a rapid detection of the guest
- They allow real time monitoring.

4. Molecular gates as sensors

The control of mass transport through gated channels that is present in the nature has inspired to many researchers. Thus, the preparation of hybrid materials that mimics these channels developing nanoscopic gated systems has been an attractive research area. These systems respond to a stimulus, and they are commonly reported as "molecular gates"[54].

Molecular gates can be defined as architectural nanoscopic supramolecular structures that incorporate various chemicals entities that allow a controlled release. Figure 11 shows a representation of a molecular gate and its working mechanism. The scheme shows an inorganic scaffolding loaded with an entrapped guest and with a suitable molecule anchored in the pore outlets, what is called molecular gatekeeper. The application of an external stimulus allows the release of the confined guest due to changes in the molecule that acts as gate.
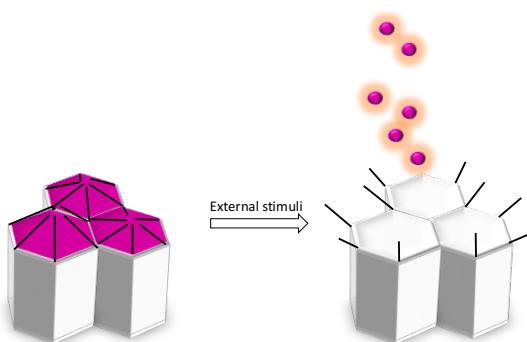
External stimuli

Fig. 11. Representation of a molecular gate working principle

[54] A.B. Descalzo, R. Martínez-Máñez, F. Sancenón, K. Hoffman, K. Rurack, *Angew. Chem.Int. Ed*, **2006**, 45, 5924.

The first example of a molecular gate was reported by Fujiwara and co-workers in 2003.[55] Since then, a number of nanoscopic gated systems using mesoporous hybrid scaffoldings have been described. Inorganic nanoparticles,[56] polymers[57], and larger supramolecular assemblies[58] have been used as blocking caps that control the opening/closing mechanism of the pore in mesoporous scaffolds. Moreover, different triggers, such as pH[59], light[60] redox potential,[61] temperature[62] or target (bio)molecules[63]

[55]a) N. K. Mal, M. Fujiwara, Y. Tanaka, *Nature*, **2003**, 421, 350. b) N. K. Mal, M. Fujiwara, Y. Tanaka, T. Taguchi, M. Matsukata, *Chem. Mater.,* **2003**, 15, 3385

[56] a)E. Aznar, M . D. Marcos, R. Martinez-Manez, F. Sancenon, J. Soto, P. Amoros, P. Guillem, *J. Am. Chem. Soc*., **2009**, 131, 6833. b) J. L. Vivero- Escoto, I. I. Slowing, C. Wu, V. S.-Y. Lin, *J. Am. Chem. Soc*. **2009**, 131, 3462.

[57] a) R. Liu, X. Zhao, T. Wu., P. Y. Feng, J. Am. Chem. Soc. 2008, 130, 14418. b) C. L. Zhu, X. Y. Song, W. H. Zhou, H. H. Yang, X. R. Wang, *J. Mater. Chem*., **2009**, 19, 7765.

[58] a) T. D. Nguyen, Y. Liu, S. Saha, K. C. F. Leung, J. F. Stoddart, J. I. Zink, J. *Am. Chem. Soc*. **2007**, 129, 626. b) R. Liu, Y. Zhang, P. Y. Feng, *J. Am. Chem. Soc*. **2009**, 131, 15128.

[59] a) V. Cauda, C. Argyo, A. Schlossbauer, T. J. Bein, *J. Mater. Chem*., **2010**, 20, 4305. b) S. Angelos, Y. W. Yang, K. Patel, J. F. Stoddart, J. I. Zink, *Angew. Chem. Int. Ed*., **2008**, 47, 2222. c) H. Meng, M. Xue, T. Xia, Y. L. Zhao, F. Tamanoi, J. F. Stoddart, J. I. Zink, E. A. Nel, *J. Am. Chem. Soc*., **2010**, 132, 12690. d) J. Liu, X. Du, *J. Mat. Chem*., **2010**, 20, 3642. e) W. Guo, J. Wang, S. J. Lee, F. Dong, S. S. Park, C. S. Ha, *Chem. Eur. J*., **2010**, 16, 8641. f) A. Popat, J. Liu, G. Q. Lu, S. Z. Qiao, *J. Mater. Chem*., **2012**, 22, 11173, Y.Y. Yan, J.H. g) Y.L. Sun, Y.W. Yang, D.X. Chen, G. Wang, Y. Zhou, C.Y. Wang, J. F. Stoddart, *Small*, **2013**, 9, 3224.

[60] a) E. Johansson, E. Choi, S. Angelos, M. Liong, J. I. Zink, *Sol. Gel Sci. Technol*., **2008**, 46, 313. b) J. Lai, X. Mu, Y. Xu, X. Wu, C. Wu, C. Li, J. Chen, Y. Zhao, *Chem. Commun*., **2010**, 46, 7370. c) Y.-L. Sun, B.-J. Yang, S.X.-A. Zhang, S. X.-A., Y.-W., Yang, *Chem.-Eur. J*., **2012**, 18, 9212.

[61] R. Mortera, J. Vivero-Escoto, I. I. Slowing, E. Garrone, B. Onida, V. S.Y. Lin, *Chem. Commun.*, **2009**, 3219.

[62] a) C. Liu, J. Guo, W. Yang, J. Hu, C. Wang, S. Fu, *J. Mat. Chem*., **2009**, 19, 4764. b) J. Lai, X. Mu, Y. Xu, X. Wu, C. Wu, C. Li, J. Chen, Y. Zhao, *Chem. Commun*., **2010**, 46, 7370. c) C. R. Thomas, D. P. Ferris, J. H. Lee, E. Choi, M. H. Cho, E. S. Kim, J. F. Stoddart, J. S. Shin, J. Cheon, J. I. Zink, *J. Am. Chem. Soc*., **2010**, 132, 10623.

[63] a) C. Coll, R. Casasús, E. Aznar, M. D. Marcos, R. Martínez-Máñez, F. Sancenón, J. Soto, P. Amorós, *Chem. Commun*., **2007**, 1957. b) E. Aznar, C. Coll, M. D. Marcos, R. Martínez-Máñez, F. Sancenón, J. Soto, P. Amorós, J. Cano, E. Ruiz, *Chem. Eur. J.,* **2009**, 15, 6877. c) Y. Zhao, B. G. Trewyn, I. I. Slowing, V. S.-Y. Lin, *J. Am. Chem. Soc*., **2009**, 131, 8398. d) Y. L. Choi, J. Jaworsky, M. L. Seo, S. J. Lee, J. H. Jung, *J. Mater. Chem*., **2011**, 21, 7882. e) A. Schulz, R. Woolley, T. Tabarin, C. McDonagh, *Analyst*, **2011**, 136, 1722. f) J. Lee, J. Lee, S. Kim, C. –J. Kim, S. Lee, B. Min, Y. Shin, C. Kim, *Bull. Korean Chem. Soc.,* **2011**, 32, 1357. g) I. Candel, A. Bernardos, E. Climent, M. D. Marcos, R. Martínez-Máñez, F. Sancenón, J. Soto, A. Costero, S. Gil, M. Parra, *Chem. Commun*. **2011**, 47, 8313. h) R. Villalonga, P. Díez, A. Sánchez, E. Aznar, R. Martínez-Máñz, J. M. Pingarrón, *Chem. Eur. J.,* **2013**, 19, 7889. i) M. Oroval, E. Climent, C. Coll, R. Eritja, A. Aviñó, M.D. Marcos, F. Sancenón, R. Martínez-Máñez, P. Amorós, *Chem. Commun*., **2013**, 49, 5480.

have been employed as the stimuli that cause the uncapping of the pores and the subsequent delivery of the guest molecules.

4.1 Mesoporous materials

According to the international Union of Pure and Applied Chemistry (IUPAC), pore sizes are classified into three main categories, namely micropores, meso-pores and macro-pores characterized by pore sizes less than 2 nm, between 2 and 50 nm, and larger than 50 nm respectively.[64] Among them, thanks to their large internal surface area, microporous and mesoporous materials are attracting considerable attention for applications in catalysis,[65] filtration and separation,[66] gas adsorption and storage,[67] enzyme immobilization,[68] biomedical tissue regeneration,[69] drug delivery,[70] and chemical/biochemical sensing.[71] Emblematic microporous materials are crystalline framework solids, such as zeolites,[72] or particular metallophosphates[73] and cacoxenite, which present the largest pore dimensions, respectively, comprised between 10 and 12 Å for zeolites and 14 Å for cacoxenite.[74]

In 1992, patents and journal publications from Mobil company disclosed the synthesis and characterization of a new class of porous materials, a family of uniform pore, silicate based, mesoporous molecular sieves, named the M41S family.[75] These materials present an orderly

---

[64] a) G. Zhao, *J. Mater. Chem*., **2006**, 12, 623. b) D. Schaefer, *MRS Bulletin*, **1994**, 14, 6.

[65] D.E. De Vos, M. Dams, B.F. Sels, P.A. Jacobs, *Chem. Rev*., **2002**, 102, 3615.

[66] X. Liu, Y. Du, Z. Guo, S. Gunasekaran, C. -B. Ching, Y. Chen, S .S .J. Leong, Y. Yang, *Microporous Mesoporous Mater*., **2009**, 122, 114.

[67] a) M. Kruk, M. Jaroniec, Chem. Mater., 2001, 13, 3169. b) A. Corma, M. Moliner, M. J. Diaz- Cabanas, P. Serna, B. Femenia, J. Primo, H. Garcia, *New J. Chem*., **2008**, 32, 1338. c) C. Ispas, I. Sokolov, S. Andreescu, *Anal. Bioanal. Chem*., **2009**, 393, 543.

[68] M. Vallet-Regi, M. Colilla, I. J. Izquierdo-Barba, Biomed. Nanotechnol., 2008, 4, 1.

[69] I. Slowing, B. G. Trewyn, S. Giri, V. S. –Y. Lin, *Adv. Funct. Mater*., **2007**, 17, 1225.

[70] a) M. Vallet-Regi, F. Balas, D. Arcos, *Angew. Chem., Int. Ed*., **2007**, 46, 7548. b) K. A. Kilian, T. Bocking, K. Gaus, J. King-Lacroix, M. Gal, J. J. Gooding, *Chem. Commun*., **2007**, 1936.

[71] a) K. A. Kilian, T. Boecking, K. Gaus, M. Gal, J. J. Gooding, *ACS Nano*, **2007**, 1, 355. b) A.Jane, R. Dronov, A. Hodges, N. H. Voelcker, *Trends Biotechnol*. **2009**,27, 230.

[72] M. E. Davis, C. Saldarriaga, C. Montes, J. Garces, C. Crowder, *Nature*, **1988**, 331, 698.

[73] M. Estermann, L. B. McCusker, C. Baerlocher, A. Merrouche, H. Kessler, *Nature*, **1991**, 352, 320.

[74] P. B. Moore, J. Shen, *Nature*, **1983**, 306, 356.

[75] a) C. T. Kresge, M. E. Leonowicz, W. J. Roth, J. C. Vartuli and J. S. Beck, *Nature*, **1992**, 359, 710. b) J. S. Beck, J. C. Vartuli, W. J. Roth, M. E. Leonowicz, K. D. Schmidt, C. T. W.

arrangement of pores, with a very homogeneous pore size, whose average value falls within the range 2- 10 nm.[76] Moreover, they have a high pore volume, from the order of 1 cm^3/g and a specific surface area between 500 m^2/g and 1000 m^2/g.

M41S materials are featured by high chemical inertness and thermal stability. Last but not least, the material synthetic procedure is well described and requires inexpensive and non-hazardous precursors. All these properties makes these materials ideal supports for adsorption processes of relatively small molecules and enables them to be suitable platforms for the preparation of hybrid systems for controlled release studies upon exposition to an external stimulus. Originally, the M41S family grouped under that name three different discrete structures, easily identifiable by X-ray diffraction MCM-41 (hexagonal phase), MCM-48 (cubic), and MCM-50 (lamellar)

4.1.1 Synthesis and functionalization of mesoporous material

Mesoporous materials research was initially motivated by the desire for ordered silica/alumina supports with pores of larger dimensions than the ones found in microporous zeolites. As it has been cited above, the first successful studies on surfactant–organised mesoporous materials were carried out on silica, and it still remains as the most studied system. Basically two main components are needed to build-up a system that presents a high ordered porous structure with homogeneous pore dimensions, a template and a polymeric precursor.

One important feature of the structure of mesoporous materials is their high concentration of structural defects in the form of silanol (Si-OH) groups. The group OH of the silanol can be replaced by a chemical species capable of joining a suitably functionalised chain by a covalent bond to the oxygen atom. In this way, a family of "hybrid materials" can be generated, in which the chemical composition of the functionalised chain is different from the inorganic framework. The most common

---

Chu, D. H. Olson, E. W. Sheppard, S. B. McCullen, J. B. Higgins and J. L. Schlenker, J. *Am. Chem. Soc.*, **1992**, 114, 10834.

[76] Liberación de fármacos en matrices biocerámicas: avances y perspectivas. Monografía XIX. Editors: María Vallet Regí – Antonio Luís Doadrio Villarejo. Real Academia Nacional de Farmacia.

cases, the functionalised chain is an organic group or silane with convenient substitutions.[77] This modification of the inorganic matrix by the incorporation of organic components, either on the silica surface, as part of the silicate walls, or trapped within the channels, permits a precise control over the surface properties and pore sizes of the mesoporous sieves for specific applications and usually stabilize the materials towards hydrolysis.[78] A big number of additional properties, achieved through the development of hybrid inorganic-organic mesoporous solids, has provided a significant progress in the last few years towards their applications in different fields.

The functionalization process involves a treatment of the starting material with a solution of an alkoxide or alkoxysilane containing the functional group in an inert solvent. Then, the organic groups can be attached or anchored to the mesoporous material framework. This process can be carried out following two different procedures: co-condesation or grafting procedure.

The co-condensation method usually leads to a homogeneous distribution of organic units along the material particles and between the surface and the inner surface corresponding to the channels and cavities. The co- condensation procedure allows the incorporation of a relatively large amount of functional groups, which generally falls between 2 and 4 meq/g, in the most favourable cases.
Some disadvantages that should be taken in account when this method is used are:
- The degree of mesoscopic order of the products decreases when the trialkoxyorganosilane concentration is increased in the reaction mixture.
- Homocondensation reactions between silane groups are increased. As a consequence, the ratio of terminal organic groups that are incorporated into the pore-wall network is, generally, lower than would correspond to the starting concentration in the reaction mixture. Also the homogeneous distribution of different organic functionalities in the framework cannot be guaranteed.

---

[77] "Liberación de fármacos en matrices biocerámicas: avances y perspectivas". Monografía XIX. Editors: María Vallet Regí – Antonio Luís Doadrio Villarejo. Real Academia Nacional de Farmacia.
[78] K. Moller, T. Bein, *Chem. Mater.*, **1998**, *10*, 2950. b) G. A. Ozin, E. Chomski, D. Khushalani, M. J. MacLachlan, *Curr. Opin. Colloid Interface Sci.*, **1998**, 3, 181.

- The incorporated organic groups can lead to a reduction in the pore diameter, pore volume, and specific surface areas.
- Only the extraction method is available to carry out the removal of the surfactant, avoiding the calcination that would destroy the structure of the material due to the presence of organic groups in the skeleton.

Grafting procedure is a post-synthesis functionalization method that allows a selective modification of the surface of the material. Trialkoxysilane derivatives are reacted in the presence of the inorganic scaffold to give the condensation reaction. The presence of the silanol groups on the silica scaffold surface guarantees the formation of a covalent bond between the trialkoxysilane precursors and the solid surface.

The selection of the grafting procedure, instead of the co-condensation method, is due to certain advantages such as:

- Grafting grants the possibility of characterize the organic trialkoxysilane derivative before functionalization.
- Functionalization by grafting allows a more rapid and efficient surfactant extraction by the calcination method.
- This method allows to firstly load the mesopore with certain molecules of interest and, then functionalizing with another category of organic compound, which is preferentially attached to the outer surface. Using this procedure, suitable hybrid materials for controlled delivery processes (see following section) are obtained.

Among important applications of this class of substrates, the most remarkable and recently studied are their use in heterogeneous-catalysis,[79] controlled delivery of chemical species,[80] chemical sensors[81] and environmental applications.[82]

---

[79] S.-E. Park, and E.-Y. Jeong, 2014, *Heterogeneous Catalysis with Organic–Inorganic Hybrid Materials in Bridging Heterogeneous And Homogeneous Catalysis: Concepts, Strategies, And Applications*, Wiley-VCH Verlag GmbH & Co. KGaA, Weinheim, Germany. doi: 10.1002/9783527675906.ch3

[80] a) J. M. Rosenholm, E. Peuhu, L. T. Bate-Eya, J. E. Eriksson, C. Sahlgren, M. Linden, *Small*, **2010**, *6*, 1234. b) M. Liong, J. Lu, M. Kovochich, T. Xia, S. G. Ruehm, A. E. Nel, F. Tamanoi, J. I. Zink, *ACS Nano*, **2008**, *2*, 889. c) K.K. Cotí, M. E. Belowich, M. Liong, M. W. Ambrogio, Y. A. Lau, H. A. Khatib, J. I. Zink, N. M. Khashab, J. F. Stoddart, *Nanoscale*, **2009**, *1*, 16.

In this thesis synthesis and application of organic-inorganic mesoporous materials for chemical sensing are explored.

---

[81] M. K Patra, K. Manzoor, M. Manoth, S. C. Negi, S. R. Vadera, N. Kumar, Defence *Sci J.,* **2008**, *58*, 636.

[82] S.S. Thakur, Chauhan G.S., *Ind. Eng. Chem. Res.,* **2014**, 53, 4838.

**Chapter 2:
Objectives**

This PhD thesis intended into address in the design and synthesis of chemosensors for detection of NOx species. The project for selective and sensitive NO_2 detection involves the use of biphenyl chromophores (chapter 3), BODIPY dyes (chapter 4) and the use of molecular gate as chemosensor (chapter 5). The NO was approached based on a BODIPY-Cu^{II} complex to selectively detection (chapter 6).

The specific objectives were:

- Design and synthesis of biphenyl chemodosimeters for NO_2 (gas) detection: Through the design, synthesis and characterization of the chemosensor containing different substituent groups to modulate the chromo-fluorogenic response in front of the target molecule. Evaluation of the selectively and sensitive of the chemosensor and applicability in real-time monitoring.

- Design and synthesis of BODIPY chemodosimeters for NO_2 (gas) detection using the same approach of the biphenyl compounds and the evaluation of the sensitive, selective, chromo-fluorogenic properties and support in different superficies.

- Design and synthesis of MCM-41 molecular gates as chemosensor for NO_2 (gas), characterization of the supramolecular material and evaluation of the liberation of the cargo in the presence of the target molecule.

- Design and synthesis of a BODIPY-Cu^{II} complex for NO (gas) detection: detection based in a displacement mechanism and evaluation of its selectivity, sensitivity as well as its response in cells.

Part I:
Nitrogen dioxide detection

I.1 Introduction

Sensitive and selective detection of NO_2 is one of the most important area of development in the chemosensors field. Nitrogen dioxide is one of the most prevalent and dangerous gases. There are several sources of this pollutant which are mainly related with un-vented gas stoves. Nitrogen dioxide appears in both indoor and outdoor air. Outdoor NO_2 is produced mainly by road traffic and other fossil fuel combustion processes at high temperatures. NO_2 in indoor air is generated from various sources such as indoor combustion, tobacco smoking and infiltration from outdoors.[83] Long-term exposure to NO_2 is associated with increased susceptibility to lower respiratory tract illness and increased risk of chronic obstructive pulmonary disease mortality.[84] In addition, NO_2 exposure is a potential inducer of neurological diseases.

The European Commission's Scientific Committee on Occupational Exposure Limits (SCOEL) has approved exposure limits of 0.5 ppm (8-hour time-weighted average) and 1 ppm (15-min short-term exposure limit) for NO_2.[85] However, NO_2 levels in certain cities and at certain hours can reach much higher values of near 100 ppm.

Due to the ubiquitous presence of this gas and its health effects, the development of selective and sensitive methods for its detection and quantification is a hot area of research. Traditionally electrochemical sensors are usually used for detection of NO_2 in real labour environments, however interference from coexisting gases have been reported to be a problem in these devices.

In fact, there is an interest in the design of new sensors capable of selectively detect NO_2. In this context chromo-fluorogenic probes are highly appealing for real-time monitoring and because they require of very inexpensive instrumentation. Moreover, in certain circumstances colour modulation can even be observed by the naked eye making chromo-fluorogenic approaches highly attractive for certain applications. However, despite the inherent advantages of optical probes the number

---

[83] Shima, M.; Adachi M. *International journal of epidemiology*, **2000**, *29*, 862-870.

[84] a) M. Shima, M. Adachi, *Int. J. Epidemiol.* **2000**, *29*, 862–870 b) X. Meng, C. Wang, D. Cao, C.M. Wong, H. Kan, *Atmos. Environ.* **2013**, *77*, 149–154.

[85] European Commission. Scientific Committee on Occupational Exposure Limits (SCOEL). Recommendations for Nitrogen Dioxide. SCOEL/ SUM/ 53. June 2014.

of publications related to the design of molecular chemodosimeters (colorimetric or fluorescent probes) for NO$_2$ detection is very scarce.[86]

I.2 Objectives

Following our interest in the development of chromo-fluorogenic probes for toxic gases, we show herein new chemosensors able to detect selectively the presence of NO$_2$ (gas) in air.

Specifically, our aims were:
- Design and synthesis of new chemosensors for selective and sensitive detection of NO$_2$ in gas phase.
- Characterization of these new molecules by the usual techniques (Nuclear Magnetic Resonance, High Resolution Mass Spectrometry…).
- Study de chromo-fluorogenic behaviour of the synthesized chemosensors in the presence of NO$_2$.
- Study of the reactivity of the chemosensor in presence of different species, specifically the most commons interferents to determinate the selectivity of the method.
- Evaluation of the chemosensor obtaining the limit of detection of the method to determinate the sensitivity.
- Development of different approaches for their application in real-time monitoring.

I.3 Chemosensor design

Actual methods for NO$_2$ detection show certain limitations such as lack of specificity, limited selectivity, operational complexity, non-portability, difficulties in real-time monitoring and false positive readings. As an alternative to these instrumental procedures, the development of

---

[86] a) Ohira S, Wanigasekara E, Rudkevich DM, Dasgupta P.K. Talanta, 2009, 77, 14b)Y. Yan, S. Krishnakumar, H. Yu, S. Ramishetti, L-W. Deng, S. Wang, L. Huang, D. Huang, *J. Am. Chem. Soc.* **2013**, *135*, 5312; c) B. Mondal, V. Kumar, *RSC Adv.* **2014**, *4*, 61944; d) Y. Yan, J. Sun, K. Zhang, H. Zhu, H. Yu, M. Sun, D. Huang, S. Wang, *Anal. Chem.* **2015**, *87*, 2087

molecular chemosensors, constructed under the chemodosimeter paradigm, has been development in this thesis.

In the first part of the study, different compounds based on the biphenyl chromophore were synthesized. Among the different reactions of NO_2 we decided to explore the utility of the generation of aromatic aldehydes from trimethylsilyl benzyl ethers[87] and oximes[88] in order to prepare suitable chemodosimeters. The synthesized biphenyl probes possess electron donor groups (such as methoxide or dimethylamine) electronically connected with trimethylsilyl or oxime (weak electron acceptor) moieties. The underlying idea is that, upon NO_2 reaction, the formed aldehyde (an electron acceptor moiety) would change the electronic properties of the probe (Scheme 1).

R: H, OMe, N(Me)$_2$
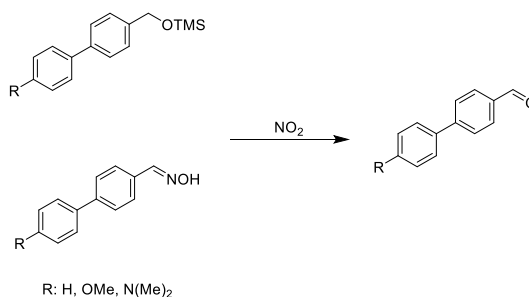
Scheme 1. Outline for the chromo-fluorogenic sensing paradigm with biphenyl chromophore.

The ability of NO_2 to react with oximes to give the corresponding carbonyl group under very soft conditions [89] (Scheme 2) has aroused the interest of developing new chemosensor. In the second part a BODIPY derivative as colorimetric and fluorescent probe for NO_2 detection in air has been prepared. In order to extend the applicability of this kind of systems, new BODIPY derivatives based on the same sensing principle were reported (Scheme 3).

---

[87] S. Ohira, E. Wanigasekara, R. D. Rudkevich, P. K. Dasgupta, *Talanta,* 2009, **79**, 14

[88] M. Javaheri, M. R. Naimi-Jamal, M. G. Dekamin, G. Kaupp, *Phosphorus Sulfur Silicon Relat. Elem.*, 2012, **187**, 142

[89] Mokhari J., Naimi-Jamal M. R., Hamzehal H.. 11th International Electronic Conference on Synthetic Organic Chemistry (ECSOC-11) 1-30 November **2007**.
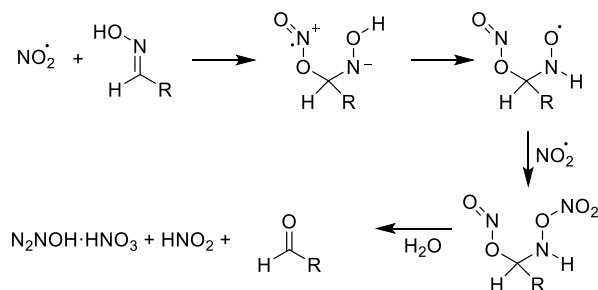
Scheme 2. Mechanism proposed for the oximes deprotection by NO_2.[90]

Moreover, the principle of generation of aromatic aldehyde from phenylhydrazone was also development in BODIPY compounds. The result of the transformation of the hydrazone into the corresponding free aldehyde in the presence of NO_2 results in a significant bathochromic shift of the maximum absorption band in the UV-vis spectrum and in a noticeable fluorogenic response.
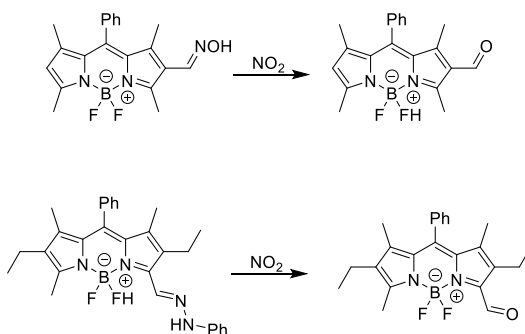
Scheme 3. Representation of sensing paradigm with BODIPY dyes based on the generation of aromatic aldehyde

---

[90] J. Mokhtari, M. R. Naimi-Jamal, H. Hamzeali, M. G. Dekamin, G. Kaupp, Chemsuschem., 2009, **2**, 248

Chapter 3.
Biphenyl derivates for NO₂ detection in air

Biphenyl derivatives containing trimethylsilyl benzyl ether or oxime groups as probes for NO₂ detection

L. Alberto Juárez,[a,b,d] Ana M. Costero,[a,b,d]* Margarita Parra,[a,b,d] Salvador Gil,[a,b,d] Javier Ródenas,[a,b] Félix Sancenón[a,c,d] and Ramón Martínez-Máñez[a,c,d]*

[a] *Instituto Interuniversitario de Reconocimiento Molecular y Desarrollo Tecnológico (IDM), Unidad Mixta Universidad Politécnica de Valencia-Universidad de Valencia, Spain.*
[b] *Departamento de Química Orgánica. Universidad de Valencia, Doctor Moliner 50, 46100, Burjassot, Valencia, Spain. E-mail: ana.costero@uv.es*
[c] *Departamento de Química, Universidad Politécnica de Valencia, Camino de Vera s/n, 46022, Valencia, Spain. E-mail: rmaez@qim.upv.es*
[d] *CIBER de Bioingeniería, Biomateriales y Nanomedicina (CIBER-BBN).*

Abstract

Four probes based in the use of a biphenyl moiety and functionalized with trimethylsilyl benzyl ether (**P1** and **P3**) and oxime (**P2** and **P4**) groups have been prepared and tested as optical probes for the detection of NO_2. Reaction of NO_2 with acetonitrile solutions of **P2**-**P4** resulted in the formation of aldehydes 7 and **8** with a concomitant redshift of the absorption bands. Probe **P2** displayed a bathochromic shift of 45 nm upon reaction with NO_2 and was able to detect this poisonous gas at concentrations as low as 0.02 ppm. **P2** was highly selective against NO_2 and other gases (i.e. NO, CO_2, H_2S, SO_2) and vapours of organic solvents (i.e. acetone, hexane, chloroform, acetonitrile or toluene) had no effect in the optical properties of the probe

Introduction

Nitrogen oxides (NOx) are formed in large quantities from fuel combustion in cars, trucks and power plants,[1] they are a major problem in urban areas and are linked to many respiratory diseases.[2] From a chemical point of view NOx mainly refers to the sum of nitric oxide (NO) and nitrogen dioxide (NO_2), although other nitrogen species can also be included, such as nitrous and nitric acids. Together with the adverse effects of direct exposure to NOx on human health, it is also remarkable its contribution to ground level ozone and fine particle pollution. Hence, strict regulations regarding levels of nitrogen oxides are currently applied by governments and the monitorization of NOx levels based in reliable analytical methods is of great interest.[3]

Among NOx species, NO_2 causes a range of harmful effects on lungs such as increased inflammation of the airways, worsened cough and wheezing, reduced lung function, increased asthma attacks and increased susceptibility to respiratory infection.[4] All these problems are more important for children and older adults.[5] Due to the ubiquitous presence of NO_2, the development of selective and sensitive sensing methods for its detection is a hot area of research.[6] No standards have been agreed upon for nitrogen oxides in indoor air, moreover ASHRAE and the US EPA National Ambient Air Quality Standards list 0.053 ppm as the average 24-hour limit for NO_2 in outdoor air.[7] However, NO_2 levels in certain cities and at certain hours can reach even higher values (near 100 ppm).

Laser-based photoacoustic spectroscopy,[8] surface acoustic wave (SAW),[9] transition metal oxide devices,[10] carbon quantum dot-functionalized aerogels,[11] or ozone treated graphene[12] are some reported analytical

techniques used to detect/monitor NO_2 levels. However, some of these methods show certain limitations such as lack of specificity, limited selectivity, operational complexity, non-portability, difficulties in real-time monitoring and false positive readings. As an alternative to these instrumental procedures, the development of molecular chemosensors, constructed under the chemodosimeter paradigm, has been gaining interest in recent years. However, the number of publications related with optical probes for NO_2 detection is still relatively scarce.[13]
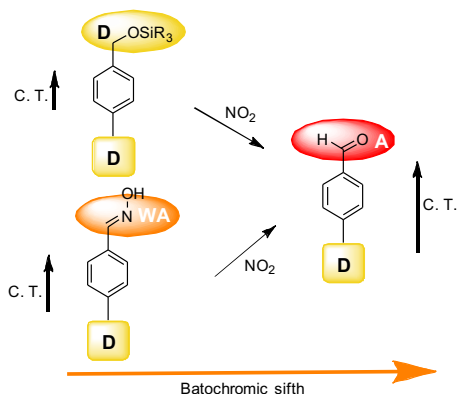
Scheme 1. Sensing protocol used for NO_2 detection.

Bearing in mind our interest in the development of chemical sensors for gas detection,[14] we report herein the synthesis and sensing behavior towards NO_2 of four new chemodosimeters based on the biphenyl chromophore. Among the different organic reactions involving NO_2 we decided to explore the utility of the generation of aromatic aldehydes from trimethylsilyl benzyl ethers [15] and oximes[16] in order to prepare suitable chemodosimeters for the detection of this poisonous and pollutant gas. These are reactions with quantitative yields, working at room temperature and at ambient pressure. The synthesized biphenyl probes (*vide infra*) possess electron donor groups (such as methoxide electronically connected with trimethylsilyl) or oxime (weak electron acceptor) moieties. The underlying idea is that, upon NO_2 reaction, the formed aldehyde (an electron acceptor moiety) would change the electronic properties of the chemodosimeter with subsequent shifts of the absorption bands (see Scheme 1).

Results and discussion

Probes **P1**-**P4** were prepared following the synthetic pathway depicted in Scheme 2. Pd(0) catalyzed cross-coupling reaction of the appropriate boronic acids (**1** and **2**) with 4-

bromohydroxymethylbenzene (**3**) or 4-bromobenzaldehyde (**4**) yielded the corresponding biphenyl derivatives bearing hydroxyl (**5** and **6**) or aldehyde (**7** and **8**) moieties.[17] Transformation of the hydroxyl group into the corresponding trimethylsilyl ether (probes **P1** and **P2**) was carried out using hexametildisilazane (HMDS) in dry CH$_2$Cl$_2$,[18] whereas the probes containing oximes (**P3** and **P4**) were obtained with hydroxylamine hydrochloride in H$_2$O/MeOH mixed with sodium carbonate.[19] All compounds were characterized by ^{1}H NMR, ^{13}C NMR and MS (see Supporting Information). Acetonitrile solutions of the four probes (1.0 x 10^{-4} M) showed intense absorption bands in the 260-300 nm region with ε values ranging from 6000 to 15000 M^{-1} cm^{-1}.
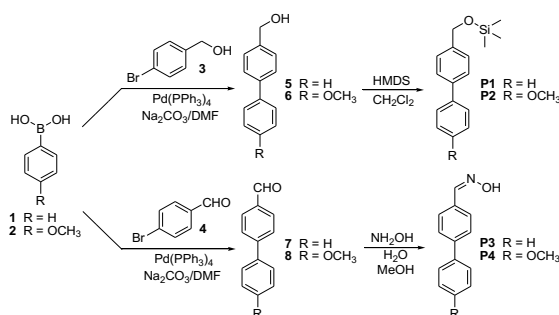
Scheme 2. Synthetic pathways used for the preparation of probes **P1**-**P4**.
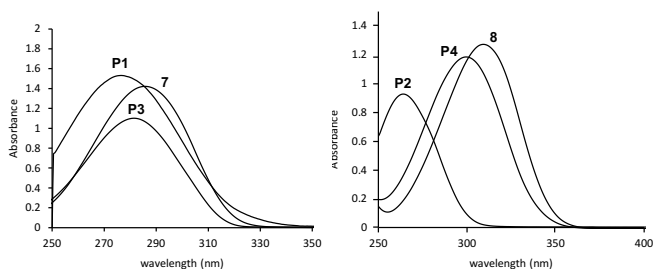
Figure 1. (Left) UV spectra of probes **P1** and **P3** (1.0 x 10^{-4} M in acetonitrile) alone and after bubbling 1 ppm of NO$_2$. (Right) UV spectra of probes **P2** and **P4** (1.0 x 10^{-4} M in acetonitrile) alone and after bubbling 1 ppm of NO$_2$. The reactions gave aldehydes **7** and **8**, respectively.

In a first step, the absorption changes of probes **P1**-**P4** (1.0 x 10^{-4} M in acetonitrile) in the presence of 1 ppm of NO$_2$ (obtained from a commercial cylinder), was tested.

Acetonitrile solutions of **P1** showed an absorption band centered at 277 nm that was redshifted to 285 nm upon bubbling air containing

1 ppm of NO_2 (see Figure 1). Interestingly, the same absorption band centered at 285 nm was observed upon bubbling NO_2 into acetonitrile solutions of probe **P3** (see also Figure 1). The new absorption band, formed upon NO_2 bubbling, was ascribed to the formation of aldehyde **7** as a consequence of the oxidative deprotection of the trimethylsilyl ether moiety in **P1** and of the rupture of the oxime group in **P3**. In fact both, the UV and ^{1}H NMR spectra of aldehyde **7**, were fully coincident with that obtained after treatment of probes **P1** and **P3** with NO_2. Optically, the transformation of an electron donor (trimethylsilyl ether in **P1**) or a weak electron acceptor (oxime in **P3**) group into an aldehyde (with a marked ability to attract electronic density) yielding **7**, resulted in a bathochromic shift of the absorption band of **P1** and **P3**. A similar redshifts of the absorption bands of acetonitrile solutions of **P2** and **P4** was observed upon bubbling NO_2 (1 ppm in air) (see Figure 1).

These changes were ascribed to the reaction of NO_2 with the probes that yielded in both cases aldehyde **8**. Also in this case it was found that the UV and ^{1}H NMR spectra of aldehyde **8**, were fully coincident with that obtained after treatment of probes **P2** and **P4** with NO_2. The best sensing performance, in terms of a larger shift of the absorption band, was obtained for probe **P2**, for which a redshift of 45 nm (from 264 to 309 nm) was observed upon bubbling 1 ppm of NO_2. For this reason, further detailed studies with **P2** were carried out in order to assess the sensitivity and selectivity of this probe toward NO_2.
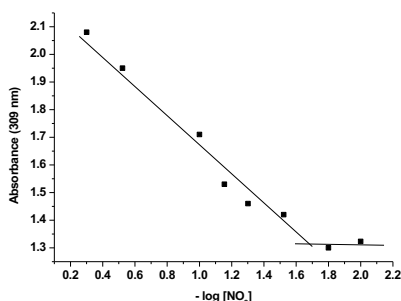
Figure 2. Absorbance at 309 nm measured after bubbling increasing quantities of NO_2 into acetonitrile solutions of probe **P2** (1.0×10^{-4} M).

The limit of detection (LOD) using **P2** for NO_2 was determined by UV measurements by bubbling increasing amounts of NO_2 into an acetonitrile solution of the probe. As shown in Figure 2, the absorbance at 309 nm was gradually enhanced when the concentration of NO_2 increases. From the titration profile a LOD as low as 0.02 ppm was calculated.

In a second step, the selectivity of **P2** was assessed. This is an important issue in the design of probes for pollutant gases in order to overcome potential interferents or false-positive readings produced by other species. Taking this into account, the potential reactivity of probe **P2** with other hazardous gases (i.e. NO, CO_2, H_2S, SO_2) or organic vapors (i.e. acetone, hexane, chloroform, acetonitrile, toluene) was tested by bubbling the selected species into acetonitrile solution of **P2** (1.0×10^{-4} M). None of the gases tested, at concentrations up to 100 ppm, induced changes in the UV spectra of probe **P2** indicating a high selective reaction of **P2** with NO_2 (see Figure 3).
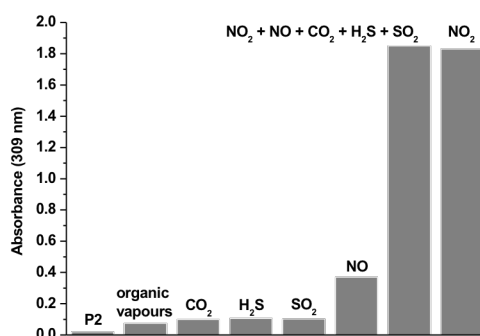
Figure 3. Absorbance at 309 nm of probe **P2** alone and in the presence of selected potential interferents (all compounds at a concentration of 100 ppm).

Competitive studies were also carried out. Thus, Figure 3 shows that the absorption of the band at 309 nm of probe **P2** in the presence of a complex gas mixture ($NO_2+NO+CO_2+H_2S+SO_2$) was the same than that observed when NO_2 was used alone. This result demonstrated a high selective response of probe **P2** toward NO_2 and suggested its possible use for the detection/monitoring of this poisonous gas.

Conclusions

Four new biphenyl-based probes **P1**-**P4** have been synthesized and used for the selective recognition of NO_2. For all four probes a bathochromic shift of the absorption bands was observed in the presence of the NO_2 and ascribed to the generation of an aromatic aldehyde upon reaction of NO_2 with trimethylsilyl benzyl ether or oxime groups contained in **P1**-**P2** and **P3**-**P4**, respectively. Among the prepared chemosensors, **P2** showed the higher shift of the absorption band and for this probe a LOD as low as 0.02 ppm was determined for NO_2 detection. Moreover, the response of

P2 was highly selective and no reaction was found in the presence of NO, CO_2, H_2S, SO_2 or organic vapors of acetone, hexane, chloroform, acetonitrile or toluene. We believe that these, or similar probes based in the same chemical reaction, can display a large potential as optical probes for the selective detection of NO_2.

Experimental Section

General remarks: Dichloromethane and acetonitrile were distilled from P$_2$O$_5$ under Ar prior to use. Silica gel 60 F254 (Merck) plates were used for TLC. Colum chromatography was performed on silica gel. ^{1}H and ^{13}C NMR spectra were determined on a Bruker AV 300 spectrometer. Chemical shifts are reported in parts per million (ppm), calibrated to the solvent peak set. High-resolution mass spectra were recorded in the positive ion mode with a VG-AutoSpec mass spectrometer. Absorption and fluorescence spectra were recorded using a Shimadzu UV-2600 spectrophotometer.

Synthesis of biphenyl alcohols 5 and 6: In a typical run, the corresponding boronic acid (**1** for the synthesis of **5**; **2** for the preparation of **6**) (2 mmol) was added, to a solution of **3** (1 mmol) in DMF (20 ml) in the presence of sodium carbonate (6 mmol). Afterward, the flask was evacuated and refilled with argon. Then, tetrakis(triphenylphosphine)palladium(0) was added and the crude obtained heated at 100 ºC for 30 minutes with vigorous stirring. The resultant mixture was diluted with H$_2$O (10 mL) and Et$_2$O (10 mL), followed by extraction twice with Et$_2$O. The ethereal extract was collected and the solvent evaporated under vacuum. The final product was isolated by column chromatography on silica, with hexane/ethyl acetate (8:2) as eluent, yielding a colourless solid (65%).
5: (65%), colourless solid. ^{1}H NMR (300 MHz, DMSO) δ (ppm): 7.68 - 7.60 (m, 4H), 7.50 - 7.32 (m, 5H), 5.21 (t, J = 5.7 Hz, 1H), 4.54 (d, J = 5.7 Hz, 2H). ^{13}C NMR (75 MHz, DMSO) δ (ppm): 142.2, 140.5, 138.9, 129.3, 127.6, 127.4, 126.9, 126.7, 62.9.
6: (67%), colourless solid. ^{1}H NMR (300 MHz, DMSO) δ (ppm): 7.50 - 7.43 (m, 4H), 7.37 (d, J = 8.4 Hz, 2H), 6.91 (d, J = 8.7 Hz, 2H), 5.20 (t, J = 5.7 Hz, 1H), 4.53 (d, J = 5.7 Hz, 2H), 3.79 (s, 3H). ^{13}C NMR (75 MHz, DMSO) δ (ppm): 159.1, 132.9, 132.8, 132.7, 127.9, 127.4, 126.2, 114.7, 63.0, 55.6.

Synthesis of probes P1 and P2: HDMS (40 mmol) was added to the corresponding alcohol (20 mmol) in dry dichloromethane (20 mL). The mixture was stirred at room temperature for 22 h (full conversion) under argon atmosphere. The solvent was evaporated and the crude was purified by column chromatography on silica using with hexane/ethyl acetate (8:2) as eluent, to give the probes **P1** (90%) or **P2** (93%) as white solids.

P1: (90%), white solid. ^{1}H NMR (300 MHz, DMSO) δ (ppm): 7.50 (m, 4H), 7.27 (m, 5H), 4.56 (s, 2H), 0.00 (s, 9H). ^{13}C NMR (75 MHz, DMSO) δ (ppm): 140.5, 140.3, 139.2, 129.2, 127.6, 127.3, 126.9, 63.8, -0.1. UV-Vis (acetonitrile) λ_{max} = 277 nm (ε= 15300 $M^{-1}cm^{-1}$).
P2: (93%), white solid. ^{1}H NMR (300 MHz, DMSO) δ (ppm): 7.45 (m, 4H), 7.22 (d, J = 8.4 Hz, 2H), 6.88 (d, J = 8.5 Hz, 2H), 4.55 (s, 2H), 3.66 (s, 3H), 0.00 (s, 9H). ^{13}C NMR (75 MHz, DMSO) δ (ppm): 139.6, 138.8, 132.6, 129.2, 127.9, 127.3, 126.2, 114.6, 63.8, 0.1. UV-Vis (acetonitrile) λ_{max} = 264 nm (ε= 8000 $M^{-1}cm^{-1}$).

Synthesis of 7 and 8: 4 (1.5 mmol) and **1** or **2** for **7** and **8** respectively (3 mmol) were dissolved in DMF (20 mL). Afterward, sodium carbonate (9 mmol) was added to this solution. The crude reaction was stirred under inert atmosphere for 30 min. Then, a catalytic amount of tetrakis(triphenylphosphine)palladium(0) was added and the reaction was stirred at 100 ºC for 10 minutes. After this time water (10 mL) was added and the mixture was extracted with ethyl acetate (2 x 20 mL). The organic phase was washed with brine (2 x 20 mL), dried with $MgSO_4$ and evaporated to give the product

7 was purified by silica column chromatography with hexane/ethyl acetate (9:1) to give a white crystalline solid (82%). ^{1}H NMR (300 MHz, DMSO-d_6) δ 10.06 (s, 1H), 8.01 (m, 2H), 7.92 (d, J = 8.3 Hz, 2H), 7.78 (m, 2H), 7.50 (m, 3H). ^{13}C NMR (75 MHz, DMSO-d_6) δ 193.20 , 146.34 , 139.27 , 135.56 , 130.62 , 129.60 , 129.06 , 127.84 , 127.60 . HRMS (EI): m/z calc. for $C_{13}H_{10}O$ 182.07 $[M+1]^+$ found: 183.0797 UV-Vis (acetonitrile) λ_{max} = 289 nm (ε= 9500 $M^{-1}cm^{-1}$).

8 was purified by silica column chromatography with hexane/ethyl acetate (8:2) to give a white crystalline solid (75%). ^{1}H NMR (300 MHz, DMSO-d_6) δ 10.03 (s, 1H), 8.01 − 7.93 (m, 2H), 7.91 − 7.85 (m, 2H), 7.74 (d, J = 9.0 Hz, 2H), 7.08 (d, J = 8.9 Hz, 2H), 3.82 (s, 3H).^{13}C NMR (75 MHz, DMSO) δ (ppm): 192.9, 160.2, 145.9, 134.8, 131.3, 130.5, 128.7, 127.0, 114.9, 55.6. HRMS (EI): m/z calc. for $C_{14}H_{12}O_2$ 212.08 $[M+1]^+$ found: 213.0901. UV-Vis (acetonitrile) λ_{max} = 309 nm (ε = 12700 $M^{-1}cm^{-1}$).

Synthesis of probes P3 and P4: The corresponding aldehyde (**7** and **8** for **P3** and **P4** respectively, 2 mmol) and hydroxylamine hydrochloride (2.2 mmol) were dissolved in methanol-water (1:1, 40 mL). A previously prepared solution of sodium carbonate (2 mmol) in water was slowly added and the reaction was stirred for 3 h at room temperature. Then, methanol was evaporated and the

aqueous phase was extracted with ether (4 x 40 mL). The organic phase was washed with brine (1 x 30 mL) and dried with $MgSO_4$. After evaporation of the solvent probes **P3** (99%) and **P4** (77%) were isolated as white solids.

P3: (99%), white crystalline solid. ^1H NMR (300 MHz, DMSO-d_6) δ 11.28 (s, 1H), 8.19 (s, 1H), 7.70 (m, 6H), 7.48 (m, 2H) 7.40 (m, 1H). ^{13}C NMR (75 MHz, DMSO) δ (ppm): 148.1, 141.2, 139.8, 132.6, 129.3, 128.1, 127.3, 127.3, 126.9. HRMS (EI): m/z calc. for $C_{13}H_{11}NO$ 197.08 [M+1]$^+$ found: 198.0913. UV-Vis (acetonitrile) λ_{max} = 282 nm (▮ = 5800 $M^{-1}cm^{-1}$).

P4:(77%), white crystalline solid. ^1H NMR (300 MHz, Chloroform-d) δ 8.09 (s, 1H), 7.50 (m, 5H), 6.92 (d, J = 8.9 Hz, 2H), 5.23 (s, 1H), 3.79 (s, 3H). ^{13}C NMR (75 MHz, DMSO) δ (ppm): 159.5, 148.2, 140.9, 134.8, 130.5, 128.7, 128.1, 127.0, 114.9, 55.6. HRMS (EI): m/z calc. for $C_{14}H_{13}NO_2$ 227.09 [M+1]$^+$ found: 228.1019. UV-Vis (acetonitrile) λ_{max} = 300 nm (ε= 11800 $M^{-1}cm^{-1}$).

Limits of detection measurements: Increasing quantities of NO_2 gas from commercially available NO_2 cylinder were bubbled for 5 min through a solution of **P2** in acetonitrile. The UV spectra were recorded in 1-cm path length cells at 25 ºC. Representation of the wavelength (nm) vs. concentration of NO_2 allowed the limit of detection to be calculated by using the equation (1)

$$LOD = 3s_b/m \quad (1)$$

in which s_b is the standard deviation of blank measurements and m is the slope of the linear regression plot.

Acknowledgements

References

1. K. Skalska, J.S. Miller, S. Ledakowicz, *Sci. Total Environ*. 2010, **408**, 3976-3989.

2. S. C. Barman, N. Kumar, R. Singh, G. C. Kisku, A. H. Khan, M. M. Kidwai, R. C. Murthy, M. P. S. Negi, P. Pandey, A. K. Verma, G. Jain, S. K. Bhargava*, J. Environ. Biol*. 2010, **31**, 913-920.

3. Analytical Techniques for Atmospheric Measurement, Editor D. Heard, John Wiley & Sons, 2008, pp. 331.

4. (a) J. L. Devalia, A. M. Campbell, R. J. Sapsford, C. Rusznak, D. Quint, P. Godard, J. Bousquet, R. J. Davies, *Am J Respir Cell Mol Biol.*, 1993, **9**, 271-278. (b) S. M. Horvath, Bull N Y Acad Med. 1980, **56**, 835–846.

5. (a) W. S. Tunnicliffe, P. S. Burge, J. G. Ayres, *Lancet*, 1994, **344**, 1733-1736. (b) M. Shima, M. Adachi, *Int. J. of E.*, 2000, **29**, 862-870.

6. H. Dehghani, M, Bezhgi, R. Malekzadeh, E. Imani, S. Pasban-Noghabi, G. Javadi, R. Faraji, M. Negahdary, R. Aghebati-Maleki, *Int. J. Electrochem. Sci.*, 2014, **9**, 1454 – 1467. (b) M. Zhao, T. Zhang, J. Wang, Z. Yuan, JNW, 2013, **8**, 405-412. (c) JZ. Ou, W. Ge, B. Carey, T. Daeneke, A. Rotbart, W. Shan, Y. Wang, Z. Fu, AF. Chrimes, W. Wlodarski, SP. Russo, YX. Li, K. Kalantar-Zadeh, ACS Nano. 2015, **9**, 10313-10323.

7. U.S. Environmental Protection Agency (EPA). Office of Environmental Health Hazard Assessment (OEHHA). Non-cancer Health Effects (RELs). [California, DC, USA]: 1999.

8. A. Mukherjee, M. Prasanna, M. Lane, R. Go, I. Dunayevskiy, A. Tsekoun, C. Kumar, N. Patel, *Appl. Opt.*, 2008, **47**, 4884-4887.

9. A. Venema, E. Nieuwkoop, M.J. Vellekoop, M.S. Nieuwenhuizen, A.W. Barendsz, *Sens. Actuators,* 1986, **10**, 47-64.

10. (a) W. K. Nomani, D. Kersey, J. James, D. Diwan, T. Vogt, Richard A. Webb, G. Koley, *Sens. Actuators B*, 2011, **160**, 251-259. (b) D. Zhang, Z. Liu, C. Li, T. Tang, X. Liu, S. Han, B. Lei, C. Zhou, *Nano Lett.*, 2004, **4**, 1919-1924. (c) S. -W. Choi, A. Katoch, G. J. Sun, P. Wu, S. S. Kim, *J. Mater. Chem. C*, 2013, **1**, 2834-2841. (d) X. Liang, S. Yang, J. Li, H. Zhang, Q. Diao, W. Zhao, G. Lu, *Sens. Actuators B* , 2011, **158**, 1-8.

11.   R. Wang, G. Li, Y. Dong, Y. Chi, G. Chen, *Anal. Chem.*, 2013, **85**, 8065-8069.

12. M. G. Chung, D. H. Kim, H. M. Lee, T. Kim, J. H.Choi, D. *K*. Seo, J. -B. Yoo, S. -H. Hong, T. J. Kang, Y. H. Kim, *Sens. Actuators B,* 2012, **166-167**, 172-176.

13. (a) L. A. Juárez, A. M. Costero, M. Parra, S. Gil, F. Sancenón, R. Martínez-Máñez, *Chem. Commun.* 2015, **51**, 1725-1727. (b) J. Mokhari, M. R. Naimi-Jamal, H. Hamzehal. 11th International Electronic Conference on Synthetic Organic Chemistry (ECSOC-11) 1-30 November 2007.

14. (a) A. Martí, A. M. Costero, P. Gaviña, M, Parra, *Chem. Commun.*, 2015, **51**, 3077-3079. (b) L. A. Juárez, A. Barba-Bon, A. M. Costero, R. Martínez-Máñez, F. Sancenón, M. Parra, P. Gaviña, M. C. Terencio, M. J. Alcaraz, Chem. Eur. J. 2015, **21**, 15450-15450.

15. S. Ohira, E. Wanigasekara, R. D. Rudkevich, P. K. Dasgupta, *Talanta,* 2009, **79**, 14-20.

16. M. Javaheri, M. R. Naimi-Jamal, M. G. Dekamin, G. Kaupp, *Phosphorus Sulfur Silicon Relat. Elem.*, 2012, **187**, 142-148.
17. C. M. Nunes, A. L. Monteiro, *J. Braz. Chem. Soc.*, 2007, **18**, 1443-1447
18. J. Marjan, *Tetrahedron,* 2012, **68**, 3861-3867.
19. S. Castellano, D. Kuck, M. Viviano, J. Yoo, F. López-Vallejo, P. Conti, L. Tamborini, A. Pinto, J. L. Medina-Franco y G. Sbardella. *J. Med. Chem.* 2011, **54**, 7663-7677.

A new simple chromo-fluorogenic probe for NO₂ detection in air

L. Alberto Juárez,[a,b] Ana M. Costero,[a,b] Félix Sancenón,[a,c d]
Ramón Martínez-Máñez,[a,c,d] Margarita Parra[a,b] and Pablo Gaviña[a,b]

[a] *Instituto Interuniversitario de Reconocimiento Molecular y Desarrollo Tecnológico (IDM), Unidad Mixta Universidad Politécnica de Valencia-Universidad de Valencia, Spain.*
[b] *Departamento de Química Orgánica. Universidad de Valencia, Doctor Moliner 50, 46100, Burjassot, Valencia, Spain. E-mail: ana.costero@uv.es*
[c] *Departamento de Química, Universidad Politécnica de Valencia, Camino de Vera s/n, 46022, Valencia, Spain. E-mail: rmaez@qim.upv.es*
[d] *CIBER de Bioingeniería, Biomateriales y Nanomedicina (CIBER-BBN).*

Abstract: A new chromo-fluorogenic probe, consisting on a biphenyl derivative containing both a silylbenzyl ether and a *N,N*-dimethylamino group, for NO$_2$ detection in gas phase has been developed. A clear color change from colorless to yellow together with an emission quenching was observed when the probe reacted with NO$_2$. A limit of detection to the naked eye of ca. 0.1 ppm was determined and the system was successfully applied to the detection of NO$_2$ in realistic atmospheric conditions.

Nitrogen dioxide, (NO$_2$) is formed when fossil fuels such as coal, oil, gas or diesel are burned at high temperatures. On-road sources like cars, trucks, and buses are the largest sources of emissions, followed by power plants, diesel-powered heavy construction equipment and other movable engines, and industrial boilers. NO$_2$ can also form indoors when fossil fuels such as wood or natural gas are burned. Moreover when heaters or stoves are not vented fully to the outside, higher levels of NO$_2$ can be reached indoor. Due to the ubiquitous presence of this gas in the atmosphere the development of selective and sensitive detection methods is a timely area of research. However, in spite of the well-known NO$_2$ toxicity, no standards have been agreed upon for nitrogen oxides in indoor air. ASHRAE and the US EPA National Ambient Air Quality Standards list 0.053 ppm as the average 24-hour limit for NO$_2$ in outdoor air.[1] However it has been found that NO$_2$ levels in certain cities and at certain hours can reach values near 100 ppb. Nitrogen dioxide causes a range of harmful effects on the lungs such as increased inflammation of the airways, worsened cough and wheezing, reduced lung function, increased asthma attacks and increased susceptibility to respiratory infection.[2]

Different approaches for NO$_2$ detection such as laser-based photoacoustic spectroscopy,[3] surface acoustic wave (SAW),[4] transition metal oxide devices[5] carbon quantum dot-functionalized aerogels,[6] or ozone treated graphene[7] have been described in the literature. However, some of these methods show certain limitations such limited selectivity, operational complexity, non-portability, difficulties in real-time monitoring and false positive readings. As an alternative to these protocols, the development of easy-to-use fluorogenic and chromogenic chemosensors has been gaining interest in recent years. Still, the number of publications related to the design of probes for NO$_2$ sensing is very scarce.[8]
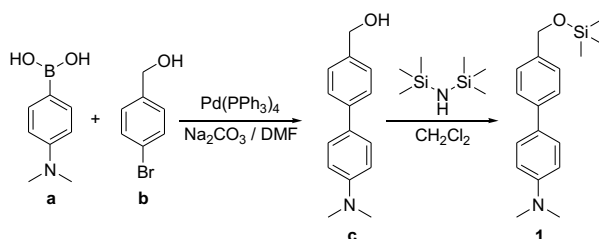
Scheme 1. Synthetic procedure used to prepare probe **1**.

Following our interest in the design of colorimetric probes for hazardous gases, we report herein a new probe for NO_2 detection both in solution and in gas phase. The probe consists of a biphenyl derivative containing a silylbenzyl ether and a *N,N*-dimethylaminophenyl group (compound **1**, see Scheme 1). The sensing protocol relies in the well-known NO_2-induced transformation of silylbenzyl ethers into the corresponding aromatic aldehydes which is a solvent-free oxidative deprotection procedure that occurs in practically quantitative yields and under very soft reaction conditions.[9] Moreover, an unexpected nitration of the *N,N*-dimethylaminobenzene ring was also observed (*vide infra*).
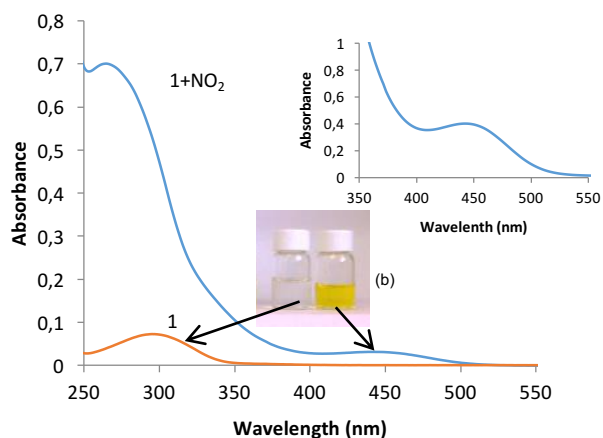
Figure 1. UV spectra of **1** (acetonitrile, 1.0×10^{-4} mol dm^{-3}) before and after exposure to air containing NO_2 at a concentration of 2 ppm for 10 min. Inset: (a) changes in the visible zone of probe **1** (acetonitrile, 1.0×10^{-3} mol dm^{-3}) in the absence and (b) in the presence of NO_2 and visual colour changes.

Probe **1** was prepared following the synthetic pathway shown in Scheme 1. Pd(0) catalyzed cross-coupling reaction of the boronic acid derivative **a**

with 4-bromohydroxymethylbenzene (**b**) gave rise to the corresponding hydroxymethyl biphenyl derivative (**c**).[10] Sylilation of the hydroxyl group in **c** to obtain probe **1** was carried out using hexamethyldisilizane in dry CH$_2$Cl$_2$.[11] All compounds were fully characterized by ^{1}H NMR, ^{13}C NMR and MS (see Supporting Information).

In a first assay, the optical response of acetonitrile solutions of probe **1** was tested by putting them in contact with air containing 2 ppm of NO$_2$ from a commercial cylinder (10 minutes). Acetonitrile solutions of probe **1** showed an intense absorption band at 303 (log ε= 4.7). Upon exposure to NO$_2$ (g) a hypsochromic shift of the UV band from 303 to 253 nm (logε= 5.2) was observed and a new absorption appeared in the visible region at 450 nm (log ε= 3.2) (see Figure 1). This band was responsible for the clear color change from colorless to yellow.
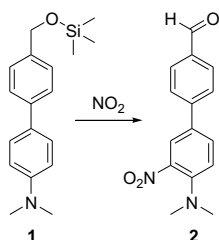
Scheme 2. Sensing NO$_2$ mechanism for probe **1**.
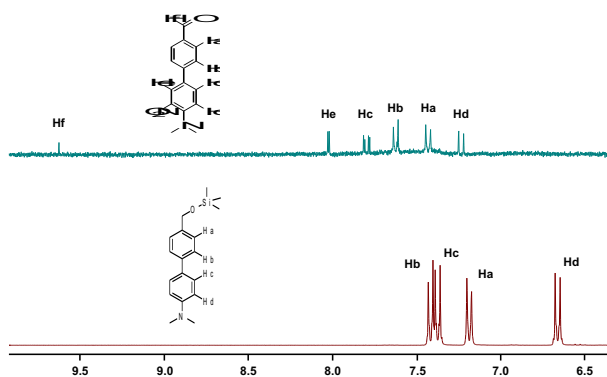
Figure 2. ^{1}H NMR spectra (CD$_3$CN) of free **1** (down), and **1** after exposure to a nitrogen atmosphere containing NO$_2$ (g) (2 ppm) for 10 minutes (up).

In order to assess the mechanism of the chromogenic response, ^{1}H NMR studies with probe **1** in the absence and in the presence of NO$_2$ in CD$_3$CN were carried out (see Figure 2). The aromatic zone of the ^{1}H NMR spectrum of probe **1** showed two pair of doublets at 7.18 (Ha) and 7.40 (Hb) ppm and at 6.65 (Hd) and 7.35 (Hc) ppm ascribable to the 1,4-

disusbtituted benzene rings. Upon NO_2 contact all the aromatic signals underwent a marked downfield shifts and a new singlet appeared at 9.65 ppm (Hf). Also the aromatic protons of the *N,N*-dimethyl aminobenzene moiety changed from a pair of doublets to three signals centered at 7.20 (d, Hd), 7.80 (dd, Hc) and 8.05 (d, He) ppm typical of an aromatic ring with a 1,2,4 tri-substitution pattern. Both facts suggested that, upon NO_2 addition two reactions occurred, (i) an oxidative deprotecion of the silyl ether and (ii) a nitration of the *N,N*-dimethyl aminobenzene ring to yield compound **2** (see Scheme 2). HRMS studies confirmed the formation of product **2** (*m/z* =271.1068 corresponding to [**2**+H]$^+$, see supporting information). It is important to remark that the presence of the trimethyl silyl moiety in **1** was mandatory in order to observe a clear colour modulation. Thus similar experiments with 4-dimethylamino-4'-hydroxymethyl biphenyl in the presence of NO_2 resulted in a complex mixture of products with no clear colour changes (data not shown).

In addition, acetonitrile solutions of probe **1** (1.0 x 10^{-4} mol dm^{-3}) were fluorescent and presented a broad emission band at 385 nm (λ_{ex} = 303 nm, ϕ=0,76). The emission was also NO_2-sensitive and a quenching was found when acetonitrile solutions of **1** were exposed to 0.05 ppm of this gas (see Figure 3). From UV-visible titration profile a limit of detection of ca. 7.2 ppb was calculated (using the *3s$_b$/m* procedure, where s_b is the standard deviation of blank and *m* is the slope of the linear regression plot, see Supporting Info). The linear fitting of absorbance at 450 nm *versus* NO_2 concentration between 0.01 and 0.1 ppm could be used for the quantification of nitrogen dioxide. In addition to this, a clear optical response to the naked eye was found for NO_2 concentrations as low as ca. 0.1 ppm.
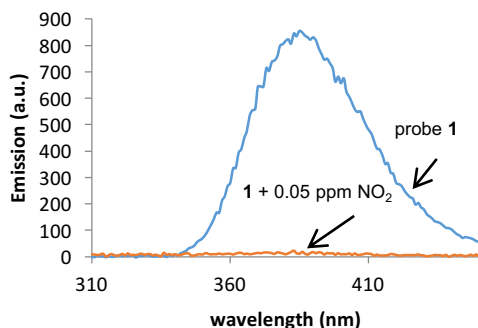
Figure 3. Fluorescence spectra of acetonitrile solutions of probe **1** (1.0 x 10^{-4} mol dm^{-3}) before and after exposure to air containing NO$_2$ at a concentration of 0.05 ppm.

Encouraged by the sensitive response to NO$_2$ observed with **1** and in order to extend the potential applicability of the probe to real monitoring, we decided to take a step further. For this purpose probe **1** was incorporated into a hydrophobic polyethylene oxide film (see Supporting Info) and the test strips prepared were placed into a container holding 1 ppm of NO$_2$ for 5 minutes. As seen in Figure 4 the colorless films clearly turned yellow upon exposure to air containing NO$_2$ at this concentration. A gradual color change from pale yellow to orange can be clearly observed in the 0.1 to 2 ppm range (see Supporting Info). Besides, changes in fluorescence were also observed by the naked eye with a conventional 254 nm UV lamp. The limit of detection to the naked eye of NO$_2$ in air, when using the polyethylene oxide films, was ca. 0.1 ppm, with a typical response time of less than 5 minutes.
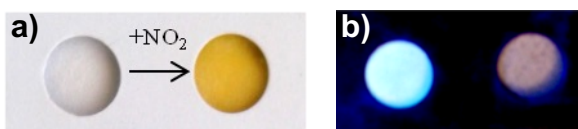
Figure 4. Sensing polyethylene oxide membranes containing probe **1**. (a) Color modulation of the sensing film in absence (left) and presence (right) of NO$_2$ (1 ppm) in air. (b) Emission of the sensing film (excitation at 254 nm) in absence (left) and presence (right) of NO$_2$ (1 ppm) in air.

One important issue related to the design of probes for pollutant gases is the role played by potential interferents or false-positive outcomes produced by other species. Bearing this concept in mind, polyethylene oxide films containing **1** were prepared and placed into a container in the presence of other hazardous gases (i.e. CO$_2$, H$_2$S, SO$_2$) or some volatile

organic compounds (i.e. acetone, hexane, chloroform, acetonitrile and toluene). No color or emission changes were observed in the presence of these tested compounds even at concentration of 100 ppm. In addition, it was also found that moisture was unable to induce any chromo-fluorogenic change in the films containing probe **1**.

Once demonstrated the selective response of **1** in air, the potential use of the films to monitor the presence of NO_2 in more realistic conditions was also tested. In particular, films containing probe **1** were placed in a car tunnel in Valencia (Spain) with heavy daily traffic and with high levels of air pollution. At the same time NO_2 detection was also carried out by means of two independent passive samplers exposed on a 5 days basis that gave accumulative values of NO_2 of 193 and 186 ppb.[12] It was found that after these 5 days of exposition the color of the films visibly changed from colorless to yellow clearly indicating the presence of NO_2.

In summary, we have developed herein a new chromogenic probe for the selective and sensitive detection of NO_2. Probe **1** contains a trimethylsilyl ether moiety that is oxidized in the presence of NO_2. Besides a nitration reaction of at the *N,N*-dimethylbenzene moiety takes place. Both reactions were responsible of the chromogenic detection. NO_2 sensing was achieved both in solution and in gas phase. Probe **1** allowed the simple colorimetric detection NO_2 with limits of detection lower than the generally accepted alarm threshold. Furthermore, the response of probe **1** towards NO_2 was selective and other common gas pollutants (such as CO_2, H_2S and SO_2) and volatile organic compounds (acetone, hexane, chloroform, acetonitrile and toluene) were unable to induce colour modulation. Moreover, probe **1** in polyethylene oxide membranes were satisfactorily used for the monitoring of NO_2 levels in real environmental samples (a tunnel with heavy daily traffic).

References

1. U.S. Environmental Protection Agency (EPA). Office of Environmental Health Hazard Assessment (OEHHA). Non-cancer Health Effects (RELs). [California, DC, USA]: **1999**.
2. a) W. S. Tunnicliffe,, P. S. Burge, J. G. Ayres, *Lancet*, **1994**, *344*: 1733-1736. b) M. Shima, M. Adachi *Int. J. Epidemiol.*, **2000**, *29*, 862-870.
3. A. Mukherjee, M. Prasanna, M. Lane, R. Go, I. Dunayevskiy, A. Tsekoun, C. Kumar, N. Patel, *Appl. Opt.*, **2008**, *47*, 4884-4887.
4. E. Nieuwkoop, M. J. Vellekoop, M. S. Nieuwenhuizen, A. W. Barendsz, *Sensor. Actuat.,* **1986**, *10*, 47-64.
5. a) W. K. Nomani, D. Kersey, J. James, D. Diwan, T. Vogt, R. A. Webb, G. Koley, *Sensor. Actuat. B: Chem.*, **2011**, *160*, 251-259. b) D. Zhang, Z. Liu, C. Li, T. Tang, X. Liu, S. Han, B. Lei, C. Zhou, *Nano Letters*, **2004**, *4*, 1919–1924. c) S. −W. Choi, A. Katoch, G. −J. Sun, P. Wu, S. S. Kim, *J. Mater. Chem. C*, **2013**, *1*, 2834-2841. d) X. Liang, S. Yang, J. Li, H. Zhang, Q. Diao, W. Zhao, G. Lu, *Sensor. Actuat. B: Chem.*, **2011**, *158*, 1-8.
6. R. Wang, G. Li, Y. Dong, Y. Chi, G. Chen, *Anal. Chem.*, **2013**, *85*, 8065-8069.
7. M. G. Chung, D. H. Kim, H. M. Lee, T. Kim, J. H. Choi, D. K. Seo, J. −B. Yoo, S. −H. Hong, T. J. Kang, Y. H. Kim, *Sensor. Actuat. B: Chem.*, **2012**, *166-167*, 172-176.
8. a) S. Ohira, E. Wanigasekara, D. M. Rudkevich, P. K. Dasgupta, *Talanta,* **2009**, *77*, 1814-1820. b) L. A. Juárez, A. M. Costero, M. Parra, S. Gil, F.Sancenón, R. Martínez-Máñez, *Chem. Commun.*, **2015**, 51, 1725-1727.c) Y. Yan, J. Sun, K. Zhang, H. Zhu, H. Yu, M. Sun, D. Huang, S. Wang, *Anal. Chem*. **2015**, *87*, 2087-2093. d) Y. Yan, S. Krishnakumar, H. Yu, S. Ramishetti, L-W. Deng, S. Wang, L. Huang, D. Huang, *J. Am. Chem. Soc.* **2013**, *135*, 5312-5315.
9. M. Javaheri, M. R. Naimi-Jamal, M. G. Dekamin, G. Kaupp, *Phosphorus Sulfur Silicon Relat. Elem.*, **2012**, *187*, 142-148.
10. C. M. Nunes, A. L. Monteiro , *J. Braz. Chem. Soc.*, **2007**, *18*, 1443-1147.
11. J. Marjan, *Tetrahedron*, **2012**, *68*, 3861-3867.

These data were submitted by Dr. A. Múñoz from the CEAM (Valencia, Spain) that were undergoing parallel experiments in the same car tunnel

Supporting information

General remarks

CH$_2$Cl$_2$ and CH$_3$CN were distilled from P$_2$O$_5$ under Ar prior to use. Silica gel 60 F254 (Merk) plates were used for TLC. Colum chromatography was performed on silica gel (60, 40-63 micras). ^{1}H NMR, ^{13}C NMR (300 MHz) spectra were determined on a Bruker AV 300 spectrometrer. Chemical shifts are reported in parts per million (ppm), calibrated to the solvent peak set. High-resolution mass spectra were recorded in the positive ion mode with a VG-AutoSpec mass spectrometer. Absorption and fluorescence spectra were recorded using a Shimadzu UV-2600 spectrophotometer and a Varian Cary Eclipse spectrofluorimeter.

Membrane Preparation

Polyethylene oxide (2 g, Mw 400,000 Dalton) was slowly added to a solution of **2** (10^{-3} M solution) in dichloromethane (40 mL). The mixture was stirred until a highly viscous mixture was formed. This mixture was poured into a glass plate (40 cm^2) and kept in a dry atmosphere for 24 h.

Spectroscopic studies

All the solvents were purchased at spectroscopic grade from Aldrich Chemicals Co., used as received, and were found to be free of fluorescent impurities. Absorption and fluorescence spectra were recorded using a Shimadzu UV-2600 spectrophotometer and a Varian Cary Eclipse spectrofluorimeter, respectively. Fluorescence quantum yields were measured at room temperature in the N$_2$-purgued solution in relation to anthracen (Φ_{EtOH} = 0.27) at 303 nm for **3.** The fluorescence quantum yields were calculated from Eq. (1). Here F denotes the integral of the corrected fluorescence spectrum, A is the absorbance at the excitation wavelength, and n is the refractive index of the medium.

$$\Phi_{exp} = \Phi_{ref} \frac{F\{1 - exp(-A_{ref} ln10)\}n^2}{F_{ref}\{1 - exp(-A\, ln10)\}n_{ref}^2}$$

Limits of detection measurements

Increasing quantities of NO_2 gas from commercially available NO_2 cylinder were bubbled 5 min to a solution of **3** in acetonitrile. The fluorescence spectra were recorded in 1-cm path length cells at 25ºC. Representation of Δ of fluorescence at the appropriate wavelength vs. concentration of NO_2 allowed the limit of detection to be calculated.

$$LOD = \frac{3S_b}{m}$$
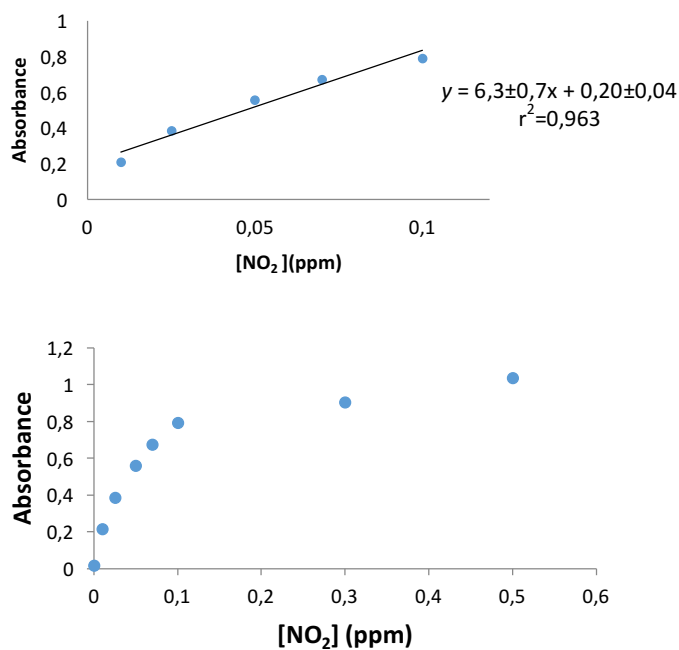
Figure S.1. Absorbance at 450 nm of **1+NO$_2$** (10^{-4}M in CH_3CN) *versus* increasing amounts of NO_2 at room temperature: (up) lineal range, (bottom) complete curve.

Synthesis of biphenyl compound intermediate c

4-(Dimethylamino)phenyl boronic acid (2 mmol) was added, to a solution of 4-bromophenylmethanol (1 mmol) in DMF (20 ml) with sodium carbonate (6 mmol). The flask was evacuated and refilled with argon. Tetrakis(triphenylphosphine)palladium(0) was added and heated at 100ºC for 30 minutes with vigorous stirring. The resultant residual mixture was diluted with H_2O (10 mL) and Et_2O (10 mL), followed by extraction twice with Et_2O. The ethereal extract was collected and stripped of solvent under vacuum. The product was isolated by column chromatography on silica, with hexane/ethyl acetate as eluent, to give the product (65%) as colourless solid. ^{1}H NMR (300 MHz, DMSO) δ (ppm) 7.54 (d, J = 8.5 Hz, 2H), 7.51 (d, J = 9.0 Hz, 2H)7.27 (d, J = 8.5 Hz, 2H), 6.73 (d, J = 9.0 Hz, 2H), 4.50 (s, 2H), 2.87 (s, 6H). (ESI): m/z calcd. for $C_{15}H_{17}NO$ [M^+H^+]: 227,1310 found 228,1383

Synthesis of product 1

Hexamethyldisilazane (HDMS) (40 mmol) was added to 20 mmol of the alcohol in 20 ml of dry dichloromethane; the mixture was stirred at room temperature for 22 h (full conversion) under argon atmosphere. The solution was evaporated and purified by column chromatography on silica, with hexane/ethyl acetate as eluent, to give the products **1** (93%) as white solid. ^{1}H NMR (300 MHz, DMSO) δ(ppm) 7.42 (d, J= 7.9 Hz, 2H) 7.38 (d, J = 8.9 Hz, 2H), 7.19 (d, J = 7.9 Hz, 2H), 6.66 (d, J = 8.9 Hz, 2H), 4.53 (s, 2H), 2.80 (s, 6H), 0.00 (s, 9H). ^{13}C NMR (75 MHz, DMSO-d_6) δ 150.07 , 139.35 , 138.77 , 127.79 , 127.29 , 127.25 , 125.56 , 112.94 , 63.94 , 40.39, 0.00 . UV-Vis (CH_3CN) λ_{max} = 303 nm, emission (CH_3CN, λ_{ex} = 300 nm) λ_{max} = 385 nm. (ESI): m/z calcd. for $C_{15}H_{14}N_2O_3$ [M^+H^+]: 270,1004 found 271,1068
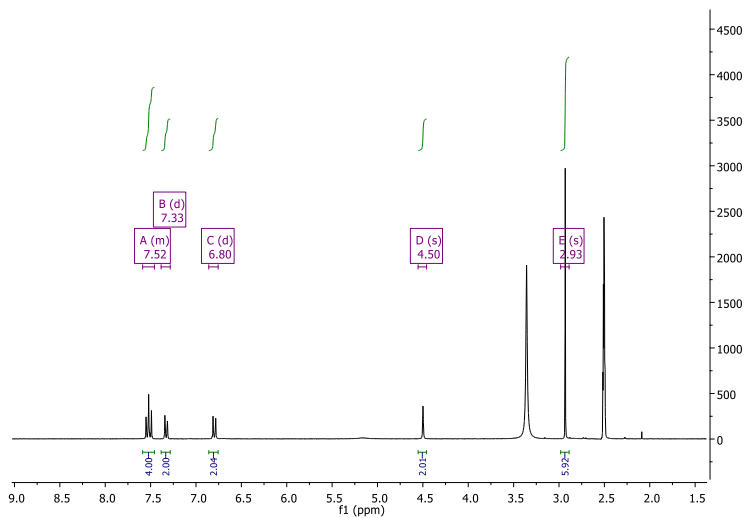
Figure S.2. ^{1}H NMR spectrum of intermediate **c** in DMSO.
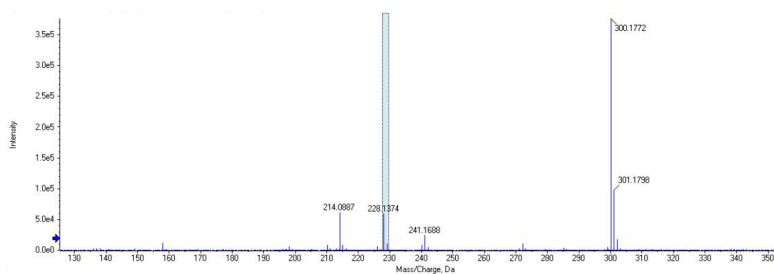
Figure S.3. HRMS (EI) of **c**
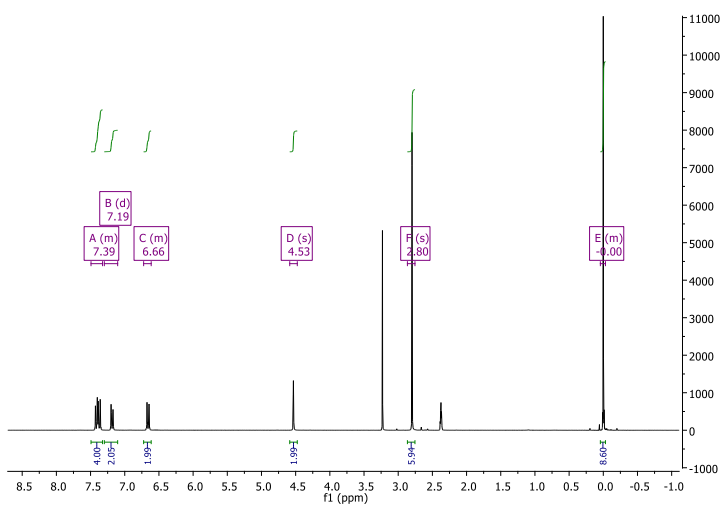
Figure S.4. ^{1}H NMR spectrum of **1** in DMSO.
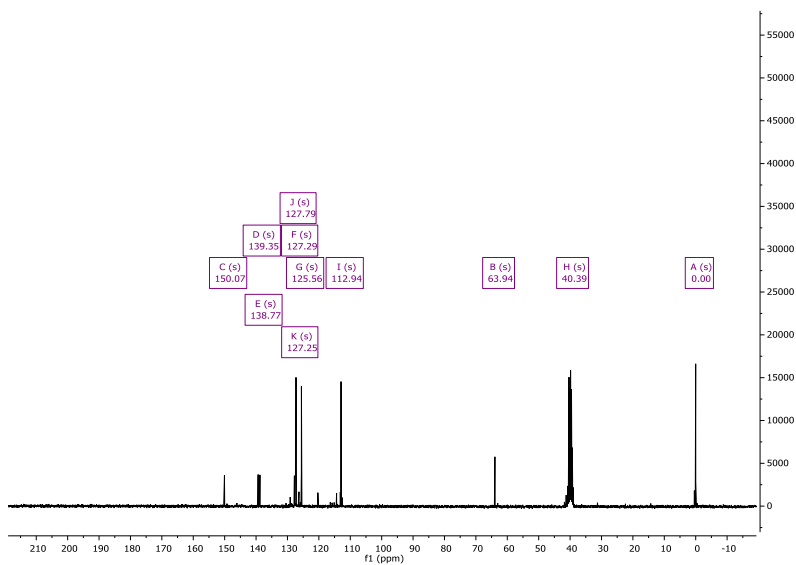
Figure S.5. ^{13}C NMR spectrum of **1** in DMSO
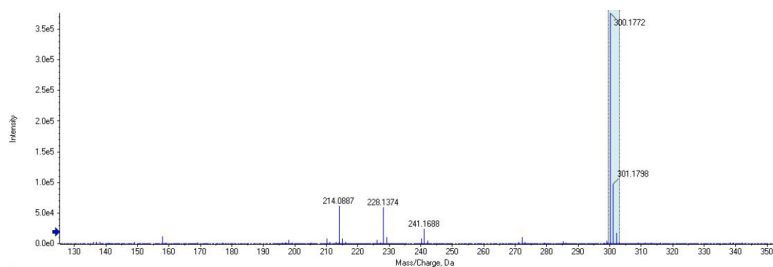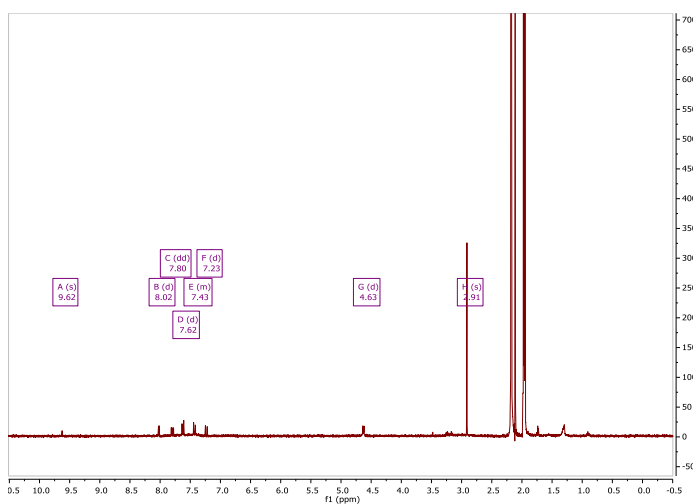

Figure S.6. HRMS (EI) of **1**
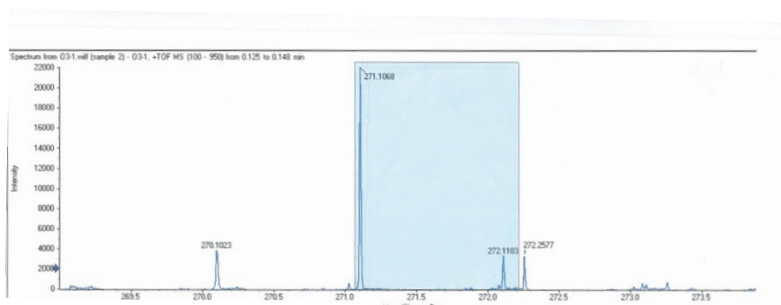

Figure S.7. ^{1}H NMR spectrum of **2** in CD$_3$CN

Figure S.8. HRMS (EI) of product **2**: m/z (%) calc for $C_{15}H_{14}N_2O_3$: 270.1004 $[M+1]^+$
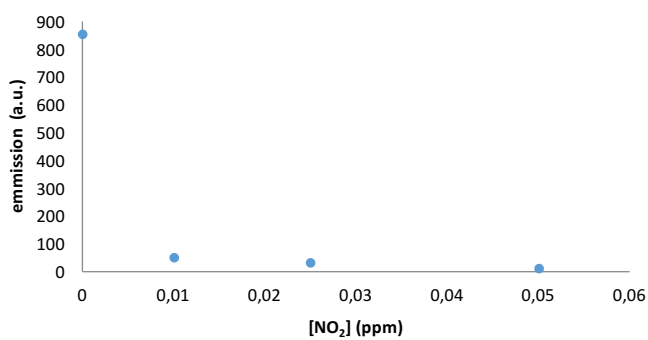found: 271.1068

Figure S.9. Emission at 385 nm (λ_{exc} = 300 nm) of **1+NO₂** (10^{-4}M in CH_3CN) *versus* increasing amounts of NO_2 at room temperature

| 0 ppm | 0.5 ppm | 1.0 ppm | 1.5 ppm | 2 ppm | 2.5 ppm | 3 ppm |

Figure S.10. Picture of the color changes observed in the film in the presence of increasing amounts of NO_2 gas.

Chapter 4:
Functionalized BODIPY for NO$_2$ detection

A new chromo-fluorogenic probe based on BODIPY for NO₂ detection in air

L. Alberto Juárez,[a,b] Ana M, Costero,[a,b]* Margarita Parra,[a,b] Salvador Gil[a,b], Félix Sancenón and R. Martínez-Máñez[a,c,d]*

[a] Centro de Reconocimiento Molecular y Desarrollo Tecnológico (IDM), Unidad Mixta Universidad Politécnica de Valencia-Universidad de Valencia, Spain.
[b] Departamento de Química Orgánica. Universidad de Valencia, Doctor Moliner 50, 46100, Burjassot, Valencia, Spain. E-mail: ana.costero@uv.es
[c] Departamento de Química, Universidad Politécnica de Valencia, Camino de Vera s/n, 46022, Valencia, Spain. E-mail: rmaez@qim.upv.es
[d] CIBER de Bioingeniería, Biomateriales y Nanomedicina (CIBER-BBN).

Abstract: A novel colorimetric probe for the selective and sensitive detection of NO$_2$ in solution and in air based in a BODIPY core containing an oxime group has been prepared.

The selective and sensitive detection of toxic gases is one of the most promising applications of optical probes and the search of new sensing systems has been investigated with increasing intensity in last years. In this context nitrogen dioxide (NO$_2$) is one of the most prevalent and dangerous gases. There are several sources of this pollutant which are mainly related with un-vented gas stoves and heaters in addition to tobacco smoke.[1] Nitrogen dioxide is a highly reactive oxidant and corrosive and it acts mainly as an irritant affecting the mucosa of eyes, nose, throat, and respiratory tract.[2] Moreover extremely high-dose exposure to NO$_2$ may result in pulmonary edema and diffuse lung injury, whereas continued exposure to high NO$_2$ levels can contribute to the development of acute or chronic bronchitis. Even low level NO$_2$ exposure may cause increased bronchial reactivity in some asthmatics, decreased lung function in patients with chronic obstructive pulmonary disease and increased risk of respiratory infections, especially in young children.[3] No standards have been agreed upon for nitrogen oxides in indoor air, moreover ASHRAE and the US EPA National Ambient Air Quality Standards list 0.053 ppm as the average 24-hour limit for NO$_2$ in outdoor air.[4] However NO$_2$ levels in certain cities and at certain hours can reach much higher values of near 100 ppm.

Traditionally electrochemical sensors are usually used for detection of NO$_2$ in real labor environments, however interference from coexisting gases have been reported to be a problem in these devices. Moreover, recent alternative approaches for detecting NO$_2$ such as laser-based photoacoustic spectroscopy,[5] surface acoustic wave (SAW),[6] transition metal oxide devices[7] carbon quantum dot-functionalized aerogels,[8] or ozone treated graphene have been reported.[9] In fact there is an interest in the design of new sensors capable of selectively detect NO$_2$. In this context chromo-fluorogenic probes are highly appealing for real-time monitoring and because they require of very inexpensive instrumentation. Moreover, in certain circumstances colour modulation can even be observed to the naked eye making chromo-fluorogenic approaches highly attractive for certain applications. However, despite the inherent advantages of optical probes the number of publications related to the design of molecular chemodosimeters for NO2 detection is very scarce.[10]
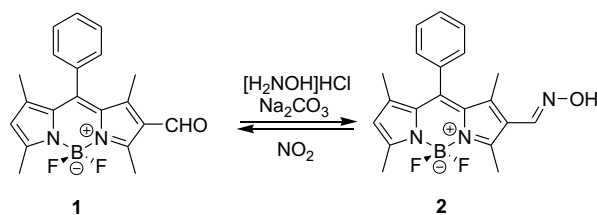
Scheme 1. Structure of the BODIPY derivatives 1 and 2.

Following our interest in the development of chromo-fluorogenic probes for toxic gases, we show herein a new chemosensor able to detect selectively the presence of NO_2 both in solution and in air (see Scheme 1). The design of the probe is based in the ability of NO_2 to react with oximes and give the corresponding carbonyl group under very soft conditions.[11] Moreover we have used as dye a BODIPY core which are a class of well-known fluorophores with widespread applications as fluorescent probes due to their valuable characteristics, such as high molar absorption coefficients and high quantum yields leading to intense absorption and fluorescence bands.[12]

Probe 2 was easily prepared from the corresponding aldehyde 2-formyl-8-phenyl-1,3,5,7-tetramethylboron-dipyrromethene (1). Moreover compound 1 was readily prepared 8-phenyl-1,3,5,7-tetramethylboton-dipyrromethene[13] by oxidation with DMF and $POCl_3$.[14] Probe 2 was then obtained by reaction of 1 with hydroxylamine hydrochloride under mild basic conditions in ethanol:water.[15] Compound 2 was fully characterized by ^1H NMR, ^{13}C NMR and MS (see Supporting Information for details). The oxime in 2 is electronically connected to the BODIPY core and it was expected that its transformation to the corresponding aldehyde in the presence of NO_2 would result in a significant optical change.
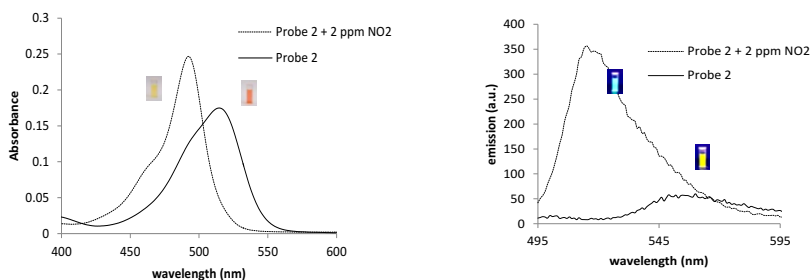
Figure 1. a) UV (a) fluorescence (b) spectra and spectra of probe 2 (acetonitrile, 10^{-5} M) alone and after bubbling air containing NO_2 at a concentration of 2 ppm. Insets display the visual changes both in color and fluorescence.

96

Acetonitrile solutions of probe 2 showed a visible absorption band at 515 nm (log ε = 4.2). Moreover the probe was weakly fluorescent due to C=N isomerization[15] with an emission band centered at 560 nm (λ_{exc} = 500 nm) and a quantum yield of only 0.19 (relative to Rhodamine B in EtOH (λ_{exc} = 500 nm)). Bubbling of air containing NO₂ at a concentration of 2 ppm to acetonitrile solutions of probe 2 immediately resulted in clear optical response. In particular a hypsochromic shift of the absorption band from 515 nm to 492 nm (log ε = 4.4) was observed (see Figure 1a). Moreover a remarkable emission change was also found (see Figure 1b); in the presence of NO₂ the weak emission at 560 nm disappeared and a new highly emissive band at 515 nm (λ_{exc} = 485 nm, ϕ = 0.77) evolved. This remarkable chromo-fluorogenic response was visible to the naked eye (see also Figures 1 and 2). Optical changes were attributed to the transformation of the oxime 2 into the corresponding aldehyde 1 that is strongly fluoresecent[14] (ϕ = 0.77 relative to Fluorescein at pH=8.06 (λ_{exc} =490 nm)). This was clearly demonstrated via a simple comparison between ^{1}H NMR and UV spectra of the reaction product between 2 and NO₂ and these of aldehyde 1. From additional titration experiments of 2 with NO₂ limits of detection (LOD) of 0.56 ppm (from UV-vis) and 0.46 ppm (from fluorescence) were determined.

Despite this interesting optical response of probe 2 in solution, the detection of NO₂ in gas phase is of greater importance. Therefore, and encouraged by the sensitive response observed with 2 in acetonitrile, in an attempt to extend the application of 2 to real-time monitoring, we decided to take a further step and developed test strips for the colorimetric detection of NO₂ in air. To this end, hydrophobic polyethylene oxide films containing probe 2 were prepared. Sensing films were readily obtained by mixing 2 and polyethylene oxide (Mw 400,000 Dalton) in dichloromethane. The mixture was then poured into a glass plate and kept in a dry atmosphere for at least 24 h (see Supporting Information). In a typical assay, films were placed into a container holding air and NO₂ (1 ppm). Immediately a clear color modulation from pink to pale yellow was observed (see Figure 2). From additional experiments using the polyethylene oxide membrane containing 2 and different amounts of NO₂ in air a visual limit of detection of 0.1 ppm was determined after ten minutes exposure. Moreover, Figure 2 also show a photograph of the emission changes (excitation using a conventional UV lamp) of the sensing polyethylene oxide membrane in the absence and presence of NO₂ also at a concentration of 1 ppm. Using emission changes a visual LOD of 0.1 was determined for the detection of NO₂ in

air after ten minutes exposure. These LOD are lower than the alarm threshold of 400 µg/m^3 (ca. 0.2 ppm) established by the European Community for nitrogen dioxide.
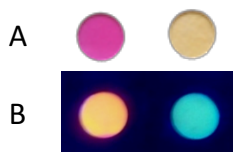

Figure 2. Sensing polyethylene oxide membranes containing probe 2. A) Colour modulation of the sensing film in absence (left) and presence (right) of NO_2 (1 ppm) in air. B) Emission of the sensing film (excitation at 254 nm) in absence (left) and presence (right) of NO_2 (1 ppm) in air.

One important issue in relation to the design of probes for pollutant gases is the role played by potential interferents or false-positive outcomes produced by other species. Bearing this concept in mind, the reactivity of probe 2 with other hazardous gases (i.e. NO, CO_2, H_2S, SO_2) was also studied. Moreover, the probe was also tested in the presence vapours of acetone, hexane, chloroform, acetonitrile and toluene. Polyethylene oxide films containing probe 2 were prepared and the films were placed into a container holding the corresponding gas. In all cases probe 2 displayed a remarkably selective response for NO_2 in air. In particular no reaction was detected in the presence of NO, CO_2, H_2S and SO_2 at very high concentrations (up to 100 ppm). Moreover, no colour or emission changes were observed in the presence of the volatile organic compounds such as acetone, hexane, chloroform, acetonitrile and toluene (up to 100 ppm in air). In addition, it was also observed that no colour changes of the probe were observed in the presence of water vapour. Such behaviour indicated that there was no reaction between 2 and these gases tested, thus rendering 2 a suitable selective probe for the detection of NO_2. In a final experiment the membrane containing 2 was introduced into a container with all the studied vapours for 24 h yet no change in the colour of the probe was observed. In contrast, when the same experiment was carried with the additional presence of NO_2 the expected colour change took place.

In summary, we reported herein a simple probe based on a BODIPY derivative that was able to chromo-fluorogenically detect the presence of NO_2 both in solution and in air. In particular, the reaction of probe 2 with

NO$_2$ induced in the transformation of the oxime to an aldehyde. The conversion of 2 in 1 resulted in a hypsochromic shift of the absorption band concomitantly with a colour change from pink to orange. In addition, a strong enhancement of the fluorescence emission together with a blue shift of the band was also observed rendering 2 a fluorimetric off-on sensing method for NO$_2$. Notably the signalling ability of 2 was also retained when incorporated onto polyethylene oxide membranes, which allowed the development of simple test strips for the chromo-fluorogenic sensing of NO$_2$ in air with a limit of detection of ca. 0.1 ppm. In addition, probe 2 was highly selective and allowed the optical detection of NO$_2$ in presence of other pollutant gases, water vapour and volatile organic compounds.

Acknowledgements

References

1 Heinsohn R. J.; Kabel R. L., *Sources and Control of Air Pollution*, Ed. Prentice Hall, **1999**.

2 Tunnicliffe, W. S.; Burge, P.S; Ayres, J.G. *Lancet*, **1994**, *344*: 1733-1736.

3 Shima, M.; Adachi M. *International journal of epidemiology*, **2000**, *29*, 862-870.

4 U.S. Environmental Protection Agency (EPA). Office of Environmental Health Hazard Assessment (OEHHA). Non-cancer Health Effects (RELs). [California, DC, USA]: **1999**.

5 Mukherjee A., Prasanna M., LaneM. , Go R., Dunayevskiy A., Tsekoun A., and Kumar C., Patel N., *Applied Optics*, **2008**, *47*, 4884-4887.

6 Venema, A., Nieuwkoop E., Vellekoop M.J., Nieuwenhuizen M.S., Barendsz A.W., *Sensors and Actuators,* **1986**, *10*, 47-64.

7 (a) Md. Nomani W.K., Kersey D., James J., Diwan D., Vogt T., Webb R. A, Koley G., *Sensors and Actuators B: Chemical*, **2011**, *160*, 251-259 (b) Zhang D., Liu Z., Li C., Tang T., Liu X., Han S., Lei B., Zhou C., *Nano Letters*, **2004**, *4*, 1919–1924 (c) Sun-Woo C., Katoch A., Wu P., Sang Sub K., *J. Mater. Chem. C*, **2013**, *1*, 2834-2841. (d) Liang X., Yang S., Li J., Zhang H., Diao Q., Zhao W., Lu G., *Sensors and Actuators B* , **2011**, *158*, 1-8.

8 Wang R., Li G., Dong Y., Chi Y., Chen G., *Anal. Chem.*, **2013**, *85*, 8065-80699.

9 Chung M. G., Kim D. H., Lee H. M., Kim T., Choi J. H., Seo D. K., Yoo J.-B., Hong S.-H., Kang T. J., Kim Y. H., *Sensors and Actuators B*, **2012**, 172-176.

10 Ohira S, Wanigasekara E, Rudkevich DM, Dasgupta P.K. *Talanta,* **2009,** *77*, 14-20.

11 Mokhari J., Naimi-Jamal M. R., Hamzehal H.. 11th international Electronic Conference on Synthetic Organic Chemistry (ECSOC-11) 1-30 November **2007**.

12 (a) Boens N., Leen V., Dehaen W. *Chem. Soc. Rev.*, **2012**, *41*, 1130-1172 (b) Wang D., Shiraishi Y., Hiari T., *Tetrahedron Lett.,* **2010**, *51*, 2545-2549; (c) X. Xie, Y. Qin, *Sens. Actuat. B-Chem.,* **2011***, 156,* 213-217; (d) Wang D., Shiraisi Y., Hirai T., *Chem. Comm.,* **2011**, *47*, 2673-2675; (e) Sun H. B., Liu S. J., Ma T. C., Song N. N., Zhao Q., W. Huang, *New J. Chem*, **2011**, *35*, 1194-1197; (f) Son H., Lee J. H., Kim Y. R., Han S., Liu X., Jaworski J., Jung H., *Analyst*, **2012**, *137*, 3914-3916. (g) Lu H., Mack J., Yang Y., Shen Z. *Chem Soc Rev.* **2014**, *43*, 4778-4823.

13 (a) Loudet A., Burgess K., *Chem. Rev.*, **2007**, *107*, 4891-4932; (b) Ulrich G., Ziessel R., Harriman A.*, Angew. Chem., Int. Ed*., **2008**, *47,* 1184-1201.

14 Jiao L., Yu C., Li J., Wang Z., Wu M., Hao E., *J. Org. Chem*. **2009**, *74*, 7525-7528.

15 Cheng G., Fan J., Sun W., Sui K., Jin X., Wang J., Peng X., *Analyst*, **2013**, *138*, 6091-6096.

Supporting information

Experimental Section
General remarks

CH_2Cl_2 and CH_3CN were distilled from P_2O_5 under Ar prior to use. Silica gel 60 F254 (Merk) plates were used for TLC. Colum chromatography was performed on silica gel (60, 40-63 micras). ^{1}H NMR, ^{13}C NMR (300 MHz) spectra were determined on a Bruker AV 300 spectrometrer. Chemical shifts are reported in parts per million (ppm), calibrated to the solvent peak set. High-resolution mass spectra were recorded in the positive ion mode with a VG-AutoSpec mass spectrometer. Absorption and fluorescence spectra were recorded using a Shimadzu UV-2600 spectrophotometer and a Varian Cary Eclipse spectrofluorimeter. 8-phenyl-1,3,5,7-tetrametilboron dipyirromethene (Ph-BDP) was prepared following the procedure described in reference 15.

Synthesis and characterization of BODIPY derivatives

Synthesis of 2-formyl-8-phenyl-1,3,5,7-tetramethylboron-dipyrromethene (1)

1
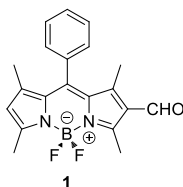
12 mL of a (1:1) mixture of DMF and $POCl_3$ were placed in a round bottom flask. A solution of 200 mg of Ph-BDP (0.62 mmol) in 60 mL of 1,2-dichloroetane was added to the flask under argon atmosphere. The mixture was stirred and heated at 60º C for 2 h. The reaction was cooled at room temperature and then, 15-20 mL of an aqueous solution of $NaHCO_3$ 1M at 0º were added. The mixture was stirred for 30 minutes and then the organic phase was separated, washed with water, dried with $MgSO_4$ and evaporated. The product was purified by column chromatography (hexane-ethyl acetate) to give a solid (0.05 g, 20%). m.p.= 208-210ºC; ^{1}H NMR (300 MHz, CDCl₃) δ 10.01 (s, 1H), 7.57 – 7.49 (m, 3H), 7.32 – 7.26 (m, 2H), 6.15 (s, 1H), 2.82 (s, 3H), 2.62 (s, 3H), 1.64 (s, 3H), 1.43 (s, 3H);^{13}C NMR (75 MHz, CDCl₃) ^{13}C NMR (126 MHz, CDCl3) δ 158.08, 154.10, 145.04, 144.83, 142.42, 139.99, 134.72, 132.51, 130.54, 129.27, 127.94, 122.46, 121.44, 14.80, 14.59, 13.96, 12.34.; HRMS (EI): m/z (%) calc for $C_{20}H_{19}BF_2N_2O$: 352.1559 [M+1]$^+$ found: 353.16. UV-Vis (CH_3CN λ_{max}/nm) 491; emission (CH_3CN λ_{max}/nm, λ_{exc} 485) 512.

Synthesis of probe 2.
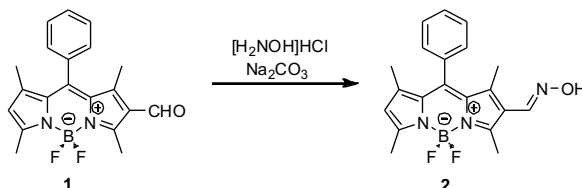
0.7116 g (2 mmol) of 2-formyl-8-phenyl-1,3,5,7-tetramethylboron dipyrromethene (**1**) and 0.161 g (2,2 mmol) of hydroxylamine hydrochloride were dissolved in 45 mL of ethanol. 0.84 g of sodium carbonate dissolved in 40 mL of ethanol:water (5:1) were added to the previously prepared solution. The reaction was stirred for 3 h and followed by TLC (dichloromethane:ethyl acetate (10:2)). The ethanol was evaporated and the residue was dissolved in diethyl ether (4x40mL). The organic phase was washed with 30 mL of brine and 30 mL of water and dried with MgSO$_4$. The evaporation of the solvend gave the wanted product that was purified by columm chromatography (dichoromethane:ethyl acetate (9:1) to give a final solid (0,052 g, 7%); m. p. = 236-238 ºC; ^{1}H NMR (300 MHz, CDCl$_3$) δ 8.09 (s, 1H), 7.57 − 7.47 (m, 3H), 7.41 − 7.27 (m, 2H), 6.04 (s, 1H), 5.30 (s, 1H), 2.71 (s, 3H), 2.60 (s, 3H), 1.46 (s, 3H), 1.38 (s, 3H). ^{13}C NMR (75 MHz, CDCl$_3$) 13C NMR (101 MHz, CDCl$_3$) δ 185.65, 170.90, 161.49, 156.46, 147.12, 143.52, 142.84, 134.11, 129.42, 127.67, 126.29, 123.87, 14.77, 13.99, 12.85, 11.33.; HRMS (EI): m/z (%) calc for C$_{20}$H$_{20}$BF$_2$N$_3$O: 367.1667 [M+1]$^+$ found: 368.17. UV-Vis (CH$_3$CN λ$_{max}$/nm) 512; emission (CH$_3$CN λ$_{max}$/nm, λ$_{exc}$ 500) 560.

Spectroscopic studies: All the solvents were purchased at spectroscopic grade from Aldrich Chemicals Co., used as received, and were found to be free of fluorescent impurities. Absorption and fluorescence spectra were recorded using a Shimadzu UV-2600 spectrophotometer and a Varian Cary Eclipse spectrofluorimeter, respectively. Fluorescence quantum yields were measured at room temperature in the N$_2$-purgued solution in relation to rhodamine B at 500 nm for **2** and in relation to fluorescein at pH= 8.06 at 490 nm for **1**. The fluorescence quantum yields were calculated from Eq. (1). Here F denotes the integral of the corrected fluorescence spectrum, A is the absorbance at the excitation wavelength, and n is the refractive index of the medium.

$$\Phi_{exp} = \Phi_{ref} \frac{F\{1 - exp(-A_{ref}ln10)\}n^2}{F_{ref}\{1 - exp(-A\,ln10)\}n_{ref}^2}$$

General Procedure for limit of detection (LOD) determinations

Increasing amounts of the corresponding gas) were added to probe **2** in acetonitrile (10^{-5} M. The UV-vis and fluorescence spectra were recorded in 1-cm path length cells at 25 ºC (termostatted). Representation of absorbance/fluorescence at the appropriate wavelength vs. concentration of NO_2 allowed the limit of detection to be calculated.

$$LOD = \frac{3S_b}{m}$$

Membrane Preparation

Polyethylene oxide (2 g, Mw 400,000 Dalton) was slowly added to a solution of **2** (10^{-3} M solution) in dichloromethane (40 mL). The mixture was stirred until a highly viscous mixture was formed. This mixture was poured into a glass plate (40 cm^2) and kept in a dry atmosphere for 24 h.
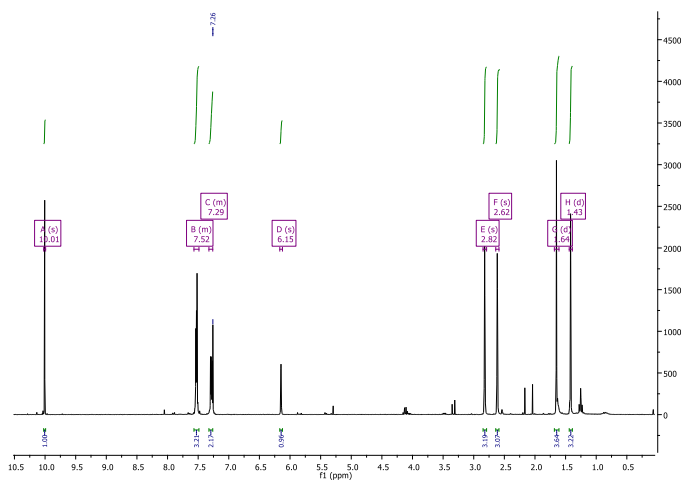
Figure S.1. ^{1}H NMR spectrum of **1** in CDCl$_3$.
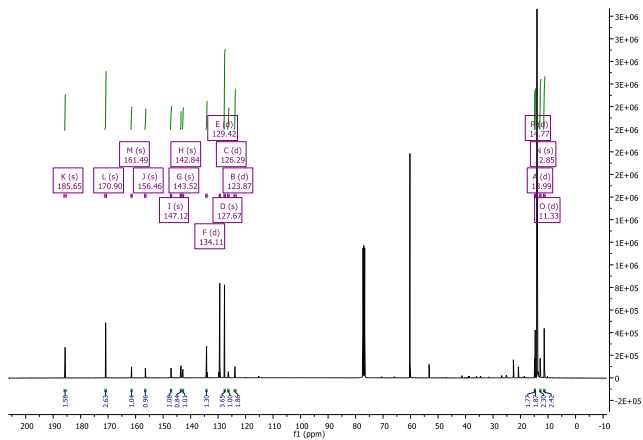
Figure S.2. ^{13}C NMR spectrum of **1** in CDCl$_3$.
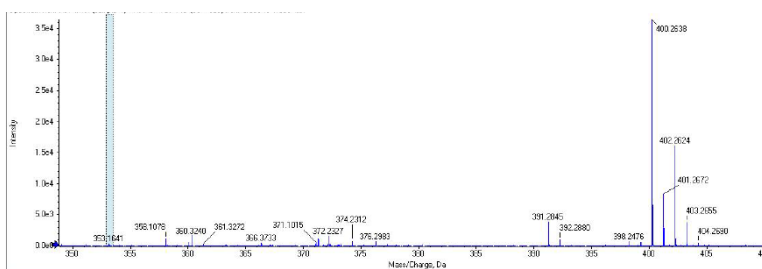
Figure S.3 HRMS of **1**.

Figure S.4. ^{1}H NMR spectrum of probe **2** in CDCl$_3$.

104
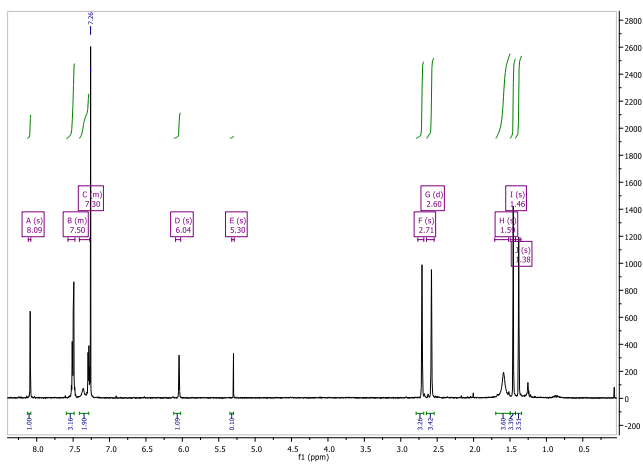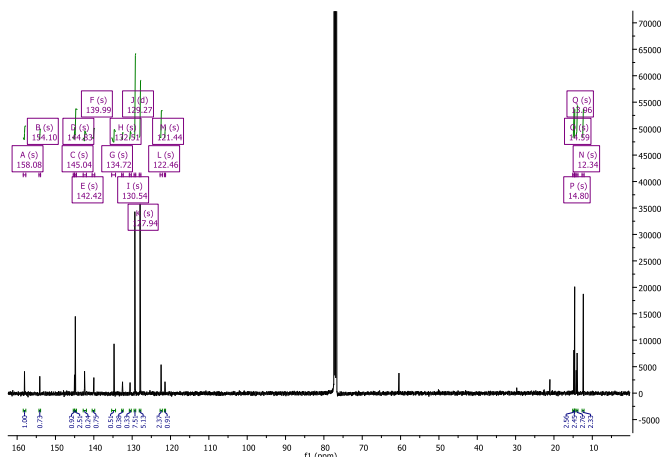
Figure S.5. ^{13}C NMR spectrum of probe **2** in CDCl$_3$.
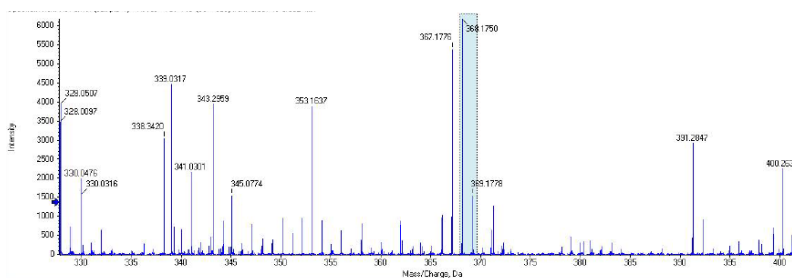
Figure S.6 HRMS of probe **2**.
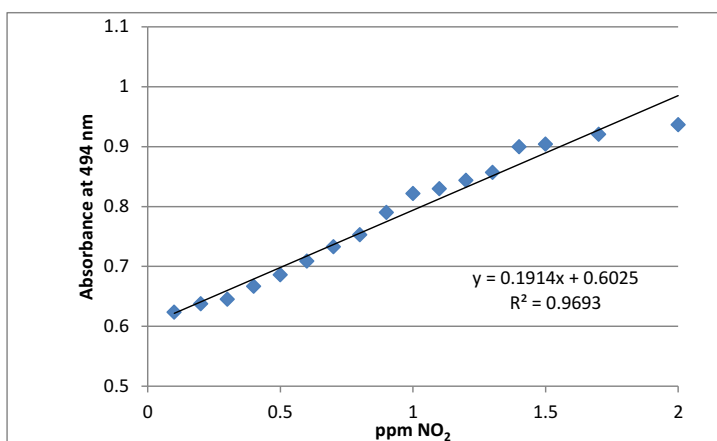
Figure S-7. Absorbance at 494 nm of **2**+**NO₂** (1.0 x 10^{-5}M in acetonitrile) *versus* increasing amounts of NO$_2$ at room temperature.

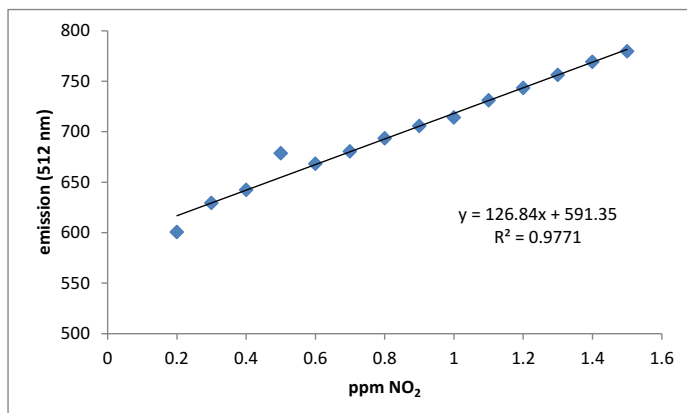Figure S-8. Emission at 512 mn of **2**+**NO₂** (1.0 x 10^{-5}M in acetonitrile) *versus* increasing amounts of NO_2 at room temperature.
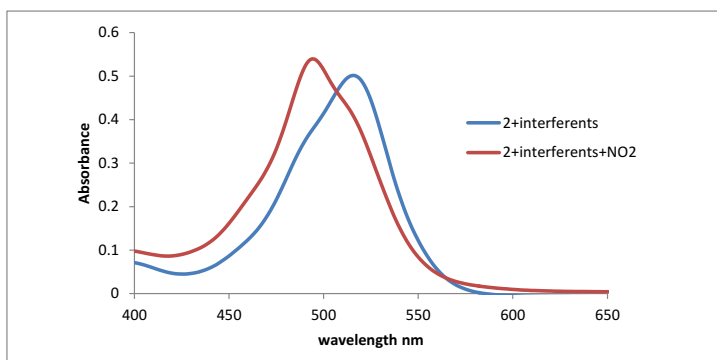
Figure S-9**.** UV spectra of probe **2**+interferents (CO_2+NO+H_2S+SO_2) and probe **2** in the presence of interferents plus NO_2.

3-Formyl-BODIPY phenylhydrazone as chromo-fluorogenic probe for selective detection of NO₂ (g)

L. Alberto Juárez,[a,b] Ana M. Costero,*[a,b,c] Margarita Parra,[a,b,c] Pablo Gaviña,[a,b,c] and Salvador Gil[a,b,c]

[a] Centro de Reconocimiento Molecular y Desarrollo Tecnológico (IDM), Unidad Mixta Universidad Politécnica de Valencia-Universidad de Valencia, Spain.
[b] Departamento de Química Orgánica. Universidad de Valencia, Doctor Moliner 50, 46100, Burjassot, Valencia, Spain. E-mail: ana.costero@uv.es
[c] CIBER de Bioingeniería, Biomateriales y Nanomedicina (CIBER-BBN).

Abstract: A new colorimetric and fluorogenic probe, based on a 3-formyl boron dipyrromethene (BODIPY) phenylhydrazone, for the sensitive and selective detection NO_2 (g) has been prepared. The probe in solution experiences a remarkable hypsochromic shift of its absorption and fluorescence emission bands in the presence gaseous NO_2 (g), leading to limits of detection of few ppb. The probe also works in the solid phase, adsorbed on filter paper strips, or chemically immobilized on the surface of silica nanoparticles, with limits of detection to the naked eye of about 0.5 ppm.

Nitrogen dioxide (NO_2) is a dangerous gas that has direct and indirect adverse health effects. Long-term exposure to NO_2 is associated with increased susceptibility to lower respiratory tract illness and increased risk of chronic obstructive pulmonary disease mortality.[1] In addition, NO_2 exposure is a potential inducer of neurological diseases.[2] Nitrogen dioxide appears in both indoor and outdoor air. Outdoor NO_2 is produced mainly by road traffic and other fossil fuel combustion processes at high temperatures. NO_2 in indoor air is generated from various sources such as indoor combustion, tobacco smoking and infiltration from outdoors.[3] The indoor reported concentrations of NO_2 vary significantly depending on environmental factors, such as the ventilation rate, burning time, and the source and strength of combustion.[4] Moreover, low air-exchange rates result in higher levels of indoor NO_2 which persist for longer times.[5] In this sense, the European Commission's Scientific Committee on Occupational Exposure Limits (SCOEL) has approved exposure limits of 0.5 ppm (8-hour time-weighted average) and 1 ppm (15-min short-term exposure limit) for NO_2.[6]

Due to the ubiquitous presence of this gas and its health effects, the development of selective and sensitive methods for its detection and quantification is a hot area of research. Several methods for NO_2 detection, such as potentiometric, [7] surface plasmon resonance (SPR),[8] laser-photoacoustic spectroscopy,[9] surface acoustic wave (SAW),[10] or transition metal oxide devices.[11] However these methods still show certain limitations such as limited selectivity, operational complexity, non-portability or difficulties in real-time monitoring.
In consequence, there is an interest in the design of new sensors capable of detecting NO_2 easily and with high selectivity. In this context, chromo-fluorogenic probes are highly appealing for real-time monitoring because they require of inexpensive instrumentation, and in the case of chromogenic probes, the colour modulation can be observed to the naked eye. Suslick and others have developed the use of arrays of

chemically responsive pigments for the colorimetric detection of volatile compounds (optoelectronic noses).[12] However, despite the inherent advantages of optical probes, there are very few reported examples of colorimetric or fluorescent probes which are specific for NO_2 detection.[13]
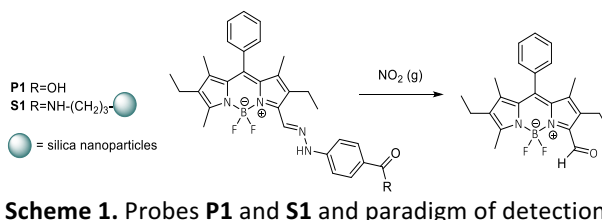
Scheme 1. Probes **P1** and **S1** and paradigm of detection.

Following our interest in the development of new chromo-fluorogenic probes for toxic gases, we have recently reported an oxime-containing BODIPY derivative as colorimetric and fluorescent probe for NO_2 detection in air.[13d] The detection reaction was based on the oxidative cleavage of the oxime into the corresponding aldehyde under very soft conditions,[14] resulting in a hypsochromic shift of the UV-vis absorption and fluorescence emission bands. In order to extend the applicability of this kind of systems, we report herein a new chromo-fluorogenic probe (**P1**) for the selective detection of NO_2 (g), based on the same sensing principle, which can be used in solution and supported on silica surfaces. Probe **P1** consists of a 3-formyl-BODIPY phenylhydrazone in which the phenyl ring of the hydrazone moiety bears a carboxylic group in *para*-position (see Scheme 1). The transformation of the hydrazone into the corresponding free aldehyde in the presence of NO_2 results in a significant bathochromic shift of the maximum absorption band in the UV-vis spectrum and in a noticeable fluorogenic response. In addition, the carboxylic acid on the phenyl ring of the hydrazine moiety allows the attachment of the probe on the surface of silica nanoparticles through covalent bonds (Scheme 1).

Firstly, studies were carried out with probe **P1**. The synthesis of **P1** is depicted in Scheme 2. Condensation of benzaldehyde with 3-ethyl-2,4-dimethylpyrrole, followed by oxidation with DDQ, deprotonation with TEA and treatment with boron trifluoride led to meso-phenyl BODIPY **1** according to literature reports.[15] Subsequently, one methyl group at the 3- position was selectively oxidized with DDQ in THF/H_2O to give the corresponding aldehyde **2**.[16] Finally, the treatment of **2** with 4-hydrazinobenzoic acid in refluxing ethanol gave the phenylhidrazone

derivative **P1** in almost quantitative yield. **P1** was fully characterized by ^{1}H NMR, ^{13}C NMR and MS (see Supporting Information for details).
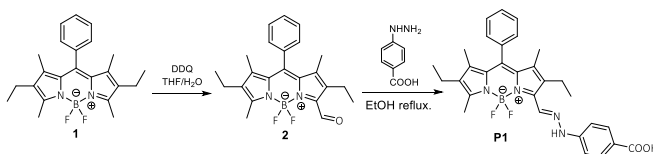
Scheme 2. Synthesis of P1

The UV-vis spectrum of **P1** (1.0 x 10^{-5} M in acetonitrile) shows an intense absorption band at 599 nm (log ε= 4.5) and a shoulder at shorter wavelength (ca. 535 nm). **P1** is also fluorescent. Its emission spectrum shows a maximum at 629 nm (λ_{exc} = 595 nm, Φ = 0.87) similarly to other BODIPY dyes.
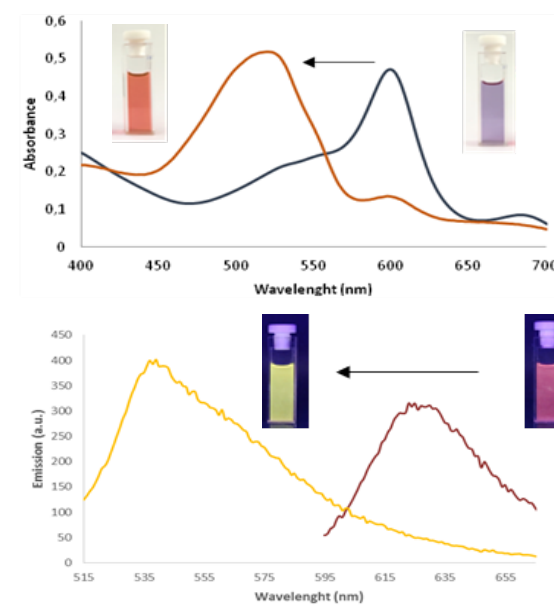
Figure 1. a) UV-Vis spectra of **P1** (acetonitrile, 1.0 x 10^{-5} M) in the absence and in the presence of NO₂ gas (1 ppm) for 5 min. Inset: visual changes observed for **P1** before and after exposure to 1 ppm of NO₂ gas. b) Fluorescence spectra of **P1** (acetonitrile, 1.0 x 10^{-5} M) in the absence (λ_{exc} = 590 nm) and in the presence (λ_{exc} = 515 nm) of NO₂ gas (1 ppm) for 5 min. Inset: visual changes (λ_{exc} = 254 nm) observed for **P1** before and after exposure to 1 ppm of NO₂ gas.

To study the response of **P1** towards gaseous NO_2, acetonitrile solutions of **P1** (1.0×10^{-5} M) were exposed to an air atmosphere containing 1 ppm of NO_2 (provided by a commercially available NO_2 cylinder diluted with N_2). After 5 min of exposure, a hypsochromic shift of the absorption band from 599 nm to 515 nm (log ε= 4.8) was observed (see Figure 1a). Moreover a remarkable change in the fluorescence emission spectrum was also observed (see Figure 1b); in the presence of NO_2 the emission at 630 nm disappeared and a new slightly higher emissive band at 545 nm (λ_{exc} = 515 nm, Φ = 0.89) evolved. These remarkable chromogenic and fluorogenic responses were visible to the naked eye (see insets in Figures 1a and 1b), and can be attributed to the transformation of **P1** into the corresponding aldehyde **2**.

Detection limits for the reaction of NO_2 with **P1** in acetonitrile were evaluated by titration experiments using UV-vis absorption and fluorescence emission spectroscopies (see Supporting Information). The titration experiments were carried out by exposing an acetonitrile solution of **P1** (1.0×10^{-5} M) to an air atmosphere containing increasing amounts of NO_2 (g) for 5 min. UV-vis limit of detection (LOD) was calculated from the plot of the ratio of the absorbance intensities at 599 and 515 nm (A_{599}/A_{515}) versus NO_2 concentration, whereas for fluorescence, the LOD was obtained from the plot of the emission peak intensity at 545 nm vs concentration of NO_2 (g) (see Figure S11 and S12). LODs were calculated by using the expression LOD= $3s_b/m$, in which s_b is the standard deviation of blank measurements and m is the slope of the linear regression plot.[17] Limits of detection of 2.9 ppb (from UV-vis) and 5.6 ppb (from fluorescence) were determined. These LODs are lower than the alert threshold of 400 $\mu g/m^3$ (0.2 ppm) established by the European Union for nitrogen dioxide [18]
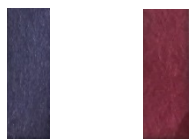

Figure 2. Filter paper strips with probe **P1** before (right) and upon exposure to 1 ppm of NO_2 (g) for 5 min. (left)

Encouraged by the sensitive response observed with **P1** in acetonitrile, in an attempt to extend its application to real-time monitoring, we decided to develop a simple test with filter paper strips for the colorimetric detection of NO_2 in air. To this end, filter paper strips containing **P1** were prepared immersing a common filter paper strip in an acetonitrile

solution of **P1** (10^{-3} M) and then drying in the air. After exposure of the films to 1 ppm of NO_2 (g) for few minutes, a significant colour change from dark blue to red was observed (Figure 2).
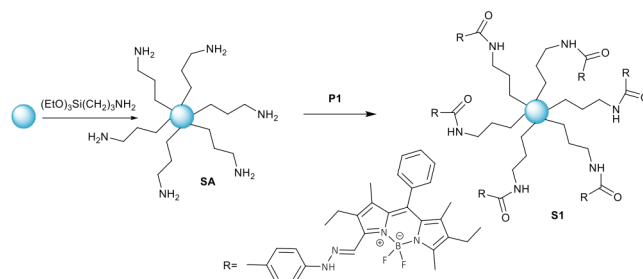

Figure 3. Preparation of BODIPY-immobilized silica nanoparticles.

In a further step to obtain supported colorimetric probes for NO_2 (g), **P1** was immobilized on the surface of silica nanoparticles to give **S1** as described in Figure 3. Aminopropyl coated silica nanoparticles **SA** were prepared from commercially available silica nanoparticles (LUDOX® (Aldrich), see Supporting Information) by reaction with (3-aminopropyl)trimethoxysilane in a water/ethanol/acetic mixture at reflux for 72 h, following the procedure reported by Montalti.[19] On the other hand, the carboxylic group of the BODIPY probe **P1** was transformed into the corresponding acid chloride by reaction with oxalyl chloride in dichloromethane. This compound was then added to a suspension of **SA** in ethanol and the mixture was refluxed overnight, to yield **S1** as a green solid. The silica supported BODIPY-phenylhydrazone probe **S1** was characterized by Transmission Electron Microscopy (TEM) and elemental analysis. TEM images for all the prepared nanoparticles showed a very homogeneous particle size (15-18 nm, see Supporting Information). The BODIPY content of the silica nanoparticles was estimated to be 0.017 mmol of BODIPY per g SiO_2 from elemental analysis.

To check the response of **S1** in the presence of NO_2 (g), air containing 0.5 ppm of NO_2 was bubbled through a suspension of **S1** in acetonitrile. A strong fluorescence of the acetonitrile solution was observed with an emission band at 544 nm, corresponding to the emission of the resulting BODIPY-aldehyde **2**, which is liberated to the solution upon reaction of **S1** with NO_2. The intensity of the band at 544 nm increased with increasing the NO_2 (g) concentration as can be seen in Figure 4. In addition, a significant colour change of the resulting nanoparticles, from green to yellow ochre, was clearly detectable by naked eye after exposure of the

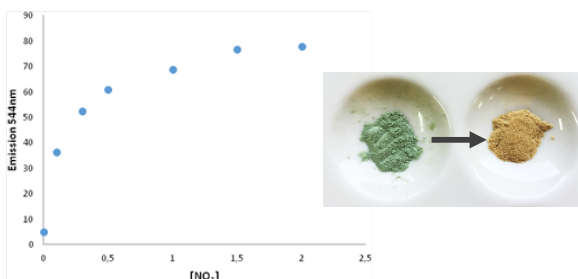solid nanoparticles to 0.5 ppm of NO_2 in a glass cylinder during 5 min (inset Figure 4).

Figure 4. Emission of a suspension of **S1** (1.0 x 10^{-6} M in acetonitrile) at 544 nm (λ_{exc} = 515 nm) in the presence of increasing concentration of NO_2 (g). Inset: Visible colour change of **S1** after exposure of the solid to 0.5 ppm NO_2 (g).

One important issue in relation to the design of probes for pollutant gases is the role played by potential interferents or false-positive outcomes produced by other species. Bearing this in mind, the reactivity of **S1** with other hazardous gases (i.e. NO, CO_2, H_2S, SO_2 up to 100 ppm each) was also studied. Moreover, the probe was also tested in the presence vapours of acetone, hexane, chloroform, acetonitrile and toluene (up to 100 ppm in air). No emission changes neither changes in colour were observed in the presence of any of the studied interferents. In addition, a remarkably good response to NO_2 was observed even in the presence of these compounds (Figure 5). Such behaviour indicated that **S1** is a suitable selective probe for the detection of NO_2 in real environments.
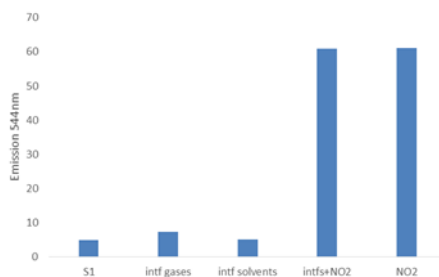

Figure 5. Interference studies of **S1** with hazardous gases, most common VOC's and competitive studies.

In conclusion a new chemodosimeter (**P1**) for detecting NO_2 (g) has been prepared with good yield. The sensing mechanism is based on the transformation of a phenylhydrazone into the corresponding free aldehyde in the presence of nitrogen dioxide, which induces strong changes in the optical properties of the BODIPY core. The probe is able to detect NO_2 (g) both in solution and adsorbed on filter paper strips. In the presence of the analyte, strong changes in colour were observed by naked-eye. Limits of detection (2.9 ppb from UV-vis measurements and 5.6 ppb from fluorescence emission) where lower than those obtained with our previous oxime-containing BODIPY probe.[13d] In addition, a new material **S1** has also been prepared by immobilizing **P1** on the surface of silica nanoparticles through covalent bonds and has been used for detecting the gas both is suspension and in solid state. Visual colour changes of the functional material **S1** (from green to yellow ochre) were observed in the presence of air contaminated with 0.5 ppm of NO_2. No changes in the probe properties were observed in the presence of up to 100 ppm of several possible interferents such as NO, CO_2, H_2S, SO_2, vapours of acetone, hexane, chloroform, acetonitrile and toluene.

Acknowledgements

References

[1]   a) M. Shima, M. Adachi, *Int. J. Epidemiol.* **2000**, *29*, 862–870 b) X. Meng, C. Wang, D. Cao, C.M. Wong, H. Kan, *Atmos. Environ.* **2013**, *77*, 149–154.
[2]   H. Li, L. Chen, Z. Guo, N. Sang, G. Li, *J. Hazard. Mater*. **2012**, *225–226*, 46–53.
[3]   SS. Park, S.Y. Cho, *J. Air Waste Manage. Assoc*. **2010,** *60*, 1434–1442.
[4]   a) K. Lee, X. Jianping, A. S. Geyh, H. Oxkaynak, B. P. Leaderer, C. J. Weschler, J. D. Spengler, *Environ. Health Perspect*. **2002**, *110*, 145–149; b) J. D. Spengler, M. Brauer, J.M. Samer, W.E. Lambert, *Environ. Sci. Technol.* **1993**, *27*, 841–845.
[5]   S. S. Park, J. H. Hong, J. H. Lee, Y. J. Kim, S. Y. Cho, S. J. Kim, *Atmos. Environ.* **2008**, *42*, 6586–6596.
[6]   European Commission. Scientific Committee on Occupational Exposure Limits (SCOEL). Recommendations for Nitrogen Dioxide. SCOEL/ SUM/ 53. June 2014.
[7]   F. Opekar, K. Stulik, *Crit. Rev. Anal. Chem.* **2002**, *32*, 253–259.
[8]   J. Brubet, V. P. Garcia, A. Pauly, C. Varenne, B. Lauron, *Sens. Actuators, B* **2008**, *134*, 632–639.
[9]   A. Mukherjee, M. Prasanna, M. Lane, R. Go, I. Dunayevskiy, A. Tsekoun, C. Kumar, N. Patel, *Applied Optics* **2008**, *47*, 4884–4887.
[10]   A. Venema, E. Nieuwkoop, M. J. Vellekoop, M. S. Nieuwenhuizen, A. W. Barendsz, *Sens. Actuators*, **1986**, *10*, 47–64.
[11]   b) X. Liang, S. Yang, J. Li, H. Zhang, Q. Diao, W. Zhao, G. Lu, *Sens. Actuators, B* **2011**, *158*, 1–8; c) D, Zhang, Z, Liu, C, Li, T, Tang, X, Liu, S, Han, B, Lei, C, Zhou, *Nano Lett.* **2004**, *4*, 1919–1924; d) S-W. Choi, A. Katoch, G. J. Sun, P. Wu, S. S. Kim, *J. Mater. Chem. C* **2013**, *1*, 2834–2841.
[12]   a) D. Filippini, A. Alimelli, C. Di Natale, R. Paolesse, A. D'Amico, I. Lundström, *Angew. Chem. Int. Ed.* **2006**, *45*, 3800–3803; b) S. H. Lim, L. Feng, J. W. Kemling, C. J. Musto, K. S. Suslick, *Nat. Chem.* **2009**, *1*, 562–567; c) L. Feng, C. J. Musto, J. W. Kemling, S. H. Lim, K. S. Suslick, *Chem. Commun.* **2010**, *46*, 2037–2039.
[13]   a)Y. Yan, S. Krishnakumar, H. Yu, S. Ramishetti, L-W. Deng, S. Wang, L. Huang, D. Huang, *J. Am. Chem. Soc.* **2013**, *135*, 5312–5315; b) B. Mondal, V. Kumar, *RSC Adv.* **2014**, *4*, 61944–61947; c) Y. Yan, J. Sun, K. Zhang, H. Zhu, H. Yu, M. Sun, D. Huang, S. Wang, *Anal. Chem.* **2015**, *87*, 2087–2093; d) L. A. Juárez, A. M. Costero, M. Parra, S. Gil, F. Sancenón, R. Martínez-Máñez, *Chem. Commun.* **2015**, *51*, 1725–1727; e) L. A. Juárez, A. M. Costero, F. Sancenón, R. Martínez-Máñez, M. Parra, P. Gaviña, *Chem. Eur. J.* **2015**, *21*, 8720–8722.
[14]   a) S. B. Shim, K. Kim, Y. H. Kim, *Tetrahedron Lett.*, **1987**, *28*, 645–648; b) J. Mokhari, M. R.Naimi-Jamal, H. Hamzehal presented in part at 11th International Electronic Conference on Synthetic Organic Chemistry (ECSOC-11), November **2007**.
[15]   G. Barin, M. D. Yilmaz, E. U. Akkaya, *Tetrahedron Lett*. **2009**, *50*, 1738–1740.
[16]   Y. Zhang, S. Swaminathan, S. Tang, J. García-Amorós, M. Boulina, B. Captain, J. D. Baker, F. M. Raymo, *J. Am. Chem. Soc.* **2015**, *137*, 4709–4719.
[17]   M. Zhu, M. Yuan, X. Liu, J. Xu, J. Liv, C. Huang, H. Liu, Y. Li, S. Wand, D. Zhu, *Org. Lett*. **2008**, *10*, 1481–1484.
[18]   European Commission, Air Quality Standards, http://ec.europa.eu/environment/air/quality/standards.htm (accessed February 2016),
[19]   M. Montalti, L. Prodi, N. Zacheronni, G. Falini, *J. Am. Chem. Soc*. **2002**, *124*, 13540–13546.

Supporting information

General procedures

All reagents were commercially available, and were used as received. CH$_2$Cl$_2$ and CH$_3$CN were distilled from P$_2$O$_5$ under Ar prior to use. Acetonitrile used for spectroscopic measurements was spectroscopic grade, and free of fluorescent impurities. BODIPY derivatives **1** and **2** were prepared acording to literature procedures.[91] Silica gel 60 F254 (Merk) plates were used for TLC. Column chromatography was performed on silica gel (60, 40-63 micras). ^{1}H NMR and ^{13}C NMR spectra were recorded with a Bruker AV 300 spectrometrer. Chemical shifts are reported in ppm, calibrated to the solvent peak set. High-resolution mass spectra were recorded in the positive ion mode with a VG-AutoSpec mass spectrometer. Absorption and fluorescence spectra were recorded with a Shimadzu UV-2600 spectrophotometer (using a 1 cm path length quartz cuvette) and a Varian Cary Eclipse spectrofluorimeter respectively. Fluorescence quantum yields were measured at room temperature in the N$_2$-purged solution in relation to rhodamine B (Φ_{EtOH} = 0.49) at 525 nm for **2** and rhodamine 101 (Φ_{EtOH} = 1) at 625 for **P1.** The fluorescence quantum yields were calculated from Eq. (1), where F denotes the integral of the corrected fluorescence spectrum, A is the absorbance at the excitation wavelength, and n is the refractive index of the medium.

$$\Phi_{exp} = \Phi_{ref} \frac{F\{1 - exp(-A_{ref} ln10)\}n^2}{F_{ref}\{1 - exp(-A\, ln10)\}n_{ref}^2}$$

Compound 2

^{1}H NMR (300 MHz, CDCl$_3$) δ 10.39 (t, J = 2.0 Hz, 1H), 7.54 – 7.50 (m, 3H), 7.30–7.25 (m, 2H), 2.70 (q, J = 7.5 Hz, 2H), 2.64 (s, 3H), 2.35 (q, J = 7.6 Hz, 2H), 1.36 (s, 3H), 1.26 (s, 3H), 1.01 (t, J = 7.5 Hz, 6H). ^{13}C NMR (75 MHz, CDCl$_3$) δ 179.8, 135.1, 132.9, 129.7, 129.1, 129.0, 128.2, 17.9, 17.5, 14.7, 14.4, 12.6, 10.8.HRMS (ESI): m/z calcd. for C$_{23}$H$_{26}$BF$_2$N$_2$O [M+H]$^+$: 395.2101, found 395.2096

UV-Vis (CH$_3$CN), λ_{max}= 515 nm; emission (CH$_3$CN) λ_{max}= 545 nm (λ_{exc} 515 nm). $\Phi_{(RhB)}$ = 0.89.

---

[91] Y. Zhang, S. Swaminathan, S. Tang, J. García-Amorós, M. Boulina, B. Captain, J. D. Baker, F. M. Raymo, *J. Am. Chem. Soc.* **2015**, *137*, 4709–4719.

Synthesis of P1

4-Hydrazinobenzoic acid (8 mg, 0.051 mmol) was added to a solution of **2** (20 mg, 0.051 mmol) in EtOH (20 mL) and the mixture was stirred at reflux overnight. Then the solution was cooled to room temperature and the resulting precipitate was isolated by filtration, washed with EtOH and dried at 70 °C for 12 h to obtain **P1** as dark blue solid with quantitative yield.

^{1}H NMR (500 MHz, CDCl$_3$) δ 8.43 (br.s., 1H), 8.37 (br.s., 1H), 8.01 (d, J = 8.7 Hz, 2H), 7.53–7.47 (m, 3H), 7.31–7.28 (m, 2H), 7.05 (d, J = 8.7 Hz, 2H), 2.79 (d, J = 7.4 Hz, 2H), 2.57 (s, 3H), 2.33 (d, J = 7.6 Hz, 2H), 1.31 (s, 6H), 1.14 (t, J = 7.4 Hz, 3H), 1.00 (t, J = 7.6 Hz, 3H). ^{13}C NMR (126 MHz, CDCl$_3$) δ 171.1, 156.7, 148.3, 144.4, 140.1, 140.0, 138.2, 135.6, 134.4, 134.1, 132.4, 130.3, 129.3, 129.1, 128.6, 128.5, 120.9, 112.2, 17.3, 14.6, 13.9, 13.0, 12.0, 11.2.

HRMS (ESI): m/z calcd. for C$_{30}$H$_{32}$BF$_2$N$_4$O$_2$ [M+H]$^{+}$: 529.2586; found 529.2577.

UV-Vis (CH$_3$CN), λ_{max} = 599 nm; emission (CH$_3$CN) λ_{max} = 629 nm (λ_{exc} 595 nm). $\Phi_{(Rh101)}$ = 0.87.

Preparation of SA

A colloidal dispersion of LUDOX AS-30 silica nanoparticles (12 mL) was added to a mixture of H$_2$O (60 mL) acetic acid (60 mL) and EtOH (100 mL). Then (3-aminopropyl)triethoxysilane (3.5 mL, 15 mmol) was added to the nanoparticle suspension and the resultant mixture refluxed at 80 °C under argon for 3 days. Ethanol was removed by evaporation under reduce pressure and the nanoparticles were isolated by filtration. The resulted solid was washed with pure water, acetone and dried at 85 °C for 1 day.

Synthesis of S1

Oxalyl chloride (50 μL, 0.04 mmol) was added dropwise to a solution of **P1** (14 mg, 0.027 mmol) in dry dichloromethane (5mL) and the mixture was stirred under Argon for 1 h. The excess of oxalyl chloride was removed by evaporation under reduced pressure and the corresponding acid chloride was dissolved in EtOH (5 mL), and added to a suspension of **SA** in EtOH (20 mL). The suspension was stirred under reflux at 80 °C for 2 h and a colour change from red to dark blue could be appreciated. The suspension was then stirred at room temperature overnight. The functionalized nanoparticles **S1** were isolated by centrifugation at 10,000

rpm, washed with water and dichloromethane and dried at 70 °C overnight.

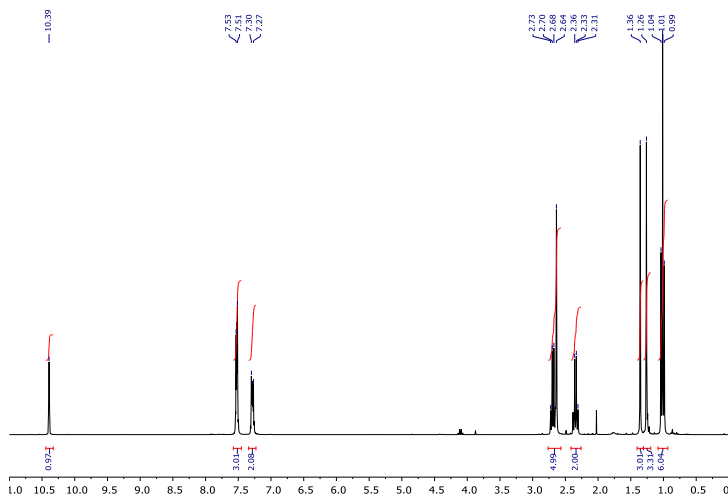UV-Vis Absorption: λ_{max} = 549 nm; fluorescence emission: λ_{max} = 617 nm (λ_{exc} 550 nm).

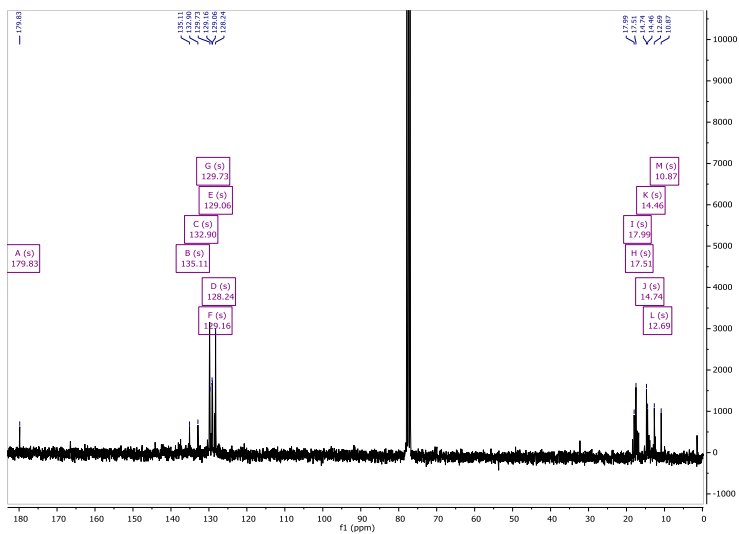**Figure S1:** ^{1}H RMN spectrum **2** in CDCl₃

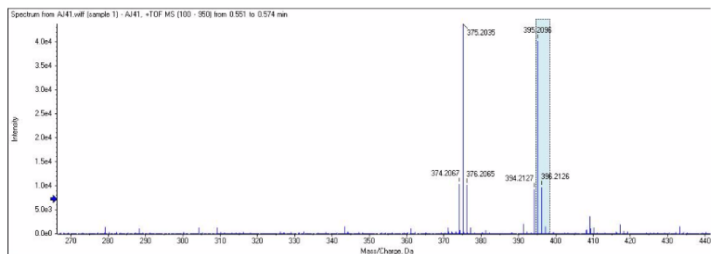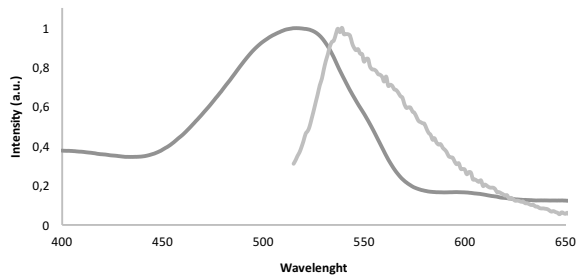**Figure S2:** ^{13}C RMN spectrum of **2** in CDCl₃

Figure S3: HRMS of **2**

Figure S4. UV-vis and normalized fluorescence emission spectra of **2** (1.0 x 10^{-5} M in acetonitrile, λ_{exc} = 515 nm)
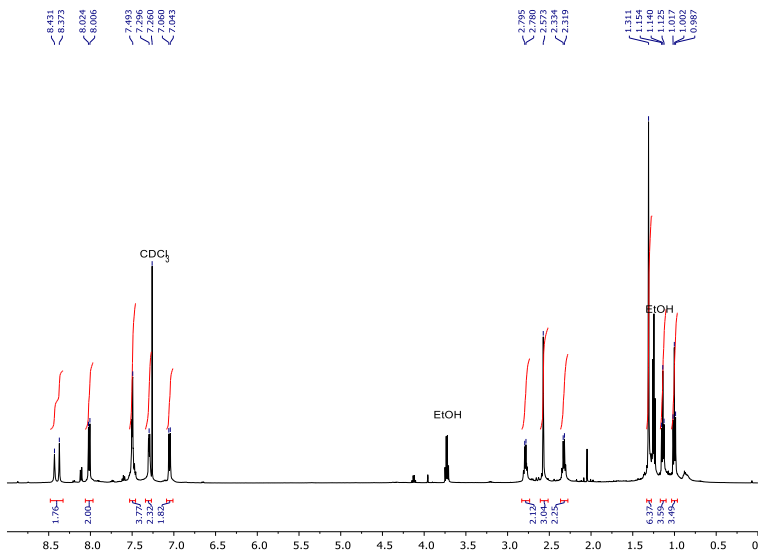

Figure S5: ^{1}H RMN spectrum **P1** in CDCl$_3$
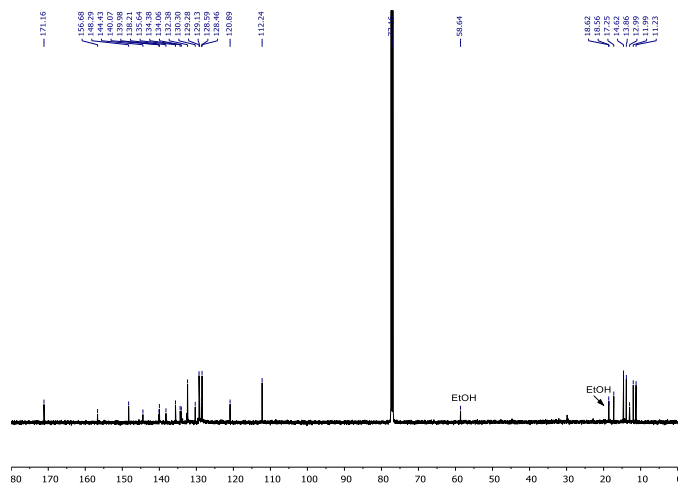
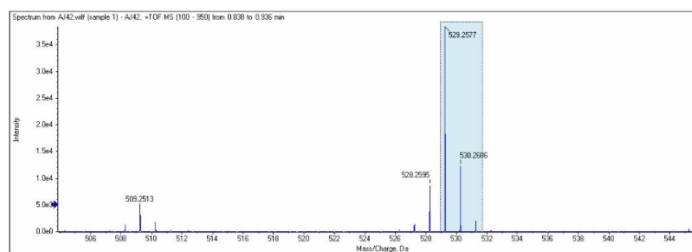**Figure S6:** ^{13}C RMN spectrum of **P1** in CDCl$_3$

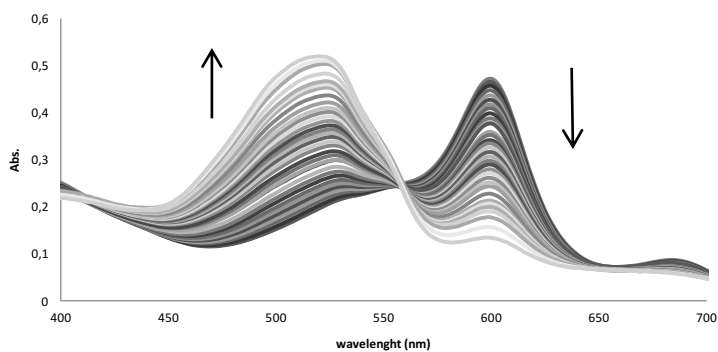**Figure S7:** HRMS of **P1**

Figure S8: UV spectra of **P1** with increasing amounts of NO$_2$ at room temperature.
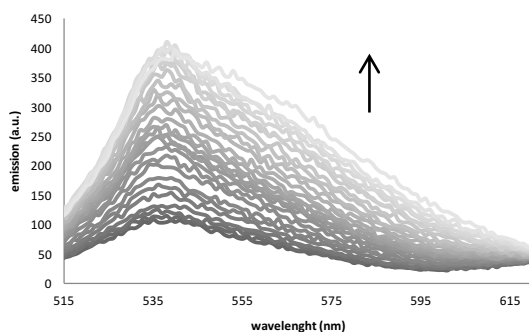
Figure S9: Emission of **P1** (1.0×10^{-5}M in acetonitrile, λ_{exc} = 515 nm) with increasing amounts of NO_2 at room temperature.
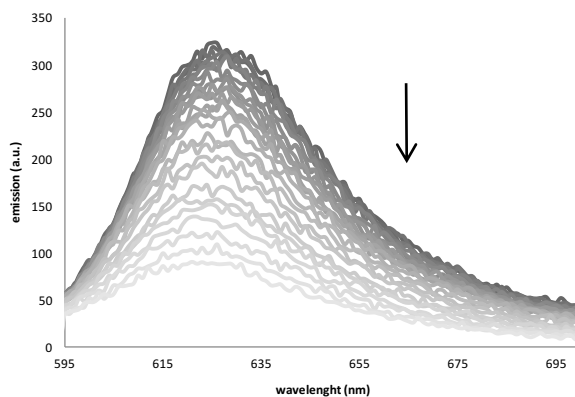

Figure S10: Emission of **P1** (1.0×10^{-5}M in acetonitrile, λ_{exc}: 590) with increasing amounts of NO_2 at room temperature.
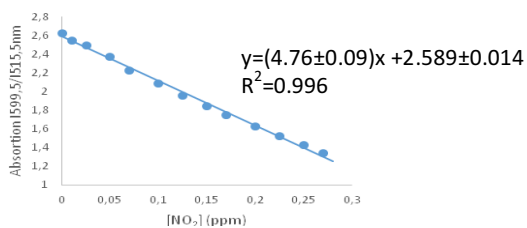

Figure S11: Absorbance intensities ratios at 599 and 515 mn of **P1** (1.0×10^{-5} mol dm^{-3} in acetonitrile) *versus* increasing amounts of NO_2.
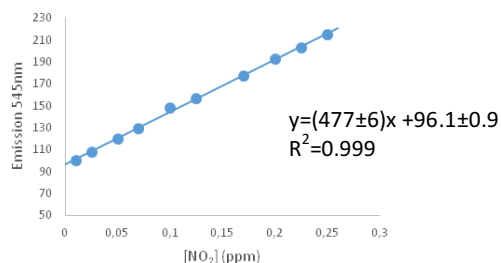
Figure S12: Emission at 545 mn of **P1** (1.0 x 10^{-5} mol dm^{-3} in acetonitrile) *versus* increasing amounts of NO$_2$
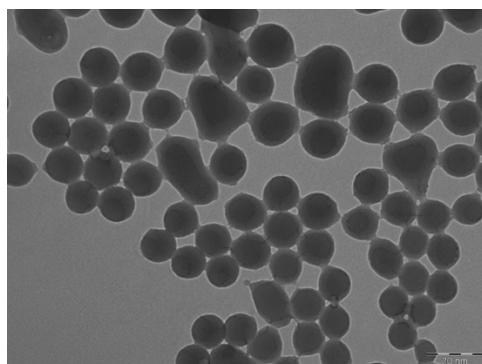
Figure S13: TEM image of **S1**

Solid	%N/mg	%C/mg	%H/mg	αP$_1$ (mmol/g SiO$_2$)
S1	0.094	0.612	0.054	0.017

Table S14: Content (α) in mmol of anchored molecules **P1** per gram of SiO$_2$ for the prepared solid **S1**.

Chapter 5:
Molecular gates as chemosensor

Self-immolative linkers as caps for the design of gated silica mesoporous supports

L. Alberto Juárez,[ab] Elena Añón,[ab] Cristina Giménez,[acd] Félix Sancenón,[acd] Ramón Martínez-Máñez,*[acd] Ana M. Costero,*[abd] Pablo Gaviña,[abd] Margarita Parra.[abd]

[a] Instituto Interuniversitario de Investigación de Reconocimiento Molecular y Desarrollo Tecnológico (IDM). Unidad Mixta Universidad de Valencia-Universidad Politécnica de Valencia, Spain.
[b] Departamento de Química Orgánica. Universidad de Valencia, Doctor Moliner 50, 46100, Burjassot, Valencia, Spain.
[c] Departamento de Química. Universidad Politécnica de Valencia, Camino de Vera s/n, 46022, Valencia, Spain.
[d] CIBER de Bioingeniería Biomateriales y Nanomedicina (CIBER-BBN).

Synthesis, characterization and controlled release behavior of a new hybrid material based on silica mesoporous nanoparticles caped with a self-immolative gate is reported.

There is a significant interest in the development of methodologies of controlled release for a diverse range of applications.[1] For this reason, a large diversity of drug nanocarriers having different size, structure and surface properties, such as liposomes and polymeric or inorganic nanoparticles, have been developed over the last decades.[2] Among these, mesoporous silica nanoparticles (MSNs) have attracted great attention in recent years due to their unique features such as stability, biocompatibility, large load capacity and the possibility of easy functionalizing their surface to obtain targeting and drug release systems.[3] In this scenario, an appealing concept when using MSNs is the possibility to functionalize the external surface with gated ensembles. The development of gated systems able to retain the payload yet releasing it upon the presence of a predefined stimulus has been proved to be an excellent approach to develop advanced nanodevices for controlled delivery applications.[4] In fact, through decoration of the mesoporous material with a wide collection of organic and biological entities or inorganic capping agents, researchers have prepared recently gated MSNs that can be triggered by target chemical (such as selected anions, cations neutral molecules, redox-active molecules, pH changes and biomolecules), physical (such as light, temperature, magnetic fields or ultrasounds) and biochemical (such as enzymes, antibodies, or DNA) stimuli.[5]

From a different point of view, self-immolative molecules are covalent aggregates that, upon application of an external trigger, initiate a disassembly reaction, through a cascade of electronic elimination processes, leading ultimately to the release of its building blocks.[6] This chemical phenomenon is usually driven by a cooperative increase in entropy coupled with the irreversible formation of thermodynamically stable products. These molecules have been extensively used in several applications including the design of prodrugs,[7] sensors[8] and drug delivery systems.[9] Self-immolative processes can commonly be found for polysubstituted, electron-rich aromatic species containing an electron-donating substituent in conjugation (ortho or para) with a suitable leaving group located in a benzylic position.[10] In classical self-immolative linkers a single activation event leads to the release of a single

group. This release can be described as non-amplified. In contrast the evolution of this technology has resulted in recent years in the design of self-immolative systems in which a single activation event leads to the delivery of multiple groups. This has been described as amplified release.[11]
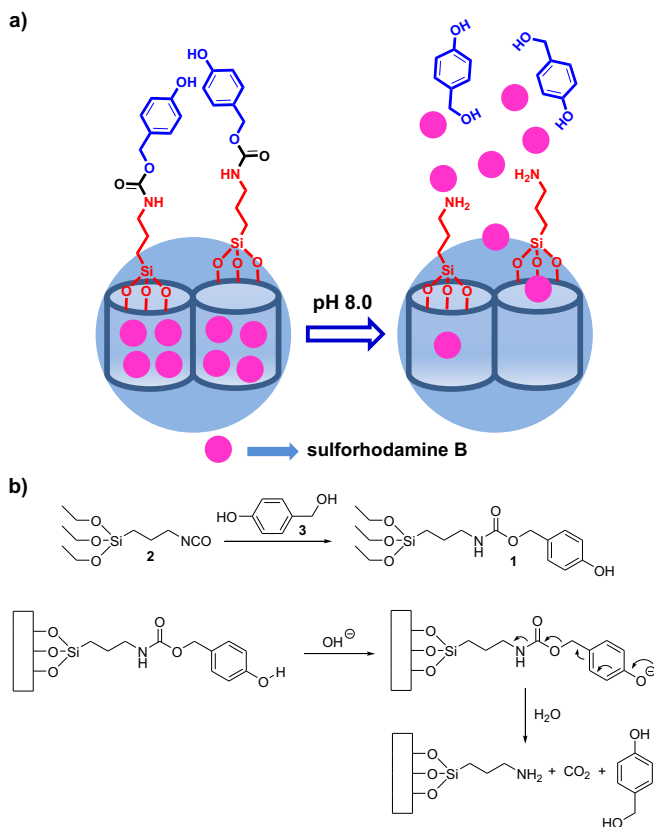
Scheme 1. (a) Schematic representation of the prepared gated nanoparticles **S1**, (b) synthesis of self-immolative molecular gate **1** and the cascade electronic elimination reaction triggered by pH.

Taking into account our interest in the preparation of capped mesoporous materials for applications in controlled release[12] and sensing/recognition[13] protocols we describe herein the possibility of combining MSNs and self-immolative derivatives in order to develop new gated MSNs supports. In this context, and as far as we are aware, the use of self-immolative molecules as caps in

conjunction with mesoporous supports for the preparation of gated nanodevices has never been described.

The design of our system is shown in Scheme 1. MCM-41 mesoporous silica nanoparticles of ca. 100 nm of diameter were selected as inorganic scaffold and were loaded with the dye sulforhodamine B. As cap we selected the simple molecule 1 in order to demonstrate that it is possible to use self-immolative linkers to prepare gated MSNs. 1 is a carbamate derivative that can suffer a 1,6 elimination reaction via a quinone-methide cascade under basic conditions (see Scheme 1).

The self-immolative molecule 1 was prepared by simple reaction of (3-isocyanatopropyl)triethoxysilane (2) with 4-hydroxymethylphenol (3) (see Scheme 1). On the other hand, MSNs were prepared following well-known procedures using tetraethyl orthosilicate (TEOS), as suitable hydrolysable inorganic precursor, and hexadecyltrimethylammonium bromide (CTAB) as a structure-directing agent.[14] The preparation of the final S1 material was carried out using a two-step procedure. In a first step, the pores of the calcined mesoporous scaffold were loaded with sulforhodamine B by simply stirring a suspension of the nanoparticles in a concentrated acetonitrile solution of the dye. In the second step, self-immolative molecule 1 was added to the suspension. Using this protocol 1 was expected to be preferentially attached onto the external surface of the nanoparticles due to the presence of the sulforhodamine B dye inside the pores. After the grafting step, the nanoparticles were filtered, washed with acetonitrile and dried at 70°C for 12 h. This procedure yielded the final **S1** material as a red-pink solid.

The starting mesoporous silica scaffold and the final nanoparticles **S1** were characterized following standard procedures (see Supporting Information for details). Powder X-ray diffraction (PXRD) and transmission electron microscopy (TEM), carried out on the starting nanoparticles showed the presence of a mesoporous structure (see Figures 1 and 2). Figure 1 shows the PXRD pattern of the as-made mesoporous nanoparticles (curve a), the calcined solid (curve b) and the final material **S1** (curve c). As it could be seen, the (100) reflection was present in the three patterns indicating the preservation of the mesoporous scaffolds The presence of the mesoporous structure on the final functionalized solid **S1** was also

confirmed by TEM. Figure 2 shows the pseudo-spherical morphology of the obtained materials and the typical channels of the MCM-41 matrix visualized as a pseudohexagonal array of pore voids or as alternate black and white strips. The prepared final **MSNs S1** have a diameter of 94 ± 5 nm (Figure 2).
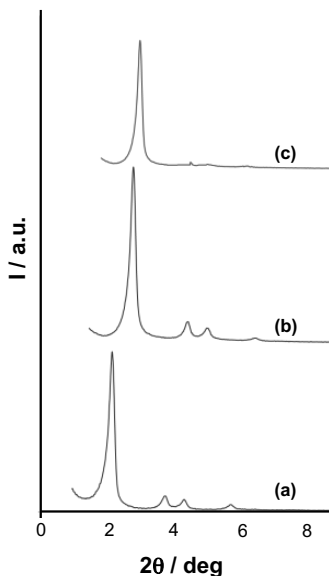

Figure 1. Powder X-ray patterns of the solids: (a) MCM-41 as synthesized, (b) calcined MCM-41, (c) **S1** nanoparticles.
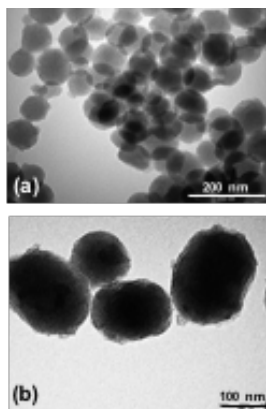

Figure 2. TEM images of (a) calcined MCM-41, (b) **S1** nanoparticles. For all the materials, the typical porosity of the mesoporous matrix is observed.

N_2 adsorption-desorption isotherms studies of the starting calcined nanoparticles and of the final material **S1** were also performed (see Supporting Information). The curve of calcined nanoparticles showed an absorption step at P/P_0 values between 0.1 and 0.3 (type IV isotherm) which is typical of mesoporous solids. This first step is attributed to N_2 condensation inside the mesopores. Application of the BJH model on the adsorption curve of the isotherm, pore diameter and pore volume were calculated (see Table 1). The absence of a hysteresis loop within this range and the low BJH distribution suggest a cylindrical uniformity of the mesopores. Applying the BET model, a total specific surface area of 895 $m^2 g^{-1}$ was calculated. A second characteristic of the isotherm of the starting calcined nanoparticles is the characteristic H1 hysteresis loop that appeared at $P/P_0 > 0.8$ and corresponding to the filling of the large pores between nanoparticles attributed to textural porosity. For the final capped nanoparticles **S1**, the N_2 adsorption-desorption isotherm (see Supporting Information) is typical of mesoporous systems with partially filled mesopores. As expected, smaller pore volume and specific surface area were found for **S1** (see Table 1), when compared with the starting MSNs. Finally, elemental and thermogravimetric analyses were used to determine the organic content in the final gated nanoparticles **S1**. The content of **1** and sulforhodamine B amounted to 0.107 and 0.39 mmol g^{-1} SiO_2, respectively.

Table 1. BET specific surface values, pore volumes and pore sizes calculated from the N_2 adsorption-desorption isotherms for calcined MSNs and **S1**.

Solid	S_{BET} ($m^2 g^{-1}$)	Pore volume ($cm^3 g^{-1}$)[a]	Pore size (nm)[b]
calcined MSNs	895	0.73	2.47
S1	265	0.35	2.45

[a] Pore volumes and pore sizes were associated with only intraparticle mesopores.
[b] Pore sizes estimated by the BJH model applied to the absorption branch of the isotherm

S1 nanoparticles contain phenolic carbamate groups as self-immolative caps that were expected to be large enough to inhibit cargo release. However, deprotonation of the phenolic hydroxyl group is expected to result in cargo delivery. In fact taking into account the designed opening protocol (*vide ante*), it was anticipated that at pH bellow the pk$_a$ of the phenolic subunit in **1** (pK$_a$ ca. 8-9) the nanoparticles S1 would remain closed. However, at

basic pH the deprotonation of the hydroxyl would result in a cascade disassembly reaction and cargo delivery.

In order to test this designed aperture mechanism kinetic cargo release profiles for solid **S1** at different pH values were obtained. In a typical experiment 1.0 mg of the solid **S1** was suspended in water at pH 4.0, 5.0, 7.5 or 8.0. Mixtures were stirred at room temperature and aliquots were taken at scheduled times. The solid was then removed by centrifugation and dye delivered to the solution was monitored by measuring the emission of sulforhodamine B in the solution at λ = 560 nm (λ_{ex} = 550 nm). The results of cargo delivery as a function of the pH are shown in Figure 3.

As seen, at pH 4.0, despite the use of a rather small molecule such as **1** anchored in the pore outlets, delivery of sulforhodamine B from the pores of **S1** nanoparticles was highly inhibited and a near "zero release" was observed. Nearly the same behavior was found when the pH was raised to 5.0 where the % of dye released was less than ca 10% after 5h. At pH 7.5 still a relatively low dye delivery was found (ca. 30% after 5h), whereas sulforhodamine B release was highly enhanced at pH 8.0 reaching the maximum cargo delivery at ca. 120 minutes. As expected (*vide ante*) the observed cargo release at basic pH was ascribed to a deprotonation of the hydroxyl moiety of **1**. The generated phenolate anion initiated a self-immolative process that induced the rupture of the gate with and the subsequent dye release (see Scheme 1). Delivery experiments at more basic pH were not carried out because of possible degradation of the inorganic mesoporous matrix.

The autonomous disassembly of the self-immolative cap upon deprotonation of the phenolic hydroxyl moiety was assessed by means of ^{1}H NMR spectra and by HRMS. For this purpose, a suspension of **S1** in water at pH 8.0 was stirred at room temperature for 3 hours. The nanoparticles were removed by centrifugation. The resulting solution rotavapored and the obtained crude dissolved in deuterated acetonitrile. The ^{1}H-NMR spectrum of the crude clearly showed the presence of signals corresponding to 4-hydoxymethylphenol which was generated by reaction of the elimination product *p*-quinone methide with water (see Scheme 1). In contrast, signals of 4-hydoxymethylphenol were not observed if **S1** was suspended in water at acidic pH. The presence of the 4-

hydoxymethylphenol derivative unequivocally confirm the occurrence of a disassembly reaction of the self-immolative gate at basic pH in **S1**.
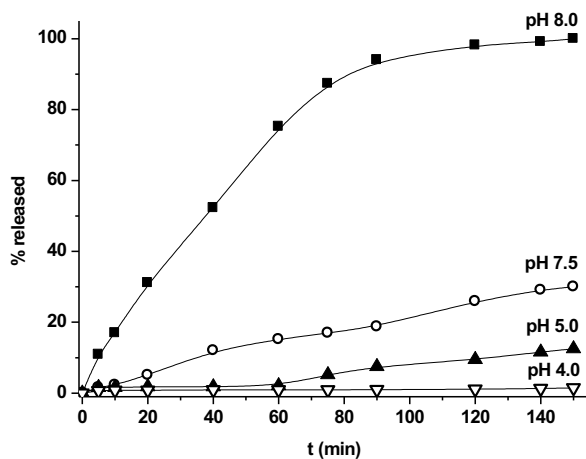

Figure 3. Release kinetic profiles of sulforhodamine B (emission at 560 nm upon excitation at 525 nm) from **S1** nanoparticles at different pH values.

As stated above in classical self-immolative chemistry a single activation event usually leads to the release of a single group whereas the design of self-immolative systems for the delivery of multiple groups is usually difficult and requires the preparation of rather complex challenging molecules from a synthesis point of view.[11] In this scenario, the anchoring as cap of a simple molecule such as **1** in MSNs allows to design systems in which a single activation in **1** induced the release of a large number of cargo molecules (in our case a dye). In fact, one reported advantage of gated materials is the existence of amplification features. For instance, it has been described that the "activation" of relatively few capping molecules usually results in the release of a relatively large quantity of entrapped cargo guests.[15] The approach of using self-immolative molecules as gates offers great potential for the preparation of new delivery systems with enhanced features compared with classical self-immolative systems for delivery applications. In particular, it is possible to select, with minimum effort, different porous supports, a large range of self-immolative gate-like systems and a number of molecules to be delivered which do not need to be anchored to the self-immolative linker. In fact,

this approach is conceptually different to classic self-immolative showing molecular amplification because our proposed protocol disconnects the triggering step from the release event therefore making delivery independent of the interaction between the activation event and the self-immolative linker.

In summary, we reported herein the synthesis, characterization and pH-triggered controlled release behavior of a new hybrid material based on silica mesoporous nanoparticles loaded with sulforhodamine B and caped with a self-immolative cap. At acidic and neutral pH the gate remained closed and negligible or poor dye release was observed. However, at slightly basic pH a marked cargo delivery was observed. Dye release was ascribed to a deprotonation of the phenol moiety in the capping molecule that resulted in the subsequent disassembly of the self immolative cap. As far as we known, this is the first example in which a self-immolative molecule is used as cap for the development of mesoporous silica-based gated materials. Self-immolative linkers have gained popularity in recent years due to the formation of stable bonds which become labile upon activation. We believe that the combination of self-immolative linkers with mesoporous materials could result in the easy preparation of a new generation of self-immolative systems. Moreover, the possibility to design capped self-immolative supports able to be opened by using pH, specific enzymes, small molecules, etc. makes this approach highly attractive for the preparation of new gated self-immolative systems for different applications.

References

1.   (a) M. W. Tibbit, J. E. Dahlman, R. Langer, *J. Am. Chem. Soc.* 2016, **138**, 714; (b) K. Nguyen, T. Kim, Y. Zhao, *Acc. Chem. Res.* 2015, **48**, 3016; (c) G. Kang, N. Tripathy, *Ther. Deliv.* 2014, **5**, 1053.

2.   (a) N. Kamaly, B. Yameen, J. Wu, O. C. Farokhzad, *Chem. Rev.* 2016, **116**, 2602; (b) Y. Li, G. Liu, X. Wang, J. Hu, S. Liu, *Angew. Chem. Int. Ed.* 2016, **55**, 1760; (c) N. Sharma, K. Neeraj, V. Kumar, *Drug Deliv. Lett.* 2014, **4**, 12; (d) I. K. Yazdi, A. Ziemys, M. Evangelopoulos, J. O. Martinez, M. Kojic, E. Tasciotti, *Nanomedicine* 2015, **10**, 3057.

3.   (a) C. Argyo, V. Weiss, C. Bräuchle, T. Bein, *Chem. Mater.* 2014, **26**, 435; (b) J. El Haskouri, D. Ortiz de Zarate, C. Guillem, J. Latorre, M. Caldés, A. Beltrán, D. Beltrán, A. B. Descalzo, G. Rodríguez-López, R. Martínez-Máñez, M. D. Marcos, P. Amorós, *Chem. Commun.* 2002, 330.

4.   (a) G. J. A. A. Soler-Illia, O. Azzaroni, *Chem. Soc. Rev.* 2011, **40**, 1107; (b) N. Song, Y. −W. Yang, *Chem. Soc. Rev.* 2015, **44**, 3474; (c) E. Aznar, R. Martínez-Máñez, F. Sancenón, *Expert Opin. Drug Deliv.* 2009, **6**, 643; (d) C. Coll, A. Bernardos, R. Martínez-Máñez, F. Sancenón, *Acc. Chem. Res.* 2013, **46**, 339.

5.   (a) E. Aznar, M. Oroval, Ll. Pascual, J. R. Murguía, R. Martínez-Máñez, F. Sancenón, *Chem. Rev.* 2016, **116**, 961; (b) F. Sancenón, Ll. Pascual, M. Oroval, E. Aznar, R. Martínez-Máñez, *ChemistryOpen* 2015, **4**, 418; (c) Z. Li, J. C. Barnes, A. Bosoy, J. F. Stoddart, J. I. Zink, *Chem. Soc. Rev.* 2012, **41**, 2590; (d) C. −H. Lu, B. Willner, I. Willner, *ACS Nano* 2013, **7**, 8320; (e) S. Saha, K. C. −F. Leung, T. D. Nguyen, J. F. Stoddart, J. I. Zink, *Adv. Func. Mater.* 2007, **17**, 685.

6.   (a) A. Alouane, R. Labruère, T. Le Saux, F. Schmidt, L. Jullien, *Angew. Chem. Int. Ed.* 2015, **54**, 7492; (b) S. Gnaim, D. Shabat, *Acc. Chem. Res.* 2014, **47**, 2970.

7.   See for example: (a) H. J. Schuster, B. Krewer, J. M. von Hof, K. Schmuck, I. Schuberth, F. Alves, L. F. Tietze, *Org. Biomol. Chem.* 2010, **8**, 1833; (b) B. E. Toki, C. G. Cerveny, A. F. Wahl, D. Seuter, *J. Org. Chem.* 2002, **67**, 1866; (c) S. Chen, X. Zhao, J. Chen, J. Chen, L. Kuznetsova, S. S. Wong, I. Ojima, *Bioconjugate Chem.* 2010, **21**, 979.

8.   See for example: (a) L. Louise-Leriche, E. Paunescu, G. Saint-Anfre, R. Baati, A. Romieu, A. Wagner, P. Y. Renard, *Chem. Eur. J.* 2010, **16**, 3510; (b) Y. Meyer, J. A. Richard, M. Massonneau, P. Y. Renard, A. Romien, *Org. Lett.* 2008, **10**, 1517; (c) X. B. Zhang, M. Waibel, J. Hasserodt, *Chem. Eur. J.* 2010, **16**, 792.

9.   See for example: (a) A. Satyam, *Bioorg. Med. Chem. Lett.* 2008, **18**, 3196; (b) M. Shamis, H. N. Lode, D. Shabat, *J. Am. Chem. Soc.* 2004, **126**, 1726; (c) R. Weinstain, E. Segal, R. Satchi-Fainaro, D. Shabat, *Chem. Commun.* 2010, **46**, 533; (d) R. J. Amir, M. Popkov, R. A. Lernes, C. F. Barbas III, D. Shabat, *Angew. Chem. Int. Ed.* 2005, **44**, 4378.

10.   (a) H. Y. Lee, X. Jiang, D. Lee, *Org. Lett.* 2009, **11**, 2065; (b) A. Alouane, R. Labruère, T. Le Saux, I. Aujard, S. Dubruille, F. Schmidt, L. Jullien, *Chem. Eur. J.* 2013, **19**, 11717; (c) R. Erez, D. Shabat, *Org. Biomo. Chem.* 2008, **6**, 2669; (d) R. M. Kevwitch, C. S. Shanahan, D. V. McGrath, *New. J. Chem.* 2012, **35**, 492.

11.   (a) M. E. Roth, O. Green, S. Gnaim, D. Shabat, *Chem. Rev.* 2016, **116**, 1309; (b) G. Liu, G. Zhang, J. Hu, X. Wang, M. Zhu, S. Liu, *J. Am. Chem. Soc.* 2015, **137**, 11645; (c) I. S. Turan, E. U. Akkaya, *Org. Lett.* 2014, **16**, 1680; (d) N. Fomina, C. L. McFearin, A. Almutairi, *Chem. Commun.* 2012, **48**, 9138.

12.   See for example: (a) A. Ultimo, C. Giménez, P. Bartovsky, E. Aznar, F. Sancenón, M. D. Marcos, P. Amorós, A. R. Bernardo, R. Martínez-Máñez, A. M. Jiménez-Lara, J. R. Murguía, *Chem. Eur. J.* 2016, **22**, 1582; (b) C. de la Torre, I. Casanova, G. Acosta, C. Coll, M. J. Moreno, F. Albericio, E. Aznar, R. Mangues, M. Royo, F. Sancenón, R. Martínez-Máñez, *Adv. Func. Mater.* 2015, **25**, 687; (c) C. de la Torre, L. Modragón, C. Coll, A. García-Fernández, F. Sancenón, R. Martínez-Máñez, P. Amorós, E. Pérez-Payá, M. Orzaez, *Chem. Eur. J.* 2015, **21**, 15506; (d) N. Mas, D. Arcos, L. Polo, E. Aznar, S. Sánchez-Salcedo, F. Sancenón, A. García, M. D. Marcos, A. Baeza, M. Vallet-Regí, R. Martínez-Máñez, *Small* 2014, **23**, 4859.

13.   See for example: (a) Ll Pascual, I. Baroja, E. Aznar, F. Sancenón, M. D. Marcos, J. R. Murguía, P. Amorós, K. Rurack, *Chem. Commun.* 2015, **51**, 1414; (b) S. El Sayed, M. Milani, M. Licchelli, R. Martínez-Máñez, F. Sancenón, *Chem. Eur. J.* 2015, **21**, 7002; (c) E. Climent, L. Modragón, R. Martínez-Máñez, F. Sancenón, M. D. Marcos, J. R. Murguía, P. Amorós, K. Rurack, E. Pérez-Payá, *Angew. Chem. Int. Ed.* 2013, **52**, 8938; (d) L. E. Santos-Figueroa, C. Giménez, A. Agostini, E. Aznar, M. D. Marcos, F. Sancenón, R. Martínez-Máñez, P. Amorós, *Angew. Chem. Int. Ed.* 2013, **52**, 13712.

14. S. Cabrera, J. El Haskouri, C. Guillem, J. Latorre, A. Beltrán, D. Beltrán, M.D- Marcos, P. Amorós, *Solid State Sci.* 2000, **2**, 405.

15. E. Climent, M. D. Marcos, R. Martínez-Máñez, F. Sancenón, J. Soto, K. Rurack, P. Amorós, *Angew. Chem. Int. Ed.* 2009, **48**, 8519

140

Supporting Information

Chemicals.

The chemicals tetraethylorthosilicate (TEOS), *n*-cetyltrimethylammonium bromide (CTABr), sodium hydroxide (NaOH), (3-isocyanatopropyl)triethoxysilane and 4-hydroxybenzyl alcohol were purchased from Sigma-Aldrich Química S. A. (Madrid, Spain) and used without further purification. THF was dried before use.

General methods.

PXRD, TGA, elemental analysis, TEM, N_2 adsorption-desorption, NMR, and fluorescence spectroscopy techniques were employed to characterize the synthesized materials. Powder X-ray measurements were performed on a Philips D8 Advance Diffractometer using CuKα radiation. Thermogravimetric analyses were carried out on a TGA/SDTA 851e Mettler Toledo balance, using an oxidant atmosphere (air, 80 mL/min) with a heating program consisting of a heating ramp of 10°C per minute from 393 to 1273 K and an isothermal heating step at the final temperature for 30 min. TEM images were obtained with a 100 JEOL JEM-1010 microscope. N_2 adsorption-desorption isotherms were recorded with a Micromeritics ASAP2010 automated sorption analyzer. The samples were degassed at 120°C in vacuum overnight. The specific surface areas were calculated from the adsorption data in the low pressure range using the BET model. Pore size was determined following the BJH method. The ^{1}H and ^{13}C NMR spectra were recorded in a deuterated solvent as the lock and in a residual solvent as the internal reference. The high-resolution mass spectra were recorded in the positive ion mode in a VG-AutoSpec. The UV-vis spectra were recorded using a 1-cm path length quartz cuvette.

Synthesis of 1.

4-hydroxybenzyl alcohol (250 mg, 2.01 mmol) was dissolved in anhydrous THF (10 mL) and a small piece of Na (ca. 1 mg) was added. After stirring 10 min under argon at room temperature**,** (3-isocyanatopropyl)triethoxysilane (2.01 mmol) was added dropwise and the mixture was stirred under reflux overnight. Evaporation of the solvent gave product **1** as light yellow oil (320 mg, 57%).

^{1}H NMR (300 MHz, CDCl$_3$) δ: 7.21 (d, *J* = 8.3 Hz, 2H), 6.98 (d, *J* = 8.5 Hz, 2H), 4.49 (s, 2H), 3.75 (m, 6H), 3.16 (dd, *J* = 15.9, 6.6 Hz, 2H), 1.59 (m, 2H), 1.15 (m, 9H), 0.58 (m, 2H). ^{13}C NMR (75 MHz, CDCl$_3$) δ: 155.19, 150.68, 138.55, 128.10, 121.85, 64.63, 58.84, 43.93, 23.41, 18.61, 8.02.

Synthesis of mesoporous MCM-41 nanoparticles.

The MCM-41 mesoporous nanoparticles were synthesised by the following procedure: *n*-cetyltrimethylammonium bromide (CTABr, 1.00 g, 2.74 mmol) was first dissolved in 480 mL of deionised water before adding 3.5 mL of a solution of NaOH 2M till getting a basic pH 8. Then, the solution was heated to 80°C and TEOS (5.00 mL, 2.57×10^{-2} mol) was added dropwise to the surfactant solution at maximum stirring. The mixture was stirred for 2 h at 80°C. A white precipitate was obtained and isolated by centrifugation. Once isolated, the solid was washed with deionised water and ethanol till obtaining neutral pH in the solution, and was dried at 60ºC (MCM-41 as-synthesised). To prepare the final porous material (MCM-41), the as-synthesised solid was calcined at 550ºC using an oxidant atmosphere for 5 h in order to remove the template phase.

Synthesis of solid S1.

Calcined MCM-41 (100 mg) and sulforhodamine B dye (100 mg, 0.17 mmol) were suspended in acetonitrile (20 mL). Then, the mixture was stirred for 24 h at room temperature with the aim of achieving the maximum loading in the pores of the MCM-41 scaffolding. Afterward, self immolative molecule **1** (0.185 g, 0.5 mmoles) was added, and the suspension was stirred for 5.5 h. Finally, the solid was filtered off and dried at vacuum.

Materials characterization.

Figure 1 (see manuscript) shows the powder X-ray diffraction (PXRD) patterns of the nanoparticulated MCM-41 matrix as-synthesized, the MCM-41 calcined and **S1** solid (loaded with sulforhodamine B and functionalized with the self immolative molecule **1**). The MCM-41 as-synthesized displayed the four typical low-angle reflections of a hexagonal-ordered matrix indexed at (100), (110), (200) and (210) Bragg peaks (curve a). In curve of MCM-41 calcined, a significant shift of the (100) peak in the PXRD is observed (curve b). These observations are in agreement with the condensation of silanols in the calcination step, which caused an approximate cell contraction of 6-8 Å. Finally, curve c shows the **S1** PXRD pattern. For **S1** a broadening of the (100) and (200) peaks are observed due to a reduction in contrast related to the functionalisation process and to the filling of mesopores with sulforhodamine B. Nonetheless, the intensity of the (100) peak in this pattern strongly indicates that the loading process with the dye and the additional functionalisation with **1** did not modify the mesoporous MCM-41 scaffold.

In Figure SI-1 (curve a), the N_2 adsorption-desorption isotherms of the MCM-41 calcined nanoparticles is represented. This curve displays an adsorption step with a P/P_0 value of between 0.1 and 0.3, corresponding to a type IV isotherm, which is typical of mesoporous materials. This first step is due to nitrogen condensation in the mesopores. With the BJH model on the adsorption curve of the isotherm, the pore diameter and pore volume were calculated to be 2.97 nm and 0.73 cm^3g^{-1}, respectively. The absence of a hysteresis loop in this range and the low BJH pore distribution suggested a cylindrical uniformity of mesopores. The total specific area was 895 m^2g^{-1}, calculated using the BET model. A second remarkable feature of the curve is the characteristic H1 hysteresis loop that appears in the isotherm at a high relative pressure ($P/P_0 > 0.8$) and associated with a wide pore size distribution. This corresponds to the filling of the large pores among the nanoparticles (2.45 cm^3g^{-1} calculated by the BJH model) due to textural porosity. For the **S1** material, the N_2 adsorption-desorption isotherm is typical of mesoporous systems with filled mesopores (see Figure SI-1, curve b). In this case, and as expected, a lower N_2 adsorbed volume (0.35 cm^3g^{-1}) and surface area (265 m^2g^{-1}) were found when compared with the starting MCM-41 material. As observed, this solid presents a curve with no gaps at low relative pressure values if compared to the mother MCM-41 matrix (curve a). Table SI-1 shows the BET-specific surface values, pore volumes and pore sizes calculated from the N_2 adsorption-desorption isotherms for MCM-41 calcined and **S1** solid. The contents of grafted **1** and cargo in solid **S1** were determined by thermogravimetric and elemental analysis and are shown in Table SI-2.

TEM images for the MCM-41 calcined sample and **S1** solid are depicted in Figure 2 (see manuscript). In both cases, a detailed look to individual nanoparticles, showed the typical channels of the MCM-41 matrix visualized as alternate black-white lines. Finally, a particle diameter of ca. 95 nm was determined.
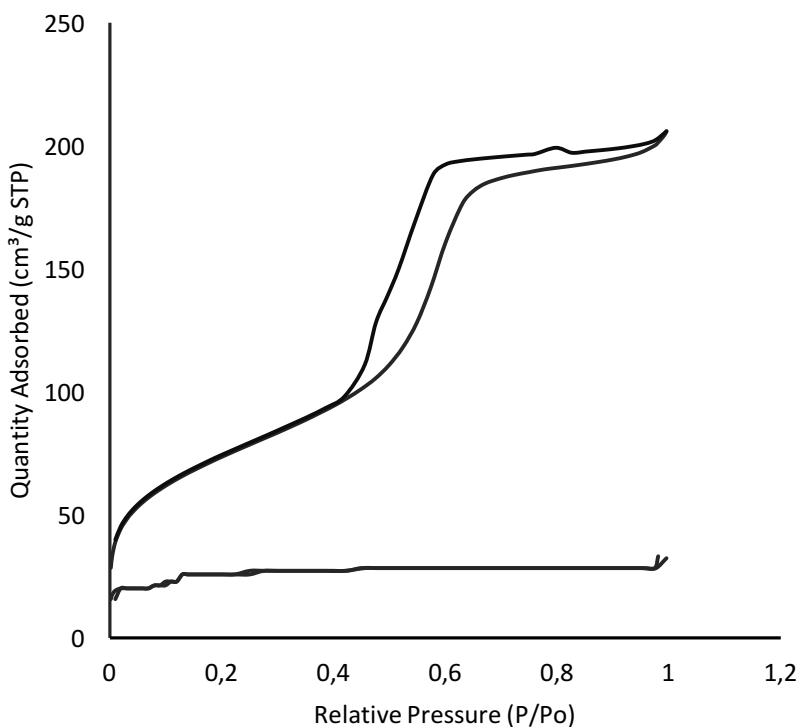
Figure SI-1. Nitrogen adsorption–desorption isotherms for: (a) MCM-41 calcined mesoporous material and (b) **S1**.

Table SI-1. BET-specific surface values, pore volumes and pore sizes calculated from the N_2 adsorption-desorption isotherms for selected materials.

Sample	S_{BET} /m^2/g	BJH Pore[a]/nm	Total Pore Volume[b]/cm^3/g
Calcined MSNs	895	2.97	0.73
S1	265	2.45	0.35

[a] Pore volumes and pore sizes were associated with only intraparticle mesopores.
[b] Pore size estimated by the BJH model applied to the adsorption branch of the isotherm.

Table SI-2. Content (α) in mmol of anchored molecules and cargo per gram of SiO_2 for the prepared solids.

Solid	α_1 (mmol/g SiO_2)	α_{cargo} (mmol/g SiO_2)
S1	0.107	0.390

Cargo release studies.

S1 consists in mesoporous MCM-41-type nanoparticles containing sulforhodamine B in the pores and capped with self-immolative molecule **1**. As part of the nanoparticles design, the grafted **1** was expected to cap the pores and inhibit cargo delivery. Subsequent deprotonation of the phenol moiety of **1** yielded a phenolate anion. The generated negative charge initiated a self-immolative process that induced the rupture of the gate with subsequent dye release. In order to check this aperture mechanism release kinetics studies at different pH were carried out. In a typical experiment, 1.0 mg of solid **S1** was suspended in 3.0 mL of water at different pH (4.0, 5.0, 7.5 and 8.0). The suspensions were stirred and at certain times aliquots were separated and centrifuged to eliminate the solid and dye delivery was determined by monitoring fluorescence of sulforhodamine B (λ_{exc} = 560 nm, λ_{em} = 550 nm) in the aqueous phase. Delivery results are shown in Figure 3 in the manuscript.
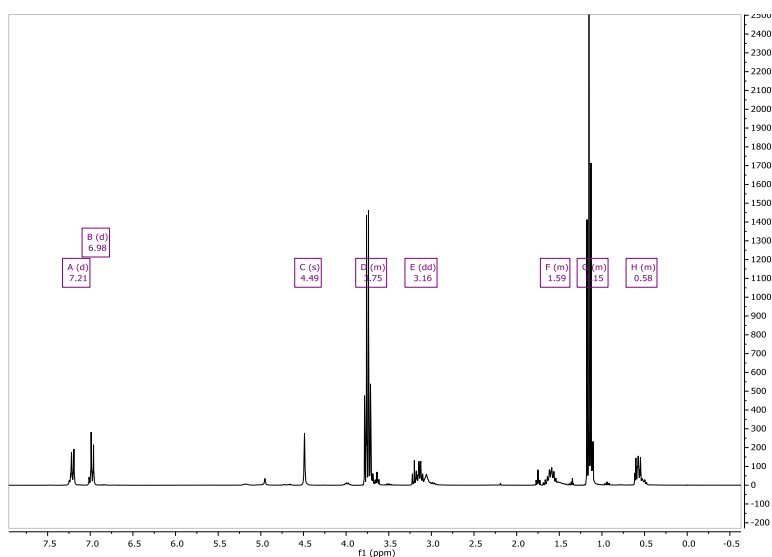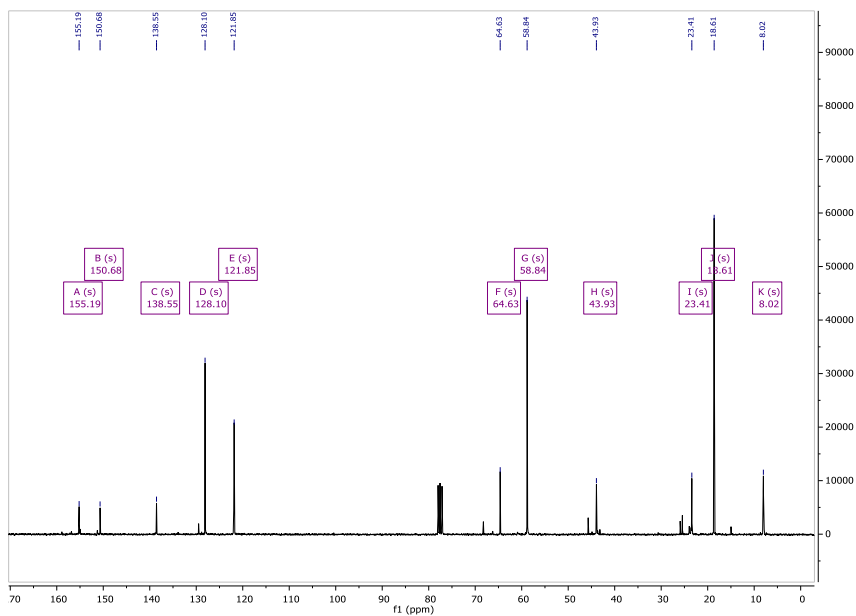

Figure SI-2. ^{1}H NMR spectrum of **1** in CDCl$_3$

Figure SI-3. ^{13}C NMR spectrum of **1** in CDCl$_3$.

DOUBLE CHECK FLUOROGENIC DETECTION OF NO$_2$ USING GATED SILICA MESOPOROUS MATERIAL

L. A. Juárez[ab], A. M. Costero*[abd], M. Parra[abd], P. Gaviña[ab], S. Gil[abd], F. Sancenón[acd], R. Martínez-Máñez[acd]

[a] Instituto Interuniversitario de Reconocimiento Molecular y Desarrollo Tecnológico (IDM), Unidad Mixta Universidad Politécnica de Valencia-Universidad de Valencia, Spain.

[b] Departamento de Química Orgánica. Universidad de Valencia, Doctor Moliner 50, 46100, Burjassot, Valencia, Spain. E-mail: ana.costero@uv.es

[c] Departamento de Química, Universidad Politécnica de Valencia, Camino de Vera s/n, 46022, Valencia, Spain. E-mail: rmaez@qim.upv.es

[d] CIBER de Bioingeniería, Biomateriales y Nanomedicina (CIBER-BBN).

Redaction process

Stimuli-responsive nanomaterials, able to show switchable behavior in response to environmental changes are novel smart materials with promising possibilities. .[1,2] One appealing application of such systems is the design of functionalized nanocontainers able to deal with cargo delivery under controlled conditions via external triggers.[3] Traditional delivery systems usually rely on simple diffusion controlled processes or degradation of the nanocarrier,[4] using for instance microcapsules,[5] micelles,[6] vesicles,[7] or liposomes.[8] In this context, silica mesoporous supports (SMPS) show unique properties such as large load capacity, biocompatibility, high thermal stability, homogeneous porosity, inertness, and tunable pore sizes with a diameter of ca. 2-10 nm.[9] Moreover, it has been demonstrated that it is possible to incorporate in the external surface of SMPS functional groups able to be opened or closed at will for functional control release applications. These hybrid mesoporous silica nanoarchitectures were developed primarily for drug delivery and molecular transport in response to chemical, physical and biological stimuli,[10] but in the last years increased advances in sensing applications are being observed, with gated materials showing good selectivity against other analytes, sensitivity and a fast response time.[11] However, to the best of our knowledge, the use of mesoporous silica-based gated materials for the detection of small gaseous species has not yet been reported in the literature. In this sense, we report here a new approach for the development of chemosensors for NO_2 gas using gated materials.

NO_2 has direct and indirect adverse health effects. Long-term exposure to NO_2 is associated with increased susceptibility to lower respiratory tract illness[12] Meng et al. reported that NO_2 was associated with increased risk of chronic obstructive pulmonary disease mortality.[13] In addition, NO_2 exposure is a potential inducer of neurological diseases.[14] Due to the ubiquitous presence of this gas the development of selective and sensitive sensing methods is a hot area of research.

Given our interest in the development of chromo-fluorogenic probes for toxic gases, we have recently reported a phenylhydrazone modified BODIPY derivative (P1) for the sensitive and selective colorimetric and fluorescent detection of NO_2 (g). The sensing mechanism takes advantage of the NO_2 induced oxidative regeneration of carbonyl compounds from the corresponding hydrazones under very soft conditions. We report herein the synthesis of silica mesoporous nanoparticles functionalized with a formyl BODIPY phenylhydrazone derivative, and loaded with an appropriate dye (NM1), and the use of

this gated material for the selective and sensitive detection of NO_2 (g). Our proposed sensing protocol is depicted in Scheme 1. The oxidative cleavage of the phenylhydrazone in the presence of the analyte should uncap the pores, releasing the both, the entrapped dye and the BODYPY aldehyde (BA) fluorophore. Thus, the designed system present two different measurement channels and a clear amplification of the signal.
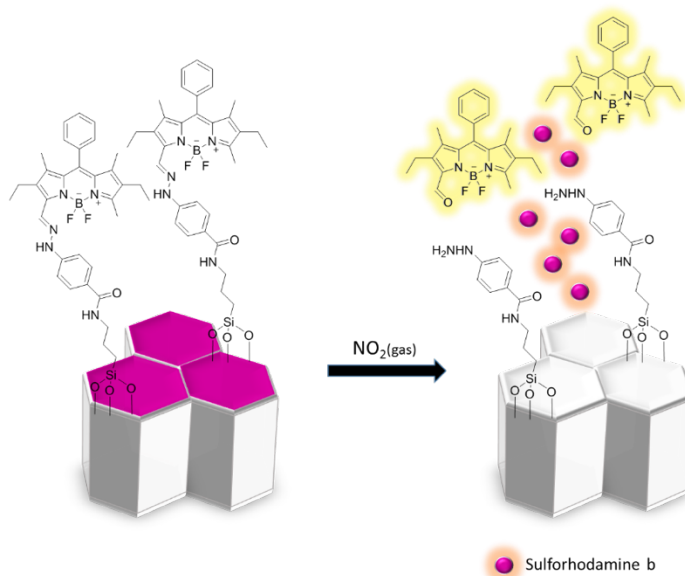

Scheme 1: Sensing protocol

First of all, the mesoporous material is charged with an appropriate dye, in this case sulforhodamine B. The porous are closed by using an organic molecule able to be broken in the presence of the analyte. Among the different reactions involving NO_2 we decided to explore the utility of this gas to react with phenyl-hydrazones and transform them into the corresponding aldehydes under very soft conditions.[15] Thus, we have thought in this strategy to build the organic gate in the prepared hybrid material. The molecular gate consists in a phenyl hydrazone derived from a BODIPY aldehyde that can be bound to the mesoporous material through an amide group. In the presence of the analyte, the hydrazone regenerates the free BODIPY-aldehyde with the corresponding optical changes.   In fact, BODIPY derivatives are a class of well-known fluorophores with widespread applications as fluorescent probes due to their valuable characteristics, such as high molar absorption coefficients and high quantum yields leading to intense absorption and fluorescence bands.[16] At the same time, this reaction induces the gate opening and the

dye contained in the mesoporous will be liberated giving rise to both a second measurement channel and an amplification of the signal.

The sensing paradigm is shown in scheme 1 where the presence of NO_2 gas can be assessed by both the release of the dye and the appearance of the BODIPY-aldehyde. At the best of our acknowledgement, this is the first time that a double check is described. This design can increase the reliability and sensibility of the detection method.

Mesoporous MCM-41 silica nanoparticles were chosen as inorganic support on account of their unique properties such as large load capacity and well-known functionalization procedures.[17] The silica nanoparticulated material (a calcined MCM-41-like solid) was prepared by following well-known procedures using TEOS as the hydrolysable inorganic precursor and the surfactant.[18] On the other, the treatment of the BODIPY phenylhydrazone **P1** with oxalyl chloride in dry dichloromethane led to the acyl chloride derivative **1** in quantitative yield.[19]

The UV-Vis spectrum of BODYPY aldehyde shows an absorption band at 525 nm and the fluorescence spectrum shows an emission band at 530 nm (λ_{ex}= 520 nm). Accordingly, with these properties sulforhodamine B was chosen as fluorophore to load the material, because its spectroscopic properties (λ_{ab}= 555 nm, λ_{em}= 570 nm (λ_{ex}= 550 nm)) do not interfere in the double check control.
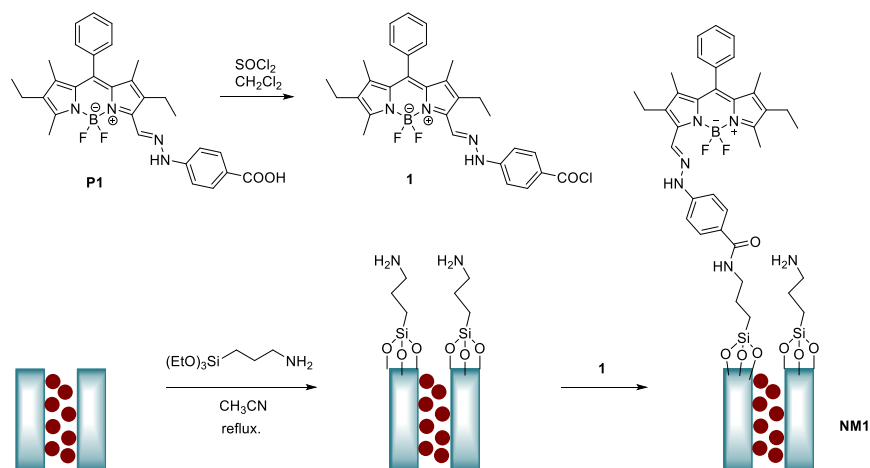
Scheme 2: preparation of NM1

The functionalization of the final hybrid material was carried out through a two-step synthetic procedure (scheme 2).[20] In the first step, the efficient loading of pores was achieved by stirring a suspension of the mesoporous nanoparticles in a highly concentrated acetonitrile solution of sulforhodamine B . After one hour, (3-aminopropyl)triethoxysilane was added and the reaction was refluxed overnight. In the second step, the external surface of the siliceous material was functionalized by adding **1** to the mixture and stirring during 5 min. In this way, the anchoring reaction of the filled nanoparticles occurred in a solution containing a high concentration of the dye, thus inhibiting dye diffusion from the inner pores to the bulk solution. Finally, the light pink solid **NM1** was filtered, washed with acetonitrile and dried at 70 ºC for 12 h.

The starting MCM-41 support, and the charged gated material **NM1** were characterized by standard techniques. Figure 1 (left) shows the powder X-ray diffraction (XRD) patterns of solids MCM-41 as-synthesized, MCM-41 calcined, and **NM1**. The XRD of the mesoporous MCM-41 material as-synthesized (Fig. 1, curve (a)) displayed the expected four peaks of a hexagonal ordered array indexed as (100), (110), (200), and (210) Bragg reflections. In the curve (b) (figure 1), corresponding to the MCM-41 calcined sample, a significant shift of the (100) reflection in the XRD is clearly observed. This displacement, together with the broadening of the (110) and (200) reflections, corresponds to an approximate cell contraction of 6–8 Å due to the condensation of silanol groups in the calcination step. For **NM1** (Fig. 1, curve (c)) reflections (110) and (200) were lost, most likely due to a reduced contrast as the result of the loading and functionalization process. Yet the presence of the d100 peak in the XRD patterns in both S1 and S1–CPT suggested that the pore loading (with sulforhodamine B) and functionalization process did not modify the mesoporous MCM-41 scaffolding.

The Transmission Electron Microscopy (TEM) images also show the preservation of the mesoporous structure in **MN1**. Figure 1 (right) show the morphology of the prepared mesoporous material. MCM-41 was obtained as spherical particles showing a mean diameter of 94±5 nm and it was observed that the loaded and functionalized **NM1** maintains the initial MCM-41 matrix morphology. In addition, the characteristic channels of a mesoporous matrix were observed as alternate black and white lines.
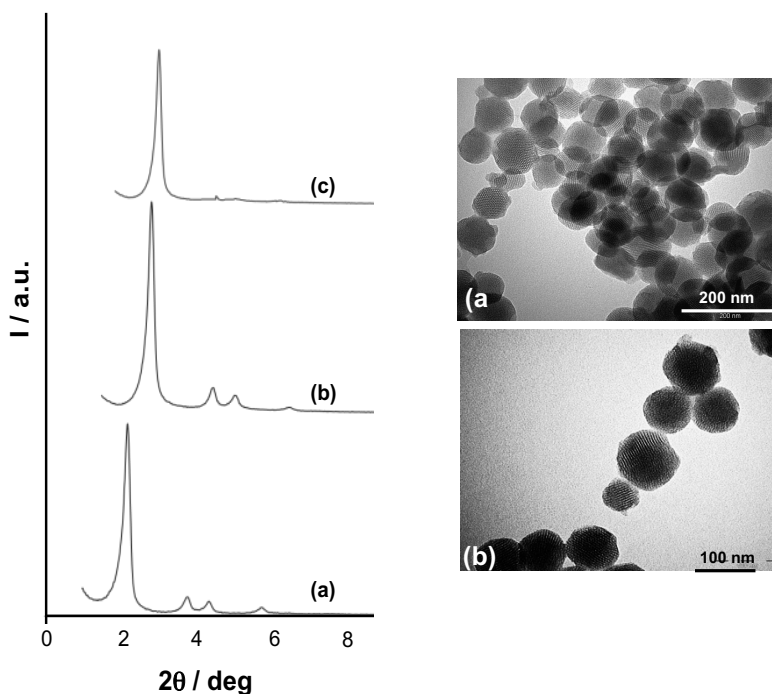
Figure 1. Left: XRD patterns for the nanoparticulated MCM-41 as-synthesized (a), calcined MCM-41 nanoparticles (b) and NM1(c); Right: TEM images of (a) calcined MCM-41 sample and (b) solid S1, showing the typical hexagonal porosity of the MCM-41 mesoporous matrix.

The contents of sulforhodamine B and the BODIPY compound **P1** in solid **NM1** were determined by elemental analysis and they were 0.110 (mmol g^{-1} SiO_2) of 0.122 (mmol g^{-1} SiO_2) of BODIPY and 0.287 (mmol g^{-1} SiO_2) of sulforhodamine b.
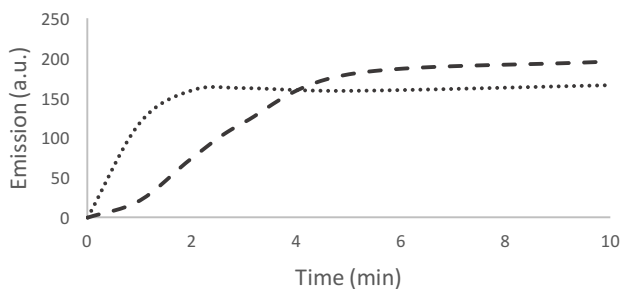
Figure 2: Fluorescence emission of **NP1** (acetonitrile, 1.0 x 10^{-5} mol dm^{-3}) (λ_{exc} = 520 nm) exposure at 1 ppm of NO_2 gas and monitorized at different times.

In a first step, to determine the optimal response time of the sensor system, 1 mg of **NM1** was suspended in 3 mL of acetonitrile and exposed to 1 ppm of NO_2(g) and the optical response was monitored by fluorescence (figure 2). An emission band at 530 nm (λ_{ex}= 520 nm) appeared first, provided by the BODIPY-aldehyde (BA) formation and then an emission band centered at 570 nm appeared slowly corresponding to the delivery of the cargo, (sulforhodamine B). The optimal time for measurement was found to be 5 min when the cargo was completely delivered and the appearance of the BODIPY-aldehyde **BA** was complete.
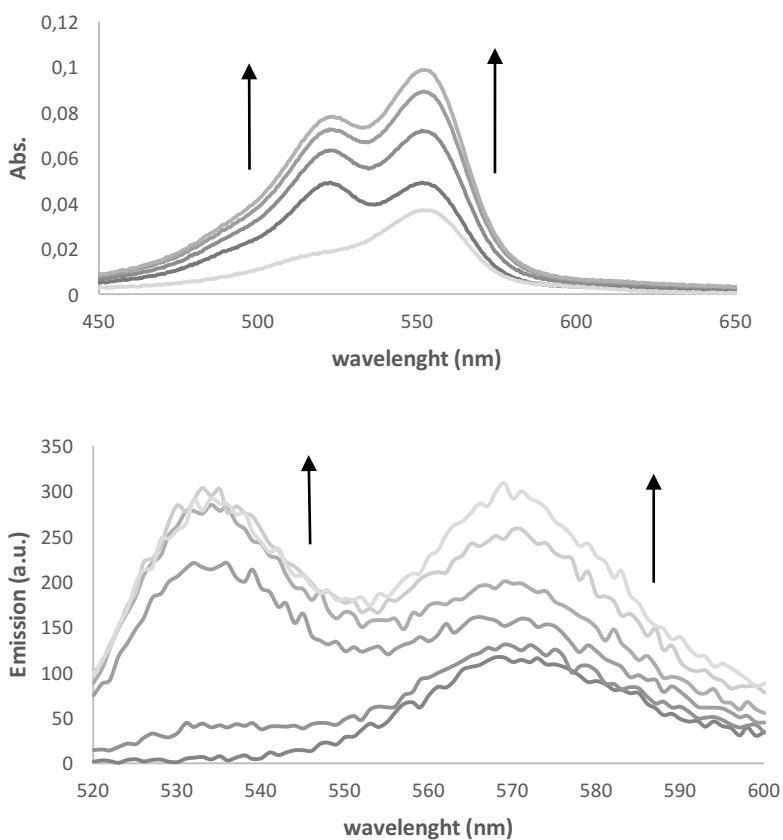
Figure 3: UV-Vis spectra (a) and fluorescence emission spectra (λ_{exc} = 520 nm) (b) of **NM1** (acetonitrile, 1.0 x 10^{-5} mol dm^{-3}) upon exposure to increasing amounts of NO_2 gas for five minutes.

To study the NO_2 detection in detail using the **NM1** in a typical experiment, 1 mg of **NM1** was suspended in 3 mL of acetonitrile at room temperature. The suspension was stirred and increasing concentrations of NO_2, provided by a commercial cylinder diluted with N_2, were bubbled through the solution, during 5 minutes and then, filtered. The apparition of BODIPY-aldehyde **BA** and the delivery of the sulforhodamine B dye were monitored by UV-vis absorption (lmax = 551 nm) and by fluorescence emission spectroscopies, following the emission band of **BA** centered at 530 nm (λ_{exc} = 520 nm) and the sulforhodamine B emission band centered at 570 nm (λ_{exc} = 520 nm) (see Figure 3).

Detection limits for the reaction of NO_2 with **NM1** in acetonitrile were evaluated by UV-vis and fluorescence titration experiments. In UV-vis spectra the detection limit was calculated using the band at 551 nm which is attributed to the delivery of the sulforhodamine b and for fluorescence emission the band at 571 nm (λ_{exc}=550 nm) *vs* concentration of NO_2 (g).

The limit of detection (LOD) was calculated by using the expression LOD=*3s_b/m*, in wich s_b is the standard deviation of blank measurements and *m* is the slope of the linear regression plot. [21] Limits of detection (LOD) of 0.19 ppm (from UV-vis) and 0.11 ppm (from fluorescence) were determined (see supporting information). These LOD are lower than the alarm threshold of 400 $\mu g/m^3$ (ca. 0.2 ppm) established by the European Community for nitrogen dioxide.[22]

Figure 4: Visual changes observed for **NM1** in acetonitrile suspension before and after exposure to 0.25 and 0.5 ppm of NO_2 gas, respectively.

NM1 (1 mg) suspended in acetonitrile (3 mL) after exposure to NO_2 shows a clear color change from pale pink to pink at 0.25 ppm and bright pink at 0.5 ppm (Figure 4). This color changes can be observed by naked-eye and suggest the possible application of **NM1** to real-time monitoring.
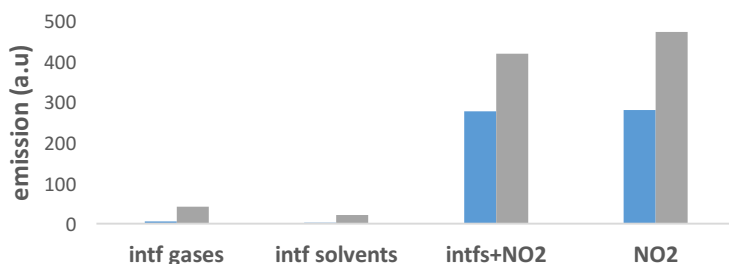
Figure 5: Interferents studies of **NM1** with hazardous gases, most common organic solvents and competitive studies. Blue emission at 530 nm and grey at 570 nm.

One important issue in relation to the design of probes for pollutant gases is the role played by potential interferents or false-positive outcomes produced by other species. Bearing this in mind, the reactivity of **NM1** with other hazardous gases (i.e. NO, CO_2, H_2S, SO_2 (up to 100 ppm)) was also studied. Moreover, the probe was also tested in the presence of vapours of acetone, hexane, chloroform, acetonitrile and toluene (up to 100 ppm in air). No changes in the fluorescence spectra were produced in the presence of any of the studied interferents. The emission at 530 nm (λ_{exc} = 520 nm) provided by the BODIPY-aldehyde **BA** and the sulforhodamine b emission band centered at 570 nm (λ_{exc}=550 nm) don't have any remarkable change, in fact the delivery of the cargo does not occur with any of the potential interferents. In addition, a remarkable response to NO_2 was observed even in the presence of these compounds (Figure 5). Such behaviour indicated that **NM1** is a suitable selective probe for the detection of NO_2 in real environments.

In summary we have demonstrated, that it is possible to use functionalized BODIPY compounds as gatekeepers of the surface of SMPS. This provides a suitable method for the design of delivery systems to release the guests in presence of NO_2. It is advisable to remark that it is a selective and sensitive method of detection of NO_2(g) with LOD notably lower than the toxicity limits. In particular, the paradigm of the monitoring occurs via double check: the cargo delivery and the generated BOPIPY-aldehyde derivative.

References

[1] Ariga, K.; Vinu, A.; Hill, J. P.; Mori, T. Coord. Chem. Rev. **2007**, *251*, 2562.

[2] Katz, E.; Willner, I. Angew. Chem. Int. Ed. **2004**, *43*, 6042

[3] Descalzo, A. B.; Martínez-Mañez, R.; Sancenón, F.; Hoffmann, K.; Rurack, K. Angew. Chem., Int. Ed. **2006**, *45*, 5924.

[4] (a) Puoci, F.; Iemma, F.; Picci, N. Curr. Drug Delivery **2008**, *5*, 85. (b) Siepmann, F.; Siepmann, J.; Walther, M.; MacRae, R.; Bodmeier, R. J. Controlled Release **2008**, *125*, 1.

[5] Hamidi, M.; Azadi, A.; Rafiei, P. AdV. Drug DeliVery ReV. **2008**, *17*, 1638.

[6] Pouton, C. W.; Porter, C. J. H. AdV. Drug DeliVery ReV. **2008**, *17*, 625.

[7] Rijcken, C. J. F.; Soga, O.; Hennink, W. E.; van Nostrum, C. F. J. Controlled Release **2007**, *120*, 131.

[8] Andresen, T. L.; Jensen, S. S.; Jorgensen, K. Prog. Lipid Res. **2005**, *44*, 69.

[9] (a) Beck, J. S.; Vartuli, J. C.; Roth, W. J.; Leonowicz, M. E.; Kresge, C. T.; Schmitt, K. D.; Chu, C. T.-W.; Olson, D. H.; Sheppard, E. W.; McCullen, S. B.; Higgins, J. B.; Schlenker, J. L. J. Am. Chem. Soc. **1992**, *114*, 10834. (b) Wright, A. P.; Davis, M. E. Chem. ReV. **2002**, *102*, 3589. (c) Kickelbick, G. Angew. Chem., Int. Ed. **2004**, *43*, 3102. (d) Stein, A. AdV. Mater. **2003**, *15*, 763.

[10] (a) Perez-Esteve, E; Ruiz-Rico, M.; Martínez-Mañez, R.; Barat, J. M. *Journal of Food Science,* **2015**, *80*, E2504; (b) Alberti, S.; Soler-Illia, G. J. A. A.; Azzaroni, O. *Chem. Commun*., **2015**, *51*, 6050.

[11] Sancenon, F.; Pascual, Ll.; Oroval, M.; Aznar, E.; Martinez-Mañez, R. Chemistry Open **2015**, *4*, 418.

[12] a) L. J. Folinsbee, Environ. Health Perspect., **1992**, *100*, 45; b)R.J.W. Melia, C. Florey, D.G. altman, A.V. Swan, Br. Med. J., **1977**, *2*, 149; c) L.M. Neas, D.W. Dockery, J.D. Spengler, F.E. Speizer, B.G. Ferris, Am. J. Epidemion., **1991**, *134*, 204.

[13] X. Meng, C. Wang, D. Cao, C.M. Wong, H. Kan, Atmos. Environ. **2013**, *77*, 149.

[14] H. Li,L. Chen, Z. Guo, N. Sang, G. Li, J. Hazard. Mater., **2012**, *46*, 225.

[15] Mokhari J., Naimi-Jamal M. R., Hamzehal H. 11th international Electronic Conference on Synthetic Organic Chemistry (ECSOC-11) 1-30 November 2007.

[16] (a) Boens N., Leen V., Dehaen W. Chem. Soc. Rev., **2012**, *41*, 1130 (b) Wang D., Shiraishi Y., Hiari T., Tetrahedron Lett., **2010**, *51*, 2545; (c) X. Xie, Y. Qin, Sens. Actuat. B-Chem., **2011**, *156*, 213; (d) Wang D., Shiraisi Y., Hirai T., Chem. Comm., **2011**, *47*, 2673; (e) Sun H. B., Liu S. J., Ma T. C., Song N. N., Zhao Q., W. Huang, New J. Chem, **2011**, *35*, 1194; (f) Son H., Lee J. H., Kim Y. R., Han S., Liu X., Jaworski J., Jung H., Analyst, **2012**, *137*, 3914.

[17] Coll. C; Bernardos. A; Martínez-Mañez. R; Sancenón. F. *Acc. Chem. Res.* **2013**, 46, 339.

[18] (a) Cabrera, S.; El. Haskouri, J.; Guillem, J.; Latorre, J.; Beltrán, A.; Beltrán, D.; Marcos M. D.; Amorós, P. *Solid State Sci.*, **2000**, *2*, 405; (b) Radu, D. R.; Lai, C.-Y.; Jeftinija, K.; Rowe, E. W.; Jeftinija S.; Lin, V. S. Y. *J. Am. Chem. Soc.*, **2004**, *126*, 13216.

[19] Kshirsagar, Umesh A.; Mhaske, Santosh B.; Argade, Narshinha P. Tetrahedron Letters, **2007**, *48*, 3243.

[20] Casasús, R.; Climent, E.; Marcos, M. D.; Martínez-Máñez, R.; Sancenón, F.; Soto, J.; Amorós, P.; Cano, J.; Ruiz, E. *J. Am. Chem. Soc.*, **2008**, *130*, 1903.

[21] M. Zhu,M. Yuan, X. Liu, J. Xu, J. Lv, C. Huang, H. Liu, Y. Li, S. Wand, D. Zhu, Org. let. **2008**, *10*, 1481.

[22] European commission (accessed February 2016), http://ec.europa.eu/environment/air/quality/standards.html

Supporting Information

Chemicals.
The chemicals tetraethylorthosilicate (TEOS), *n*-cetyltrimethylammonium bromide (CTABr), sodium hydroxide (NaOH), (3-isocyanatopropyl)triethoxysilane and 4-hydroxybenzyl alcohol were purchased from Sigma-Aldrich Química S. A. (Madrid, Spain) and used without further purification. THF was dried before use.

General methods.
PXRD, TGA, elemental analysis, TEM, N_2 adsorption-desorption, NMR, and fluorescence spectroscopy techniques were employed to characterize the synthesized materials. Powder X-ray measurements were performed on a Philips D8 Advance Diffractometer using CuKα radiation. Thermogravimetric analyses were carried out on a TGA/SDTA 851e Mettler Toledo balance, using an oxidant atmosphere (air, 80 mL/min) with a heating program consisting of a heating ramp of 10°C per minute from 393 to 1273 K and an isothermal heating step at the final temperature for 30 min. TEM images were obtained with a 100 JEOL JEM-1010 microscope. N_2 adsorption-desorption isotherms were recorded with a Micromeritics ASAP2010 automated sorption analyzer. The samples were degassed at 120°C in vacuum overnight. The specific surface areas were calculated from the adsorption data in the low pressure range using the BET model. Pore size was determined following the BJH method. The ^{1}H and ^{13}C NMR spectra were recorded in a deuterated solvent as the lock and in a residual solvent as the internal reference. The high-resolution mass spectra were recorded in the positive ion mode in a VG-AutoSpec. The UV-vis spectra were recorded using a 1-cm path length quartz cuvette.

Synthesis of mesoporous MCM-41 nanoparticles.
The MCM-41 mesoporous nanoparticles were synthesised by the following procedure: *n*-cetyltrimethylammonium bromide (CTABr, 1.00 g, 2.74 mmol) was first dissolved in 480 mL of deionised water before adding 3.5 mL of a solution of NaOH 2M till getting a basic pH 8. Then, the solution was heated to 80°C and TEOS (5.00 mL, 2.57 x 10^{-2} mol) was added dropwise to the surfactant solution at maximum stirring. The mixture was stirred for 2 h at 80°C. A white precipitate was obtained and isolated by centrifugation. Once isolated, the solid was washed with deionised water and ethanol till obtaining neutral pH in the solution, and was dried at 60ºC (MCM-41 as-synthesised). To prepare the final porous

material (MCM-41), the as-synthesised solid was calcined at 550ºC using an oxidant atmosphere for 5 h in order to remove the template phase.

Materials characterization.

Figure 1 (see manuscript) shows the powder X-ray diffraction (PXRD) patterns of the nanoparticulated MCM-41 matrix as-synthesized, the MCM-41 calcined and **NM1** solid (loaded with sulforhodamine B and functionalized with the Bodipy phenyl hydrazone **1**). The MCM-41 as-synthesized displayed the four typical low-angle reflections of a hexagonal-ordered matrix indexed at (100), (110), (200) and (210) Bragg peaks (curve a). In curve of MCM-41 calcined, a significant shift of the (100) peak in the PXRD is observed (curve b). These observations are in agreement with the condensation of silanols in the calcination step, which caused an approximate cell contraction of 6-8 Å. Finally, curve c shows the **NM1** PXRD pattern. For **NM1** a broadening of the (100) and (200) peaks are observed due to a reduction in contrast related to the functionalisation process and to the filling of mesopores with sulforhodamine B. Nonetheless, the intensity of the (100) peak in this pattern strongly indicates that the loading process with the dye and the additional functionalisation with **1** did not modify the mesoporous MCM-41 scaffold.

In Figure SI-1 (curve a), the N_2 adsorption-desorption isotherms of the MCM-41 calcined nanoparticles is represented. This curve displays an adsorption step with a P/P_0 value of between 0.1 and 0.3, corresponding to a type IV isotherm, which is typical of mesoporous materials. This first step is due to nitrogen condensation in the mesopores. With the BJH model on the adsorption curve of the isotherm, the pore diameter and pore volume were calculated to be 2.97 nm and 0.73 cm^3g^{-1}, respectively. The absence of a hysteresis loop in this range and the low BJH pore distribution suggested a cylindrical uniformity of mesopores. The total specific area was 895 m^2g^{-1}, calculated using the BET model. A second remarkable feature of the curve is the characteristic H1 hysteresis loop that appears in the isotherm at a high relative pressure ($P/P_0 > 0.8$) and associated with a wide pore size distribution. This corresponds to the filling of the large pores among the nanoparticles (2.45 cm^3g^{-1} calculated by the BJH model) due to textural porosity. For the **S1** material, the N_2 adsorption-desorption isotherm is typical of mesoporous systems with filled mesopores (see Figure SI-1, curve b). In this case, and as expected, a lower N_2 adsorbed volume (0.35 cm^3g^{-1}) and surface area (265 m^2g^{-1}) were found when compared with the starting MCM-41 material. As observed, this solid presents a curve with no gaps at low relative

pressure values if compared to the mother MCM-41 matrix (curve a). Table SI-1 shows the BET-specific surface values, pore volumes and pore sizes calculated from the N_2 adsorption-desorption isotherms for MCM-41 calcined and **NM1** solid. The contents of grafted **1** and cargo in solid **NM1** were determined by thermogravimetric and elemental analysis and are shown in Table SI-2.

TEM images for the MCM-41 calcined sample and **NM1** solid are depicted in Figure 1 (see manuscript). In both cases, a detailed look to individual nanoparticles, showed the typical channels of the MCM-41 matrix visualized as alternate black-white lines. Finally, a particle diameter of ca. 95 nm was determined.
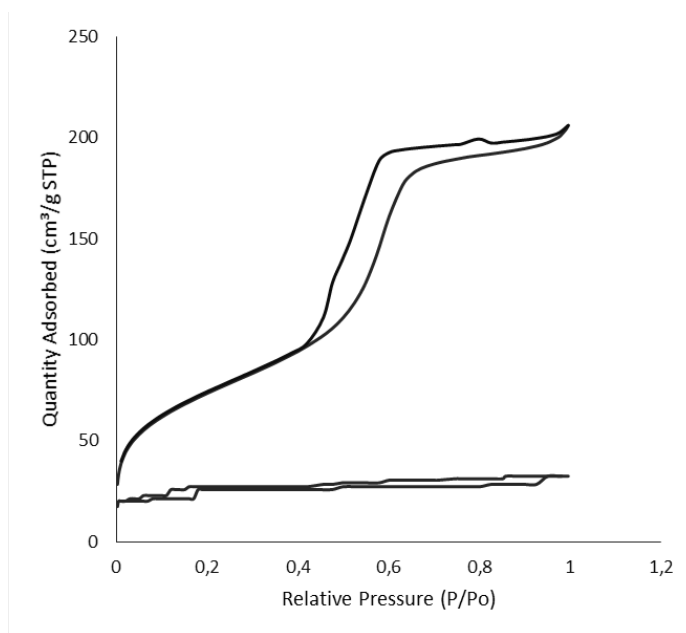
Figure SI-1. Nitrogen adsorption–desorption isotherms for: (a) MCM-41 calcined mesoporous material and (b) **NM1**.

Table SI-1. BET-specific surface values, pore volumes and pore sizes calculated from the N_2 adsorption-desorption isotherms for selected materials.

Sample	$S_{BET}/m^2/g$	BJH Pore[a]/nm	Total Pore Volume[b]/cm^3/g
MCM-41	895	2.97	0.73
NM1	235	2.11	0.17

[a] Pore volumes and pore sizes were associated with only intraparticle mesopores.

[b] Pore size estimated by the BJH model applied to the adsorption branch of the isotherm.

Table SI-2. Content (α) in mmol of anchored molecules and cargo per gram of SiO_2 for the prepared solids.

Solid	α_1 (mmol/g SiO_2)	α_{P1} (mmol/g SiO_2)	α_{cargo} (mmol/g SiO_2)
NM1	0.110	0.122	0.287

Cargo release studies.

NM1 consists in mesoporous MCM-41-type nanoparticles containing sulforhodamine B in the pores and capped with Bodipy phenyl hidrazone **P1**. As part of the nanoparticles design, the grafted **1** was expected to cap the pores and inhibit cargo delivery. Subsequent exposure to NO_2 (g) yielded a Bodipy Aldehyde. In order to check this aperture mechanism release kinetics studies at different NO_2 concentration were carried out. In a typical experiment, 1.0 mg of solid **NM1** was suspended in 3.0 mL of Acetonitrile at different concentrations. The suspensions were stirred and at certain times aliquots were separated and centrifuged to eliminate the solid and dye delivery was determined by monitoring fluorescence of sulforhodamine B (λ_{exc} = 520 nm, λ_{em} = 570 nm) and the appearing of the Bodipy Aldehyde (λ_{exc} = 520 nm, λ_{em} = 530 nm) in the organic phase. Delivery results are shown in Figure 3 in the manuscript.
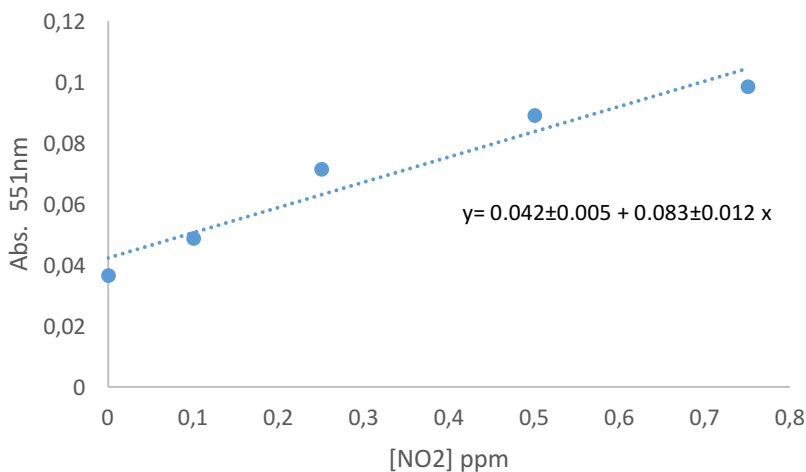
y= 0.042±0.005 + 0.083±0.012 x

Figure SI-2: Absortion at 551 mn of **NM1** (in acetonitrile) *versus* increasing amounts of NO_2
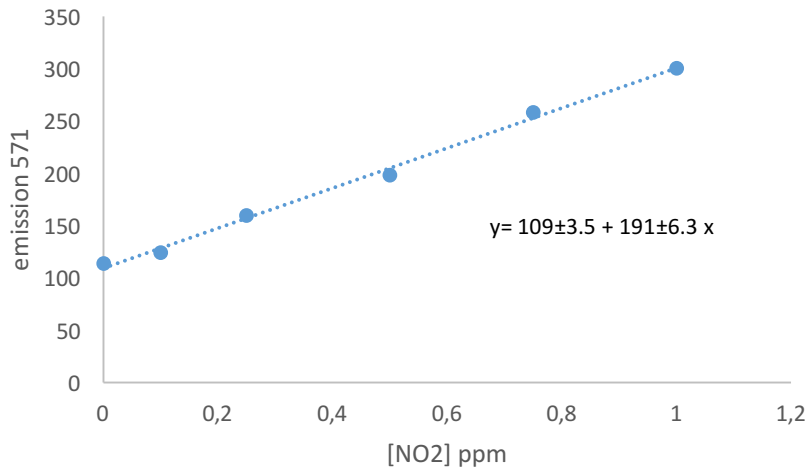
Figure SI-3: Emission at 571 mn of **NM1** (in acetonitrile) *versus* increasing amounts of NO_2

Part II:
Nitric oxide detection

II.1 Introduction

Nitric oxide (NO) is a well-known bioactive molecule that participates in a wide range of bioregulatory and immune response processes.[92] Detection and quantification of NO in biological systems presents significant analytical challenges for several reasons being the low concentration of NO *in vivo* a major concern. NO is endogenously generated by NO synthases (NOS), of which there are three isoforms. NO is release in the nanomolar rages, whereas iNOS can release NO in the micromolar ranger for extended periods of time.

NO can also be scavenged by reactions with electron-rich biomolecules such as haemoglobin and interaction with the d-orbitals of transition metal (particularly iron), or by oxidation with endogenous reactive oxygen species form nitrite and nitrate in the cells. As a result, the average lifetime of NO is in the range of milliseconds to seconds.

Detection *in vivo* and *in situ* of NO was developed in the last decade. NO is considerate a relatively stable free radical, that in biological media reacts with other free radicals and metaloproteins. On the metabolism, NO presents also other properties as: high diffusely, short life time and variable concentrations in some case lower than micromolar. This factor makes its analysis and detection difficult *in vivo* and *in situ*. For these reasons, the development of new systems for its detection is an important research area nowadays.

A huge number of strategies for NO detection has been developed, such as those base on:

- Chemiluminescence[93]
- Spectroscopic methods: UV, Fluorescence, EPR, electrochemistry. [94]

Metal-based probes that take advantage of the reactivity of NO at the metal site have also been reported; for instance, nitric oxide sensing has

---

[92] M. A. Marletta, *Cell* **1994**, *78*, 927-930.

[93] P. Wardman, *Free Radic. Biol. Med*., **2007**, 43, 995.

[94] a) E. M. Hetrick, M. H. Schoenfisch, *Annu. Rev. Anal. Chem*., **2009**, 2, 2620. b) D. Tiskas, *J. Chromatogr. B*, **2007**, 851, 51 c) X. Che, X. Tian, I. Shin, Y. Yoon, *Chem. Soc. Rev*., **2011**, 40, 4783.

been accomplished with Co^{II}, Fe^{II}, Ru^{II}, Rh^{II} and Cu^{II} complexes.[95] However, some of these probes display drawbacks, such as dependence on pH or the tendency of certain dyes to form aggregates.

II.2 Objectives

Following our interest in the development of chromo-fluorogenic probes for NO and the detection *in vivo* and *in situ* our purpose were:

- Synthesis of a new BODIPY-Cu^{II} complex

- To study the chromo-fluorogenic properties of the complex and the presence/absence of NO.

- Evaluation of the behaviour of BODIPY-complex in presence of potential interferents to test their applicability.

- Evaluation of the response in cells for its application *in vivo* and *in situ* detection.

II.3 Chemosensor design

The main focus was to prepare a BODIPY-Cu^{II} complex for detecting NO. The design was carried out bearing in mind that the copper centre can undergo reduction to Cu^{I} in the presence of NO followed by demetallation.

S. J. Lippard and coworkers[96] develop a copper fluorescein complex ($Cu^{II}FL$) which exhibits NO-triggered fluorescence enhancement. NO reduces the Cu^{II} of **21** to Cu^{I} (scheme 1) forming NO^{+}. NO^{+}

---

[95] a) M. H. Lim, B. A. Wong, W. H. Pitcock Jr., D. Mokshagundam, M. -H. Balk, S. J. Lippard, *J. Am. Chem. Soc.* **2006**, *128*, 14364-14373; b) M. H. Lim, S. J. Lippard, *Acc. Chem. Res.* **2007**, *40*, 41-51; c) C. Khim, M. C. Lim, K. Tsuge, A. Iretskii, G. Wu, P. C. Ford, *Inorg. Chem*. **2007**, *46*, 9323-9331; d) M. D. Pluth, M. R. Chan, L. E. McQuade, S. J. Lippard, *Inorg. Chem*. **2011**, *50*, 9385-9392.
[96] a) Z. J. Tonezetich, L. E. Mc. Quades, S. L. Lippard, Inorg. Chem., **2010**, 49, 6338. b) M. H. Lim, S. J. Pillard, Acc. Chem. Res., **2007**, 40, 41

nitrosates the ligand and release Cu[I]. This fact immediately turns on the fluorescence.

$$Cu^{II} + FL \rightleftharpoons Cu^{II}FL + NO \longrightarrow Cu^{I} + FL-NO$$

$$21$$
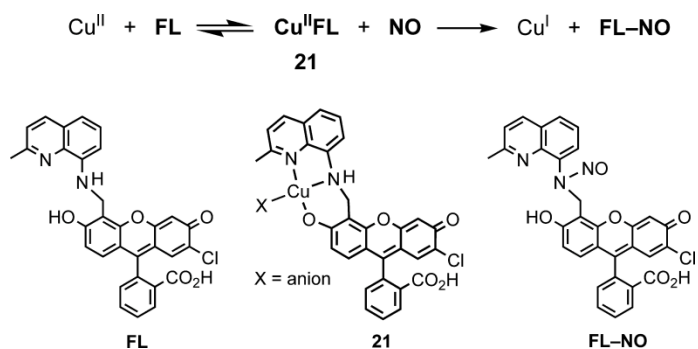
Scheme 1: Nitric oxide sensor development by Lippard

On the other hand, it is known that BODIPY derivatives that bear a 4-pyridine moiety attached to the meso position induce fluorescence quenching when the pyridine group is protonated, through the formation of a weakly emissive charge-transfer state.[97]

---

[97] a) A. Harriman, L. J. Mayon, J. Ulrrich, R. Ziessel, *Chem. Phys. Chem*. **2007**, *8*, 1207-1214; b) J. Bartelmess, W. W. Weare, R. D. Sommer, *Dalton Trans.* **2013**, *42*, 14883-14891.

Chapter 6:
BODIPY-CU(II) complex for NO detection

A BODIPY-based Cu^{II}-bipyridine complex for highly selective NO detection

L. Alberto Juárez,[a,b] Andrea Barba-Bon,[a,c,d] Ana M. Costero,*[a,b] Ramón Martínez-Máñez,[a,c,d] Félix Sancenón,[a,c,d] Margarita Parra,[a,b] Pablo Gaviña,[a,b] M. Carmen Terencio,[a,e] and M. José Alcaraz[a,e]

^{a} *Instituto Interuniversitario de Reconocimiento Molecular y Desarrollo Tecnológico (IDM), Unidad Mixta Universidad Politécnica de Valencia-Universidad de Valencia, Spain.*
^{b} *Departamento de Química Orgánica. Universidad de Valencia, Doctor Moliner 50, 46100, Burjassot, Valencia, Spain. E-mail: ana.costero@uv.es*
^{c} *Departamento de Química, Universidad Politécnica de Valencia, Camino de Vera s/n, 46022, Valencia, Spain. E-mail: rmaez@qim.upv.es*
^{e} *Departamento de Farmacología. Universidad de Valencia. Vicente Andrés Estellés s/n. 46100- Burjassot. Valencia. Spain*
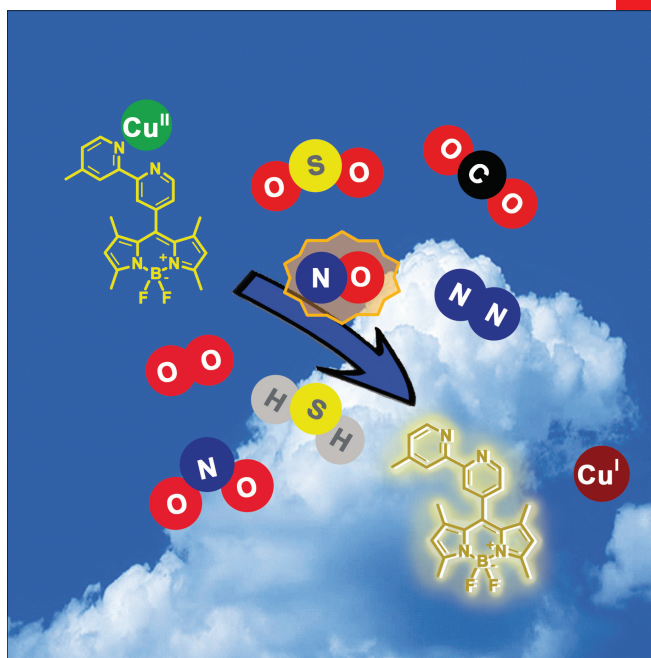
Cover Picture:
A. Costero et al.
A Boron Dipyrromethene (BODIPY)-Based Cu[II]–Bipyridine Complex for Highly Selective NO Detection

177

Abstract:

A new BODIPY-containing Cu^{II}-bipyridine complex for the simple selective fluorogenic detection of NO in air and in live cells is reported. The detection mechanism is based on NO-promoted Cu^{II} to Cu^{I} reduction, followed by demetallation of the complex, which results in the clearly enhanced emission of the BODIPY unit.

In recent years, environmental awareness has grown due to social dissatisfaction with the state of the environment.[1] As a result, more restrictive environmental laws have been introduced. In this context, air pollution is one of the major problems in urban areas, whose main sources of pollutants are the combustion processes of fossil fuels used in power plants, vehicles and other incineration processes. The main combustion-generated air contaminants are nitrogen oxides (NO_x), considered primary pollutants of the atmosphere as they are responsible for photochemical smog, acid rain and ozone layer depletion.[2] On the other hand, NO is a well-known bioactive molecule that participates in a wide range of bioregulatory and immune response processes.[3]

For these reasons, intensive experimental research is being conducted for NO monitoring, and several analytical techniques, such as electrophoresis, electron paramagnetic resonance (EPR) or GC-mass spectroscopies, chemiluminescence or electrochemical methods, have been developed to detect this hazard.[4] Even though these methods offer certain benefits, they also show some limitations which typically involve poor specificity and the use of expensive experimental apparatus, which restrict their application in practice. Recently, the development of fluorogenic probes has gained growing interest as an alternative to classical instrumental procedures.[5] In this context, fluorogenic probes are especially appealing because they allow simple detection *in situ* or/and at site, usually without any sample pre-treatment. Moreover, changes in emission can be detected by simple equipment and it is a very sensitive detection technique. Changes in emission properties can also be detected to the naked eye, which makes this procedure very appealing.

Several probes for the fluorogenic detection of NO have been reported. For instance, poorly fluorescent vicinal diamines can be transformed into triazoles by NO, which results in a significant increase in fluorescence.[6] Other sensing protocols based on NO-induced ring closure,[7] de-amination reactions[8] or NO-induced aromatization,[9] have been recently

studied. Metal-based probes that take advantage of the reactivity of NO at the metal site have also been reported; for instance, nitric oxide sensing has been accomplished with Co[II], Fe[II], Ru[II], Rh[II] and Cu[II] complexes.[10] However, some of these probes display drawbacks, such as dependence on pH or the tendency of certain dyes to form aggregates. Given the significance of NO to human health and diseases, most probes have been tested to monitor NO production *in vivo*, whereas very few studies have been conducted into nitric oxide detection in air.
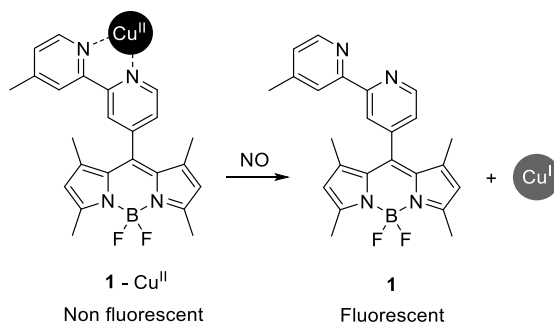
Scheme 1. Complex 1-Cu[II] and schematic outline of the sensing paradigm.

Following our interest in designing probes for the fluorogenic detection of gases,[11] we focused on the potential use of BODIPY for designing NO sensing probes. BODIPY is a well-known fluorophore that possesses valuable optical characteristics, such as absorption and fluorescence transitions in the visible spectral region with high molar absorption coefficients and fluorescence quantum yields, good stability and no dependence on pH.[12] Yet despite these advantageous BODIPY fluorophore optical properties, as far as we know, no metal-complexes based on BODIPY derivatives have been reported for fluorogenic NO detection.

The design of our probe was based on two concepts. First, it is known that the BODIPY derivatives that bear a 4-pyridine moiety attached to the meso position induce fluorescence quenching when the pyridine group is protonated, through the formation of a weakly emissive charge-transfer state.[13] We postulated that similar BODIPY-bipyridine derivatives which coordinate metal cations would also be poorly emissive. On the other hand, it has been well-established that the copper centre in Cu[II] complexes undergoes reduction to Cu[I] in the presence of NO, followed by demetallation. Based on these concepts, we prepared complex **1**-Cu[II] (see Scheme 1). This complex is expected to be poorly fluorescent, whereas

significant fluorescence enhancement is expected to be selectively observed in the presence of NO.

The synthesis of BODIPY derivative **1** began with the preparation of bipyridine aldehyde **2** by the oxidation of 4,4'-dimethyl-2,2'-bipyridine with selenium oxide.[14] Compound **1** was readily obtained by the condensation of **2** with 2,4-dimethylpyrrole following standard BODIPY synthesis procedures (see Scheme 2).[15] BODIPY **1** was characterised by ^{1}H-NMR, ^{13}C-NMR and MS (see the Supporting Information for details).
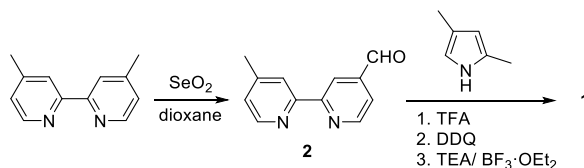
Scheme 2. Synthesis of ligand **1**.

Solutions of **1** (1.0×10^{-4} M in acetonitrile) showed an intense absorption band at λ = 500.5 nm (log ε= 7.6) and an intense emission band at λ = 520.5 nm (λ_{exc} = 478 nm, Φ = 0.570). Moreover, fluorescence quenching was observed when Cu^{II} (as nitrate salt) was added (see Table 1). This was in agreement with the coordination of the Cu^{II} cation to the bipyridine binding group. This metal complexation likely triggered an intramolecular charge-transfer process in the excited state from the BODIPY core to the bipy-Cu^{II} unit, and the resulting charge-transfer state became weakly fluorescent.[13]

Table 1. The UV-vis and fluorescence data of **1** and **1**-Cu^{II}.

	λ_{abs} (nm)	log ε	λ_{em} (nm)	$\Phi^{[a]}$
1	500.5	7.6	520.5	0.570
1-Cu (II)	504.0	7.1	519.0	0.071

[a] Quantum yields were calculated using rhodamine B in ethanol as a standard (Φ_{EtOH} = 0.49, λ_{exc} = 478 nm)

The formation of 1:1 complexes between **1** and Cu^{II} was confirmed through titration experiments in acetonitrile. The stability constant for the formation of the corresponding **1**-Cu^{II} complex was calculated from fluorescence titration experiments (Figure 1) with the SPECFIT program.[16] A value of log K = 4.9±1.6 was determined. Additional experiments demonstrated that addition of Cu^I to the acetonitrile solutions of **1** induced no changes in either the UV or emission spectra,

which suggests this cation's poor coordination with the bipy unit. It was also found that the emission quenching of **1,** which was similar to that found for **1** with Cu^{II}, was observed in the presence of diamagnetic cation Zn^{II}. This finding indicates that the poor emission observed for the **1**-Cu^{II} complex was not due to the presence of a paramagnetic cation, but resulted from the coordination of the metal with the pyridine moiety attached to the meso position of the BODIPY fluorophore. Finally, the fluorescence emission intensity of **1** was evaluated at different pH values, with only minor changes in the pH range between 4–12 (see the Supporting Information).
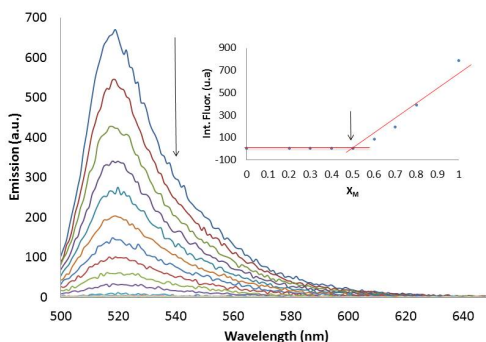
Figure 1. Fluorescence spectra of **1** (acetonitrile, 1.0 x 10^{-5} M) with increasing amounts of Cu^{II}. Inset: mole ratio graphic.
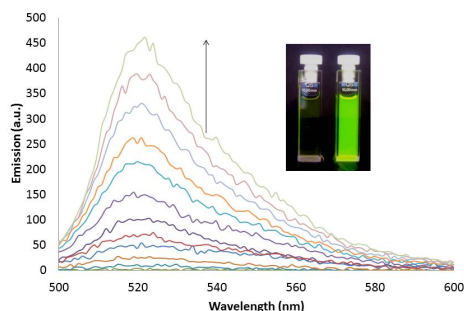
Figure 2. Fluorescence spectra of complex **1**-Cu^{II} (water: acetonitrile 9:1 v/v, 1.0 x 10^{-5} M) in the presence of increasing NO concentrations from 0 to 80 ppm after 5 min. Inset: the visual changes (λ_{ex} = 254 nm) observed for **1**-Cu^{II} before and after exposure to 1 ppm of NO.

Complex **1**-Cu^{II} was easily isolated by simply stirring **1** with one equivalent of Cu(NO$_3$)$_2$ in EtOH-water for 2 h. The resulting yellow precipitate was recrystallised from EtOH-water, filtered and dried. In order to evaluate the sensing ability of **1**-Cu^{II}, the water:acetonitrile (9:1 v/v) mixtures of the complex (1.0 x 10^{-5} M) were exposed for 5 min to N$_2$

atmospheres, which contained increasing quantities of NO, and the corresponding emission spectra were recorded. Presence of NO greatly increased the fluorescence emission at 520.5 nm, (λ_{exc} = 478 nm), which was attributed to the presence of free **1** (Figure 2). In fact, exactly the same emission band was observed for the solutions of **1** in the water:acetonitrile (9:1 v/v) mixtures. The fluorogenic sensing ability of probe **1**-Cu^{II} was also observed by the naked eye. In particular, a bright green emission was clearly seen when the solutions of **1**-Cu^{II} exposed to NO were illuminated at 254 nm with a conventional UV lamp (see Figure 2).

From the titration studies, limits of detection (LOD) of 3 ppm (from fluorescence) and 0.5 ppm (from UV-vis) were calculated by the 3Sb1/S procedure (Sb1 is the standard deviation of the blank solution and S is the slope of the calibration curve).[17] In addition, **1**-Cu^{II} was recovered after the oxidation of Cu^{I} to Cu^{II} induced by atmospheric oxygen. In particular, the regeneration of the **1**-Cu^{II} probe was achieved after keeping the **1**-Cu^{II}-NO mixture in NO-free air. This process was repeated at least 5 times with only minimal loss of fluorescence intensity (see Figure 3)
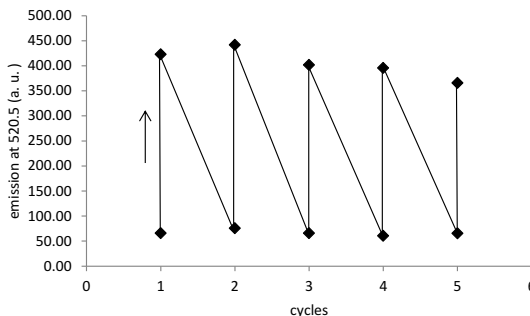
Figure 3. The cycles of emission intensity of **1**-Cu^{II} (1.0 x 10^{-5} M in acetonitrile) at λ_{em}= 520.5 nm (λ_{exc}= 500.5 nm) upon successive exposures to NO (5 min) and to a NO-free air atmosphere (24 h).

Encouraged by the sensing ability of BODIPY derivative **1**-Cu^{II}, we decided to move another step forward and we studied the potential use of the probe for detecting NO in air. To this end, a membrane that contained **1**-Cu^{II} was designed.
In a typical preparation, polyethylene oxide (Mw 400,000 Dalton) was slowly added to a solution of **1**-Cu^{II} in dichloromethane. The mixture was stirred until a highly viscous mixture was formed and finally poured into a

glass plate. The system was kept in a dry atmosphere for 24 h to obtain the corresponding sensing membrane.

In a typical assay, the membrane was placed into a container that held NO (1 ppm). After 5 min, fluorescence clearly enhanced, as observed by the naked eye with a conventional 254 nm UV lamp (Figure 4). A LOD of 0.3 ppm to the naked eye after 10 min for sensing NO in air was determined.[18]
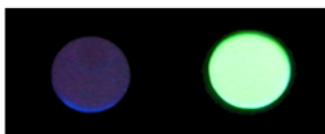

Figure 4. Emission of a polyethylene oxide membrane of **1**-Cu^{II} (λ_{ex} = 254 nm) (left) and after exposure to 1 ppm of NO in air for 5 min (right).

One important issue for designing probes for pollutant gases is the role played by the potential interferents or false-positive outcomes produced by other species. When bearing this in mind, the potential reactivity of **1**-Cu^{II}-containing membranes to other hazardous gases (i.e., NO_2, CO_2, H_2S, SO_2) at a concentration of up 100 ppm in air was also studied. The probe was also tested in the presence of vapours of acetone, hexane, chloroform, acetonitrile and toluene, and up to a concentration of 100 ppm in air. No emission changes were observed in the presence of any of these chemical species. Besides, competitive experiments demonstrated that the membrane was able to detect NO in a mixture that also contained the aforementioned gases and vapours (see the Supporting Information for details). Such behaviour indicated that **1**-Cu^{II} was a suitable highly selective probe for detecting nitric oxide in complex air samples.

Finally, we also assessed the ability of the probe to detect NO release in cells. In order to further demonstrate the biological application of BODIPY-copper complex 1-Cu^{II}, RAW 264.7 macrophages were stimulated for 18 h with *Escherichia coli* lipopolysaccharide to induce NO synthase (iNOS).[19] After washing cells with phosphate buffered saline, 1-Cu^{II} (10 µM) was added and NO release was initiated by the addition of L-Arginine as a substrate of iNOS. RAW 264.7 macrophages stimulated with only arginine or only **1**-Cu^{II} showed low fluorescence, whereas the addition of arginine in the presence of **1**-Cu^{II} significantly increased fluorescence, which demonstrates this compound's ability to detect NO released by cells (see Figure 5).
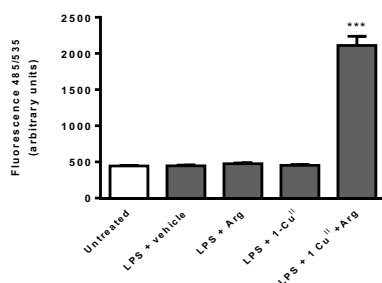
Figure 5. NO detection in RAW 264.7 macrophages stimulated with lipopolysaccharide (LPS). After cell washing, **1**-Cu^{II} (1.0 x 10^{-5} M), dissolved in water:acetonitrile 95:5 v/v (vehicle), was incubated for 30 min with cells, and Arginine (Arg) 100 μM was added to induce NO release. Data are expressed as mean±SEM (n=8-12). ***p < 0.001 compared to the LPS+vehicle-treated cells. Dunnett's t test for multiple comparisons.

Even though these results indicate that other components of the complex cellular matrix did not interfere with the detection results, further sensing experiments were carried out with some possible biological competitors in Cu(II) binding, such as cysteine, glutathione or histidine. No significant increment in fluorescence was observed in any case (see the Supporting Information, Fig. S14)
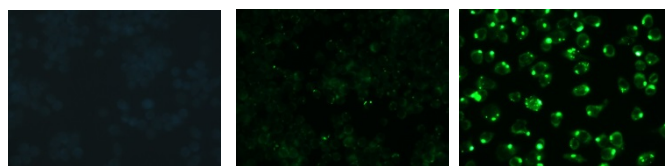
Figure 6. Fluorescence imaging of RAW 264.7 stimulated with LPS and incubated for 30 min with **1**-Cu^{II} (10 μM) in the presence or absence of Arginine (Arg) 100 μM.

Figure 6 also shows the fluorescence images of the RAW 264.7 cells stimulated with LPS and the incubation of **1**-Cu^{II} (10 μM) in the absence or presence or arginine (100 μM). Emission was clearly enhanced in the cells that contained NO. In a parallel experiment, absence of the cytotoxicity of **1**-Cu^{II} under the same conditions was demonstrated by the mitochondrial-dependent reduction of 3-(4,5-dimethylthiazol-2-yl)-2,5-diphenyltetrazolium bromide (MTT) to formazan (see the Supporting Information).

In summary, we report herein the synthesis and sensing properties of a new BODIPY-Cu^{II} complex for NO detection. Probe **1**-Cu^{II} contains a BODIPY fluorophore and a bipyridine unit capable of coordinating Cu^{II}. Reduction of Cu^{II} to Cu^{I} mediated by NO resulted in demetallation and a significant enhancement of the emission of the BODIPY unit. NO sensing was achieved in solution and in the gas phase. In particular, probe **1**-Cu^{II} in the polyethylene oxide membranes was satisfactorily used to monitor NO levels in air. Furthermore, the response of probe **1**-Cu^{II} to NO was selective in air and other hazardous gases, such as NO_2, CO_2, H_2S, SO_2, and vapours of different solvents at concentrations of up 100 ppm were unable to induce emission modulations. A LOD as low as 0.3 ppm to the naked eye after 10 min for NO sensing in air was calculated. Probe **1**-Cu^{II} was also suitable for NO detection in live RAW 264.7 macrophages with no cytotoxic effects.

Acknowledgements

References

[1]   K. Skalska, J. S. Miller, S. Ledakowicz, *Sci. Total Environ.* **2010**, *408*, 3976-3989.

[2]   M. A. Gomez-García, V. Pitchon, A. Kiennemann, *Environ. Int.* **2005**, *31*, 445-467.

[3]   M. A. Marletta, *Cell* **1994**, *78*, 927-930.

[4]   a) T. Nagano, *Luminescence* **1999**, *14*, 283-290; b) S. Ma, D.-C. Fang, B. Ning, M. Li, L. He, B. Gong, *Chem. Commun*. **2014**, *50*, 6475-6478 and references therein.

[5]   a) A. M. Costero, S. Gil, M. Parra, P. M. E. Mancini, R. Martinez-Mañez, F. Sancenon, S. Royo, *Chem. Commun*. **2008**, *44*, 6002-6004; b) T. J. Dale, J. Rebek, *Angew. Chem. Int. Ed*. **2009**, *48*, 7850-7852; c) S. Han, Z. Xue, Z. Wang, T. B. Wen*, Chem. Commun.* **2010**, *46*, 8413-8415; d) L. Ordronneau, A. Carella, M. Pohanka, J. -P. Simonato, *Chem. Commun*. **2013,** *49,* 8946-8948; e) W.-M. Xuan, Y.-T. Cao, J. -H. Zhou, W. Wang, *Chem. Commun*. **2013**, *49*, 10474-10476; f) G. H. Dennison, M. R. Sambrook, M. R. Johnston, *Chem. Commun*. **2014**, *50*, 195-197.

[6]   See for instance: a) Y. Gabe, Y. Urano, K. Kikuchi, H. Kojima, T. Nagano, *J. Am. Chem. Soc*. **2004**, *126*, 3357-3367; b) E. Sasaki, H. Kojima, H. Nishimatsu, Y. Urano, K. Kikuchi, Y. Hirata, T. Nagano, *J. Am. Chem. Soc*. **2005**, *127*, 3684-3685.

[7]   Y. Yang, S. K. Seidlits, .M. Adams, V .M. Lynch, C. E. Schmidt, E. V. Anslyn, J. B. Shear, *J. Am. Chem. Soc*. **2010**, *132*, 13114-13116.

[8]   A. Beltran, M. I. Burguete, D. R. Abánades, D. Pérez-Sala, S. V. Luis, F. Galindo, *Chem. Commun*. **2014**, *50*, 3579-3581.

[9]   S. Ma, D. C. Fang, B. Ning, M. Li, L. He, B. Gong, *Chem. Commun.* **2014**, *50*, 6475-6478.

[10]   See for instance: a) M. H. Lim, B. A. Wong, W. H. Pitcock Jr., D. Mokshagundam, M. -H. Balk, S. J. Lippard, *J. Am. Chem. Soc.* **2006**, *128*, 14364-14373; b) M. H. Lim, S. J. Lippard, *Acc. Chem. Res*. **2007**, *40*, 41-51; c) C. Khim, M. C. Lim, K. Tsuge, A. Iretskii, G. Wu, P. C. Ford, *Inorg. Chem*. **2007**, *46*, 9323-9331; d) M. D. Pluth, M. R. Chan, L. E. McQuade, S. J. Lippard, *Inorg. Chem*. **2011**, *50*, 9385-9392.

[11]   a) L. A. Juárez, A. M. Costero, M. Parra, S. Gil, F. Sancenón, R. Martínez-Máñez, *Chem. Commun.* **2015**, *51*, 1725-1727; b) J. Esteban, J. V. Ros-Lis, R. Martínez-Máñez, M. D. Marcos, M. Moragues, J. Soto, F. Sancenón, *Angew. Chem. Int. Ed.* **2010**, *49*, 4934-4937; c) M. E. Moragues, J. Esteban, J. V. Ros-Lis, R. Martínez-Máñez, M. D. Marcos, M. Martínez, J. Soto, F. Sancenón, *J. Am. Chem. Soc.* **2011**, *133*, 15762-15772; d) M. E. Moragues, A. Toscani, F. Sancenón, R. Martínez-Máñez, A. J. P. White, J. D. E. T. Wilton-Ely, *J. Am. Chem. Soc.* **2014**, *136*, 11930-11933.

[12]   a) A. Loudet, K. Burgess, *Chem. Rev*. **2007**, *107*, 4891-4932; b) G. Ulrich, R. Ziessel, A. Harriman*, Angew. Chem. Int. Ed*. **2008**, *47,* 1184-1201.

[13]   a) A. Harriman, L. J. Mayon, J. Ulrrich, R. Ziessel, *Chem. Phys. Chem*. **2007**, *8*, 1207-1214; b) J. Bartelmess, W. W. Weare, R. D. Sommer, *Dalton Trans.* **2013**, *42*, 14883-14891.

[14]   L. A. Eckermann, D. K. Barker, R. M. Hartings, A. M. Ratner, J. T. Meade, *J. Am. Chem. Soc*. **2005**, *127*, 11880-11881.

[15]   M. Kollomannsberger, K. Rurack, U. Resch-Genger, J. Daub., J*. Phys. Chem. A*. **1998**, *102*, 10211-10220.

[16]   SPECFIT/32TM GLOBAL ANALYSIS SYSTEM v.3.0, Spectrum Associates (Marlborough, MA, USA). www.bio-logic.info/rapid-kinetics/specfit.html.

[17]   M. Zhu, M. Yuan, X. Liu, J. Xu, J. Lv, C. Huang, H. Liu, Y. Li, S. Wang, D. Zhu, *Org. Lett*. **2008**, *10*, 1481-1484.

[18]   The permissible exposure limit for NO established by the US Occupational Safety and Health Administration (OSHA) is 25 ppm.

[19]   M. J. Alcaraz, A. M. Vicente, A. Araico, J. N. Dominguez, M. C. Terencio, M. L. Ferrándiz, *Br. J. Pharmacol*. **2004**, *142*, 1191-1199.

Supporting Information

General remarks: CH_2Cl_2 and CH_3CN were distilled from P_2O_5 under Ar prior to use. All the other solvents and starting materials were purchased from commercial sources where available, and were used without purification. Silica gel 60 F254 (Merck) plates were used for TLC. Column chromatography was performed on silica gel (60, 40-63 μm). ^{1}H NMR (300 MHz) and ^{13}C NMR spectra were determined in a Bruker AV 300 spectrometer. Chemical shifts are reported in parts per million (ppm), calibrated to the solvent peak set. High-resolution mass spectra were recorded in the positive ion mode with a VG-AutoSpec mass spectrometer.

Membrane Preparation: Polyethylene oxide (2 g, Mw 400,000 Dalton) was slowly added to a solution of 1-Cu(II) (10^{-3} M solution) in dichloromethane (40 mL). The mixture was stirred until a highly viscous mixture was formed. This mixture was poured into a glass plate (40 cm^2) and kept in a dry atmosphere for 24 h.

Synthesis of 4-formyl-4'-methyl-2,2'-bipyridine (2)

Compound 2 was prepared 4,4'-dimethyl-2,2'-bipyridine (0.402 g 2.18 mmol) by oxidation with SeO_2 (0.269 g, 2.40 mmol) in dioxane (15 mL), following the procedure described at literature[98] (90.4 mg, 23%) ^{1}H NMR (300 MHz, CDCl$_3$) δ 10.18 (s, 1H), 8.90 (d, *J* = 4.9Hz, 1H), 8.83 (dd, *J* = 1.5 and 0.9 Hz, 1H), 8.58 (d, *J* = 4.9 Hz, 1H), 8.28 (s, 1H), 7.73 (dd, *J* = 4.9and 1.5 Hz, 1H), 7.20 (dd, *J* = 4.9and 0.9 Hz, 1H), 2.47 (s, 3H).

Synthesis of 1

Trifluoroacetic acid (5 μL, 0.115 mmol) was added to a solution of aldehyde 2 (47 mg 0.23 mmol) and 2,4-dimethylpyrrole (55 μL, 0.50 mmol) in anhydrous dichloromethane (10 mL). The mixture was stirred for 50 min at r.t. Subsequently, a solution of 2,3-dichloro-5,6-dicyano-p-benzoquinone (52.2 mg, 0.23 mmol) in anhydrous dichloromethane (10 mL) was added to the solution and the reaction was stirred for 50 min at r.t. Triethylamine (497 μL, 3.56 mmol) was added and the mixture was stirred for 30 min. Then BF_3-OEt_2 (497 μL, 17.5 equiv) was added and the reaction was stirred at r.t and followed by TLC (hexane: ethyl acetate (1:1)) until completion (3 h). Solvent was evaporated and the residue

---

[98] L. Amanda Eckermann, D. Kyle Barker, R. Mathew Hartings, A. Mark Ratner, J. Thomas Meade, J. of the A. Chem. Soc., 127, 2005, 11880-11881

purified by column chromatography (hexane: ethyl acetate (1:1)) to yield yellow solid (30.6 mg, 37 %)

^{1}H NMR (300 MHz, CDCl$_3$) δ 8.82 (dd, J = 4.9 and 0.8 Hz, 1H), 8.51 (d, J = 5.2 Hz, 1H), 8.48 (dd, J =1,6 and 0.8 Hz, 1H), 8.11 (s, 1H), 7.31 (dd, J = 4.9 and 1.6 Hz, 1H), 7.18 (d, J = 5.2 Hz, 1H), 5.92 (s, 2H), 2.49 (s, 6H), 2.39 (s, 3H), 1.40 (s, 6H). ^{13}C NMR (75 MHz, CDCl$_3$) δ 158, 157, 156, 155, 154, 150, 149, 125, 123, 122, 121, 21, 15, 14. UV-Vis (CH$_3$CN) λ_{max} = 500.5; emission (CH$_3$CN, λ_{exc} 476) λ_{max} = 520.05 nm. Φ(Rhodamine B) 0.49. HRMS (ESI): m/z calcd. for C$_{24}$H$_{23}$BF$_2$N$_4$ [M+H]$^+$ 417.1984, found 417.2065

Synthesis of 1-Cu(II)

A solution of P1 (200 mg, 0.41 mmol) in EtOH (5mL) was added dropwise to a solution of Cu(NO$_3$)$_2$·3H$_2$O (96.6 mg; 0.40 mmol) in H$_2$O (20 mL). The mixture was stirred for 2 h at rt. The product precipitated as a yellow solid, which was separated by filtration and recrystallized from EtOH-water (1:1) to give 1-Cu(II). HRMS (ESI): m/z calcd. for C$_{26}$H$_{28}$BCuF$_2$N$_4$O [M]: 524.16, found 524.1246

Spectroscopic studies: All the solvents were purchased spectroscopic grade from Aldrich Chemicals Co., and were used as received, and they were found to be free of fluorescent impurities. Absorption and fluorescence spectra were recorded using a Shimadzu UV-2600 spectrophotometer and a Varian Cary Eclipse spectrofluorimeter, respectively. Fluorescence quantum yields were measured at room temperature in the N$_2$-purgued solution in relation to Rhodamine B at 525 nm for 1 (Φ_{EtOH} = 0.49)[24]. The fluorescence quantum yields were calculated from Eq.(1) where F denotes the integral of the corrected fluorescence spectrum, A is the absorbance at the excitation wavelength, and n is the refractive index of the medium.

$$\Phi_{exp} = \Phi_{ref} \frac{F\{1 - exp(-A_{ref} ln10)\}n^2}{F_{ref}\{1 - exp(-A\ ln10)\}n_{ref}^2}$$

Limits of detection measurements: Increasing quantities of NO gas from a commercially available NO cylinder were exposure to a solution of 1-Cu(II) (1.0 x 10^{-5} mol dm^{-3}) in acetonitrile during 5 min. The fluorescence spectra were recorded in 1-cm path length cells at 25ºC. Representation of Δ of fluorescence at the appropriate wavelength vs. concentration of NO allowed the limit of detection to be calculated.

$$LOD = \frac{3S_b}{m}$$

In which S_b is the standard deviation of blank measurements and m is the slope of the linear regression plot.
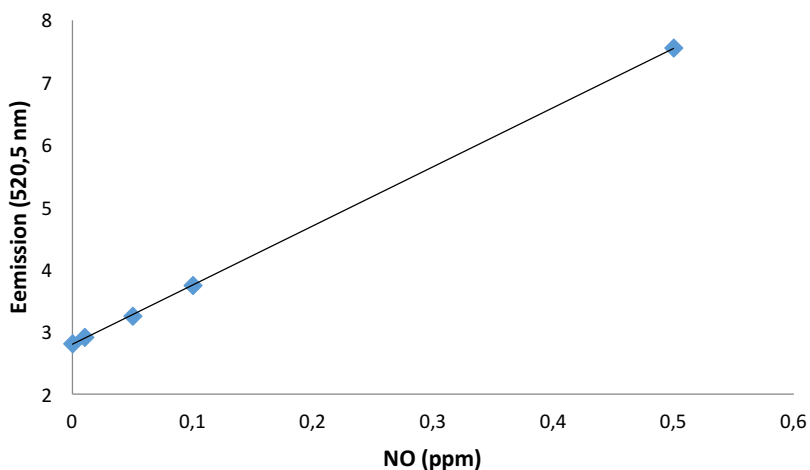

Figure S1: Emission at 520.5nm (λ_{exc}=500.5nm) of **1**-Cu(II) versus increasing amounts of NO (g) at room temperature.

Membrane Preparation: Polyethylene oxide (2 g, Mw 400,000 Dalton) was slowly added to a solution of **1**-Cu^{II} (10^{-3} M solution) in dichloromethane (40 mL). The mixture was stirred until a highly viscous mixture was formed. This mixture was poured into a glass plate (40 cm^2) and kept in a dry atmosphere for 24 h.
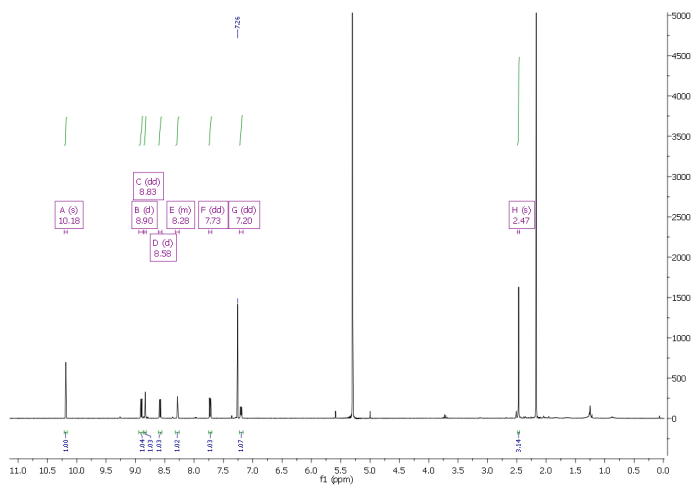
Figure S2: ^{1}H RMN spectrum of the aldehyde **2** in CDCl$_3$
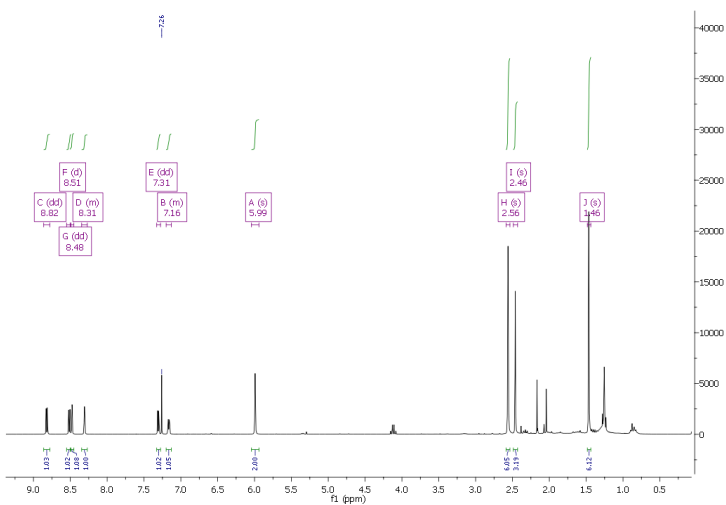
Figure S3: ^{1}H RMN spectrum of the **1** in CDCl$_3$
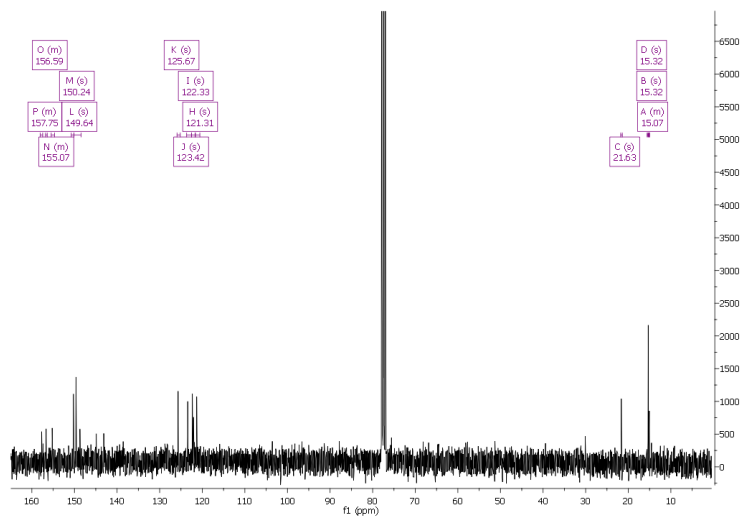
Figure S4: ^{13}C RMN spectrum of the **1** in CDCl$_3$
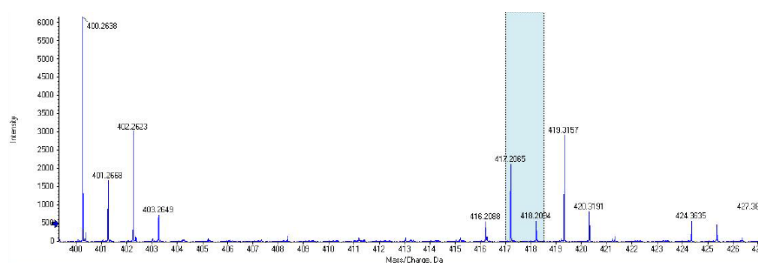
Figure S5: HRMS of the **1**
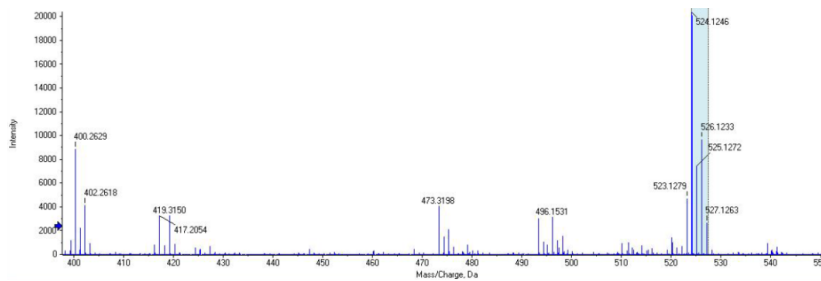
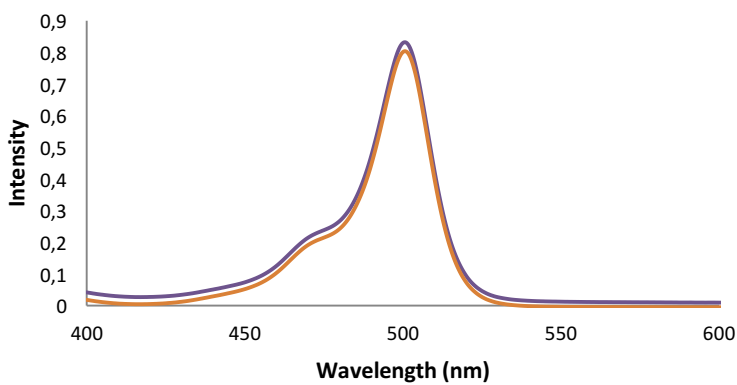Figure S6: HRMS of the **1**-Cu(II)

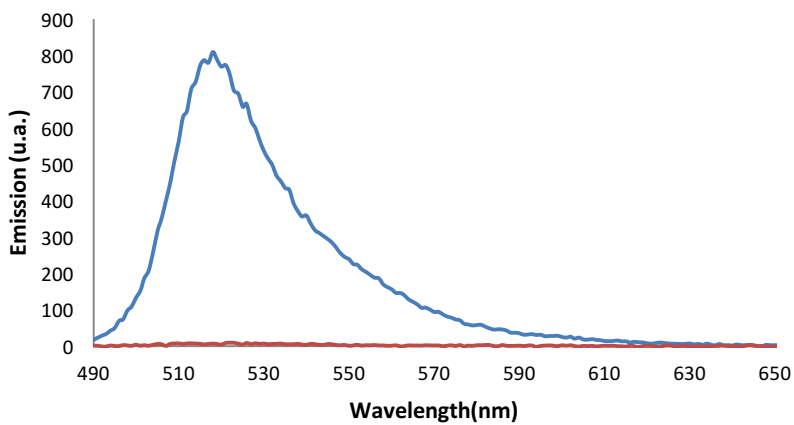Figure S7: UV spectrum of **1** and **1**-Cu(II) (acetonitrile solution, 10^{-5}M)

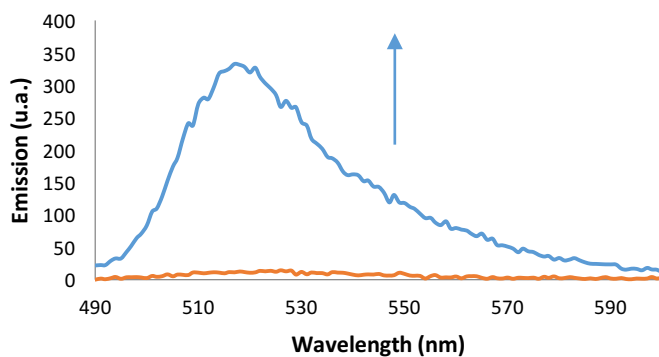Figure S8: Fluorescence spectrum of **1** and **1**-Cu(II) (acetonitrile solution, 10^{-5}M)

Figure S9: Fluorescence spectrum (λ_{exc}=500.5nm) of **1**-Cu(II) (10^{-5}M) in acetonitrile-water solution (1:9) upon exposure to NO (g) (80ppm)
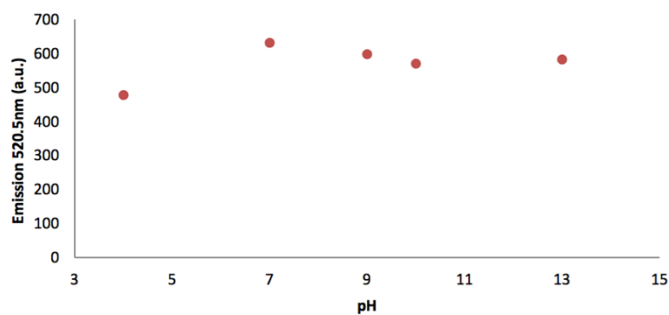

Figure S10. Fluorescence emission of **1** ($1\cdot10^{-5}$ M) in water:acetonitrile (9:1 v/v) in the pH range from 4 to 13

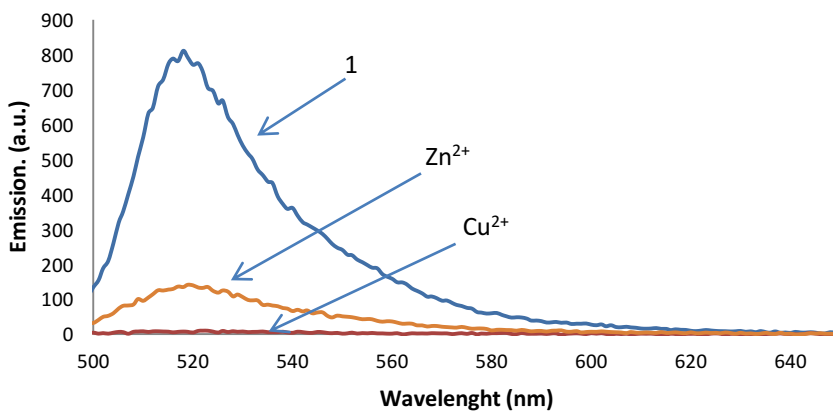Figure S11: Fluorescence spectra (λ_{exc}=500.5nm) of **1** (CH$_3$CN, 10^{-5}M) free and upon addition of 1 eq. of Zn(II) and Cu(II)
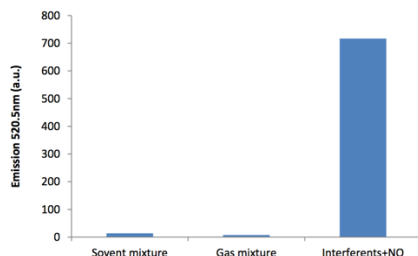
Figure S12. Competitive sensing experiments with **1**-Cu^{II} ($1\cdot10^{-5}$ M in water:acetonitrile 95:5 v/v) in the presence of mixtures of gases (NO_2, CO_2, H_2S, SO_2) and solvents (acetone, hexane, chloroform, acetonitrile and toluene) at a concentration above 100 ppm in air, and mixtures of all of them and NO

NO detection in cells and viability studies: To further demonstrate the biological application of **1**-Cu^{II}, RAW 264.7 macrophages (4x105/well) where stimulated during 18 h with Escherichia coli lipopolysaccharide (LPS) (1 µg/ml) in order to induce NO synthase (iNOS)[99]. After washing cells with phosphate buffered saline, **1**-Cu^{II} (10 µM) was added and NO release was initiated by addition of L-Arginine (100 µM) as substrate of iNOS. LPS-stimulated RAW 264.7 macrophages with only arginine or **1**-Cu^{II} showed low fluorescence determined in a Wallac 1420 VICTOR2TM (PerkinElmer) multilabel counter. In contrast, the addition of arginine in the presence of **1**-Cu^{II} produced a significant increase of fluorescence, demonstrating the ability of this compound to detect NO released by the cells. In a parallel experiment, the absence of cytotoxicity of **1**-Cu^{II} in the same conditions was demonstrated by the mitochondrial dependent reduction of 3-(4,5- dimethylthiazol-2-yl)-2,5-diphenyltetrazolium bromide (MTT) to formazan[100].

---

[99] M.J. Alcaraz, A.M. Vicente, A. Araico, J.N. Dominguez, M.C. Terencio, M.L. Ferrándiz, Br. J. Pharmacol. 2004, 142, 1191-1199.

[100] E. Borenfreund, H. Babich, N. Martin-Alguacil, *N. Toxicol In vitro*, 1988, 2, 1-6
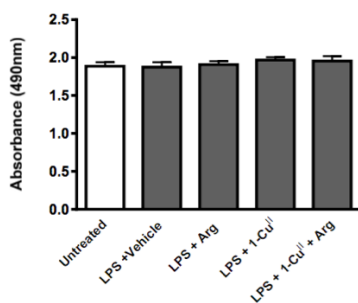
Figure S13. Cell viability determined by MTT assay in RAW 264.7 macrophages after co-incubation with **1**-Cu^{II} (1.0 x 10^{-5} M). Vehicle: water:acetonitrile 95:5 v/v. Arg: arginine. Data are expressed as mean ± SEM (n = 8−12).
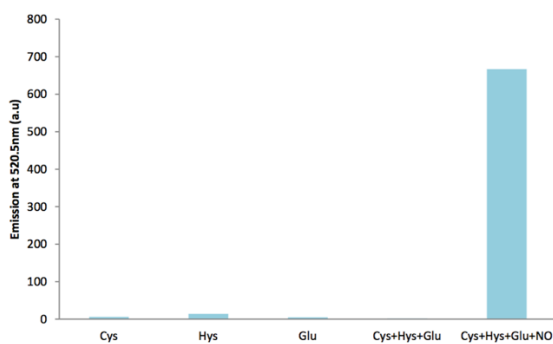

Figure S14. Interference studies of **1**-Cu^{II} (1·10^{-5} M in water:acetonitrile 95:5 v/v) with excess amounts of different possible Cu(II) coordinating compounds.

**Chapter 7:
Conclusions**

In the present thesis we wanted to develop new sensors for the selective and sensitive detection of nitrogen oxides, in particular nitic oxide and nitrogen dioxide.

In the Introduction, the main aspects of molecular recognition and optical sensing were described. In particular, the chemistry and properties of BODIPY-dyes and and the preparation of mesoporous materials and their properties were emphasized, to understand the basis of the new prepared sensors ant their sensing strategy.

In the first part including chapters 3, 4 and 5 different colorimetric and fluorogenic probes for detection of nitrogen dioxide were described. The design, synthesis and characterization of the recognition system were reported.

In the first case, chapter 3, different biphenyl chemodosimeters were tested the response to NO_2 gas and evaluated with limits of detection lower than the generally accepted alarm threshold and the color modulation can be observed by the naked eye. The applicability in real-time monitoring were development of simple colorimetric test for detection in real environment (a tunnel with heavy daily traffic).

In the fourth chapter, the design, synthesis and characterization of BODIPY-dyes was reported. Subsequently the chromogenic response to the different gaseous species was evaluated and we were able to state that our sensor displayed a great selectivity with remarkably low limits of detection, in ppb range. The additional advantage of the colour change could be observed by the naked eye encourage us to developed new systems supporting in different superficies.The high selectivity of the system avoiding a false negative response in the presence of other pollutant gases, water vapour and volatile organic compounds was stablished.

In the last chapter of the first part, the development of new silica mesoporous materials, as molecular gates were reported. The design, synthesis and characterization of molecular gates as chemosensor were described. In particular, a new gate paradigm was reported with a self-inmolative gate . The application of the MCM-41 molecular gate as chemosensor for NO_2 (g) was stablished using a double check system, using a BODIPY-dye as gate and the liberation of the cargo induced by the target molecule. The limits of detection were notably lower than the toxicity limits.

In the second part of these thesis a new BODIPY-complex fluorogenic chemosensor for nitric oxide was described. The mechanism of the detection occurs via displacement. The developed chemosensor contains a BODIPY fluorophore and a bipyridine unit capable of coordinating Cu^{II}. Reduction of Cu^{II} to Cu^{I} mediated by NO resulted in demetallation and a significant enhancement of the emission of the BODIPY unit. The study of the chemosensor sensitive showedremarkably low limits of detection, in ppb range, and good selectivity. Finally, the ability of the probe to detect NO release in cells was also assessed.

Publications

The result of this PhD thesis have been included in the following scientific publications:

- *A New Simple Chromo-fluorogenic Probe for NO$_2$ Detection in Air*
  L. Alberto Juárez, Prof. Ana M. Costero, Dr. Félix Sancenón, Prof. Ramón Martínez-Máñez, Prof. Margarita Parra and Dr. Pablo Gaviña
  Chemistry, a European Journal, **2015**, *24*, 8720-8722.

- *A Boron Dipyrromethene (BODIPY)-Based Cu^{II}–Bipyridine Complex for Highly Selective NO Detection*
  L. Alberto Juárez, Dr. Andrea Barba-Bon, Prof. Ana M. Costero, Prof. Ramón Martínez-Máñez, Dr. Félix Sancenón, Prof. Margarita Parra, Dr. Pablo Gaviña, Dr. M. Carmen Terencio and Prof. M. José Alcaraz
  Chemistry, a European Journal, **2015**, *44*, 15486-15490.

- *A new chromo-fluorogenic probe based on BODIPY for NO$_2$ detection in air.*
  L. Alberto Juárez, Ana M. Costero, Margarita Parra, Salvador Gil, Félix Sancenón and Ramón Martínez-Máñez
  Chemical Communications, **2015**, *51*, 1725–1727.

- *Biphenyl derivatives containing trimethylsilyl benzyl ether or oxime groups as probes for NO$_2$ detection.*
  L. Alberto Juárez, Ana M. Costero, Margarita Parra, Salvador Gil, Javier Ródenas, Félix Sancenón and Ramón Martínez-Máñez
  RSC Advances, **2016**, *6*, 43719–43723.

- *3-Formyl-BODIPY Phenylhydrazone as a Chromo-Fluorogenic Probe for Selective Detection of NO$_2$ (g)*
  L. Alberto Juárez, Prof. Ana M. Costero, Prof. Margarita Parra, Dr. Pablo Gaviña and Prof. Salvador Gil
  Chemistry, a European Journal, **2016**.

- *Self-immolative linkers as caps for the design of gated silica mesoporous supports*

L. Alberto Juárez, Elena Añón, Cristina Giménez, Félix Sancenón, Ramón Martínez-Máñez, Ana M. Costero, Pablo Gaviña, Margarita Parra.